

Semiclassical hybrid dynamics for open quantum systems

D I S S E R T A T I O N

zur Erlangung des akademischen Grades

Doctor rerum naturalium

(Dr. rer. nat.)

vorgelegt

der Fakultät Mathematik und Naturwissenschaften

der Technischen Universität Dresden

von

Christoph-Marian Goletz

geboren am 16. November 1981 in Zeitz

Eingereicht am 10. Februar 2011

**Die Dissertation wurde in der Zeit von 07/2007 bis
02/2011 im Institut für Theoretische Physik angefertigt.**



1. Gutachter: Prof. Dr. rer. nat. habil. Rüdiger Schmidt
 2. Gutachter: Prof. Dr. rer. nat. habil. Michael Thoss
- Verteidigt am _____

Abstract

Realistic physical systems can never be fully isolated from their environment, they rather interact with each other. Therefore it is of high interest to study open quantum systems, particularly effects coming from the influence of the surrounding.

In the present thesis, we consider environments with a finite number of degrees of freedom. However, a full quantum treatment of such an overall system can still be computationally very costly if not impossible. Therefore, we use a recently derived semiclassical hybrid method [Grossmann, *J. Chem. Phys.* **125**, 014111 (2006)], which is extended to the propagation of reduced densities in the context of system-bath problems. The essential idea behind this method is the treatment of different degrees of freedom on different levels of semiclassical approximations with different computational efforts.

In the first part of this thesis, for the first time, the hybrid method is applied to systems coupled to thermal baths, consisting of harmonic oscillators. First, non-resonant baths are considered allowing for the investigation of pure decoherence in the absence of dissipation. With the anharmonic Morse oscillator serving as a test system, we show that the developed hybrid method is a very efficient method, capable of reproducing decoherence effects, like the quenching of interference fringes, quantum-to-classical transition and the mixing of quantum states. In the same test system, quantum revivals and their bath-induced suppression are investigated along with the underlying semiclassical mechanism. A fundamental experiment from the early days of quantum physics is then studied in the framework of non-resonant baths, i.e. the double slit scenario. Here, the coupling to the bath is locally restricted and we show, that the hybrid method is an appropriate tool for the treatment of similar problems containing a coupling form factor.

Furthermore, we study resonant baths allowing for dissipation. With both, the harmonic and anharmonic oscillators at hand, we investigate the accuracy of the hybrid method as well as the importance of particular bath modes by comparing the respective results with results obtained with an implicit method, which describes an infinite bath.

In the last part of this thesis, we shift away from systems in Caldeira-Leggett baths towards systems in environments, whose specific form or geometry is fully describable and that are nonlinearly coupled to the system. For this purpose, we refer to an experiment, where the vibrational dynamics of an Iodine diatomic molecule in a Krypton environment are studied. In a model with reduced dimensionality, we first compare full quantum results with hybrid ones showing an excellent agreement even for the degrees of freedom treated with the cruder semiclassical approximation. In the next step we increase the number of degrees of freedom beyond the applicability of full quantum methods, like the split-operator scheme, and find the hybrid approach to be appropriate for the investigation of the present problem opening the door for studying further and larger systems of a similar kind.

Nomenclature

a.u.	Atomic units
CL	Caldeira-Leggett
DOF	Degree of freedom
GWP	Gaussian wave packet
HK	Herman-Kluk
LSC-IVR	Linearized semiclassical initial value representation
SC-IVR	Semiclassical initial value representation
SCBM	Semiclassical Brownian motion
SCHD	Semiclassical hybrid dynamics
SOI	System of interest
SPO	Split-operator method
TGWD	Thawed Gaussian wave packet dynamics
VVG	Van Vleck-Gutzwiller propagator

Contents

1	Introduction	1
2	Open Quantum Systems in Heat Baths	5
2.1	The Caldeira-Leggett Model	6
2.2	Frequency Shift	7
2.2.1	Harmonic Oscillator	7
2.2.2	Anharmonic Molecular Oscillator	10
2.3	The Initial State	12
2.3.1	Thermal Bath Density Operator in Position Representation	12
2.3.2	Thermal Bath Density Operator in Coherent State Representation	13
2.4	Quantifying the Coherence of a System - The Purity	15
3	Semiclassical Propagators	19
3.1	Semiclassical Initial Value Representations	19
3.1.1	Herman-Kluk Propagator	20
3.1.2	Thawed Gaussian Wave Packet Dynamics	22
3.1.3	Linearized Semiclassical Initial Value Representation	23
3.2	Semiclassical Hybrid Dynamics for Systems in a Thermal Bath	25
4	Pure Decoherence	31
4.1	Vibrational Dynamics of Diatomics	31
4.1.1	SCHD vs Various Semiclassical Approximations for $T=0$	33
4.1.2	From the Quantum to the Classical Regime at $T=0$	35
4.1.3	From the Quantum to the Classical Regime at Finite Temperature	37
4.1.4	Purity Dynamics and Decoherence	39
4.2	Long Time Quantum Dynamics - Wave Packet Revivals	41
4.2.1	Quantum Revival Time Analysis	42
4.2.2	Revivals in Semiclassics	43
4.2.3	Suppression of Revivals due to Decoherence	46
4.3	Diffraction at a Double Slit	50
4.3.1	Free Double Slit	50
4.3.2	Damping of Diffraction	52
5	Energy Dissipation	57
5.1	Damped Harmonic Oscillator	57
5.1.1	Analytical Expectation Values	57
5.1.2	Comparison With an Infinite Bath	59
5.2	Damped Molecular Oscillator	61
5.2.1	Comparison With an Infinite Bath	61
5.2.2	Dissipation vs Decoherence	64

5.2.3	Decoherence in a Resonant and Non-resonant Bath	65
6	A realistic system - Iodine in a Krypton environment	67
6.1	The Model	67
6.2	Vibrational Dynamics	70
6.2.1	Three Normal Modes	70
6.2.2	Four Normal Modes	73
7	Summary and Outlook	77
A	Sampling the Bath Frequencies	81
A.1	Exponential Density	81
A.2	“Inverse Square Root” Distribution	81
A.3	Lorentzian Density	82
A.4	Gaussian Density of Frequencies	82
B	Symplectic Integration	85
B.1	Derivatives for the Caldeira-Leggett Model	86
B.2	Derivatives for the I_2Kr_{17} Problem	86
C	From Herman-Kluk to Thawed Gaussian Wave Packet Dynamics	89
D	Expectation Values, Survival Probability and the Wigner Function in SCHD	97
D.1	The Wigner Function	97
D.2	Some Expectation Values	99
D.2.1	Energy Expectation Value for the Morse Oscillator	99
D.2.2	Norm, Position Expectation Value and Second Moment of Position .	101
D.3	Survival Probability...	102
D.3.1	... within SCHD	102
D.3.2	... within the LSC-IVR	103
	Bibliography	105

1 Introduction

Simplifications are an essential part of research in physics. They may allow for the investigation respectively numerical treatment of a given problem, which otherwise would not be possible at all, or at least very time-consuming. A common simplification in numerous fields of physics, particularly in atomic and molecular physics, is the assumption, that a studied system is completely isolated from its surroundings. Although this assumption often works well, it rarely matches reality. Realistic systems can never be fully isolated. Moreover, in some experiments, the significant influence of the surrounding system, which henceforth is identified as the environment, is a challenge affecting the properties of the observed system in an unwanted way. Prominent examples of this problem can be found in all fields of physics, where a system needs to be cooled down to very low temperatures, and in the currently very popular field of quantum computation [1, 2].

Such quantum systems that interact with and thus are influenced by an environment are called open quantum systems. They have been under thorough investigation in the past 30 years [3, 4, 5, 6] and are also the topic of this thesis. Within the theory of open quantum systems, the environment is a bath or thermal bath, i.e. a thermally equilibrated surrounding system, which commonly is considered to be infinitely large, although here this term is also used in the context of finite environments. In principle, two approaches can be considered regarding the way the bath degrees of freedom (DOFs) are handled. One possibility is a formalism, in which the bath dynamics are captured *implicitly*, e.g. the well-established Feynman-Vernon path integral formalism [7], which has been used in the case of a free and harmonic system [8], electron-molecule scattering [9], anharmonic Morse oscillator [10], double-well potential [11], and the dissipative two-state system [12]. In the same spirit master equation respectively stochastic Schrödinger equation approaches have been employed [13, 14, 15, 16] as well as generalized Langevin equations [17, 18, 19, 20], where the influence of the bath is realized by a noise force.

The other approach to open quantum systems is the *explicit* treatment of the bath DOFs together with the system DOFs including all interactions. This was employed in spin-boson and tunneling problems [21, 22, 23, 24, 25] as well as to both harmonic and anharmonic oscillators coupled to a bath [26, 27, 28].

Both explicit and implicit methods have in common that restrictions and approximations have to be made due to the formidable complexity of usual open systems. A widely used approximation for the implicit methods is the Markov approximation, where the future state of the bath is assumed to depend only on the present one.

The approach used in this thesis, however, is based on the explicit treatment of the bath DOFs along with the open quantum system, particularly in the time domain. To be more specific, the Caldeira-Leggett (CL) model is employed, in which the bath consists of a number of harmonic oscillators that are linearly coupled to the open system [29]. Depending on the size of the overall system, the use of exact propagation methods like the split-operator method (SPO) [30] can become an impossible endeavor. A possibility to deal with such large systems is the multi-configuration time-dependent Hartree [31] method, which is often

used in chemical physics. However, the approach used here is a semiclassical initial value representation (SC-IVR). For the sake of clarity, here the term “semiclassics” means the approximation of quantum mechanics using objects from classical mechanics, i.e. trajectories. Tracing back to the first semiclassical propagator in boundary value representation, the so-called Van Vleck-Gutzwiller (VVG) propagator [32, 33], SC-IVRs have experienced a renaissance since the early 90s after some pioneering work had been done already in the 70s and early 80s [34, 35, 36]. It was Kay who showed that a whole family of SC-IVRs exists [37], of which the the so-called Herman-Kluk (HK) propagator turned out to be the most effective one [38]. It has been shown to be a very good approximation to quantum mechanics in a number of systems. Since then, semiclassical methods have been applied successfully to numerous systems in molecular [39, 40, 41, 42, 43, 44, 45] and atomic [46, 47, 48, 49] physics. Even open quantum systems have been treated using the so-called semiclassical forward-backward method [50, 51, 52], which, however, is less accurate than the full method by Herman and Kluk, since an additional stationary phase approximation is made within the derivation [53, 54].

The specific semiclassical approach used in this thesis is the semiclassical hybrid dynamics (SCHD) [55], which is a combination of two semiclassical approximations of different accuracies. It combines the HK approximation with Heller’s thawed Gaussian wave packet dynamics (TGWD) [35, 56], which on the one hand is computationally much less costly than the HK method, but which on the other hand is only valid for (almost) harmonic DOFs. In this work, the SCHD is extended to the density matrix level of description considering systems embedded in a thermal bath, whose harmonicity is exploited in such a way that (almost) all bath DOFs can be treated on the level of the TGWD. For the open system the HK method can still be employed ensuring a high level of accuracy with respect to the quantum result. It is shown, that this new hybrid method is an efficient tool for the treatment of continuous variable systems in *finite* baths capturing all interactions and thus including non-Markovian effects. In particular, pure decoherence effects in systems of different levels of complexity are analyzed qualitatively and quantitatively. In this thesis it is shown, that long time dynamics in isolated molecular oscillators are reflected by SC-IVRs until the quantum revival regime and beyond. At the same time the mechanism of the suppression of revivals due to decoherence is studied with the SCHD for the open system. Moreover, for the first time, the SCHD description of a finite bath is compared with an implicit treatment of an infinite bath [57].

This thesis is organized as follows:

In Chapter 2, the theoretical framework for open quantum systems, which is relevant for this work, is given. In particular, the CL model, which is used to describe the bath, is introduced. Also, a way to discretize a bath described by a continuous spectral density is discussed, so that a finite number of bath DOFs can be considered. Furthermore, the frequency blue shift, that occurs in bound systems and that will also be observed in some numerical results in later chapters, will be investigated. Although predicted nearly 25 years ago by Pollak [17] and also observed in [53], this effect has never been studied quantitatively in more detail, regarding the dependence on the bath parameters. Subsequently, the initial thermal density operator is given in different representations, as it will be needed later on. At the end of this chapter, the purity is presented as a convenient quantity used within the investigation of decoherence.

Chapter 3 focuses on the semiclassical method of choice in this work. To this end, well-known semiclassical propagators in initial value representation will be reviewed. Starting

with the HK and the TGWD, the SCHD will then be derived in more detail in a density matrix formalism.

First numerical results obtained with the previously derived SCHD are then presented in Chapter 4. Here the effect of pure decoherence without dissipation is studied by using a low frequency cutoff. First this is done for the Morse oscillator on relatively short time scales of a few oscillation periods. In the next step, long time dynamics in the quantum revival regime is considered. After answering the question if the HK SC-IVR is capable of reproducing quantum revivals, revival dynamics in the presence of a finite bath is investigated. Subsequently a different scenario is studied, namely a wave packet propagating through a double slit. This problem describes a fundamental experiment in quantum mechanics. Also, the system-bath coupling is slightly modified.

Chapter 5 then turns towards dissipative systems by using a cutoff frequency beyond the uncoupled system frequency. Here, the harmonic as well as the physically more meaningful anharmonic Morse oscillator serve as benchmark systems, where the SCHD results are compared with results from an alternative implicit approach, called semiclassical Brownian motion (SCBM). In this formalism the influence of the bath is captured with a complex stochastic noise force. The comparison of both approaches, the explicit and implicit, allows to optimize the discretization of the finite bath in order to best mimic the results of the implicit approach.

In Chapter 6, we show that the SCHD can go beyond the treatment of system-bath problems within the CL model. To this end, we consider a molecular system in a noble gas environment, i.e. I_2 in Kr_{17} . We show, that the SCHD is an appropriate method for the study such a system, which is anharmonic in every DOF. Furthermore, we investigate the behavior of the DOFs treated on the level of TGWD, showing that these do not stay Gaussian as might have been expected but rather agree very well with the full quantum result.

Finally, in Chapter 7, a summary of this thesis is given together with an outlook on possible future work.

2 Open Quantum Systems in Heat Baths

This chapter gives the theoretical background and some necessary prerequisites for the treatment of open quantum systems in finite baths. Here, the open quantum system is assumed to be in contact with a heat bath forming the closed overall system. Hence, for the corresponding total Hamiltonian, the standard decomposition

$$\hat{\mathcal{H}} = \hat{\mathcal{H}}_{\text{S}} + \hat{\mathcal{H}}_{\text{SB}} + \hat{\mathcal{H}}_{\text{B}}, \quad (2.1)$$

can be employed, which is a sum of the system part (index S), the bath part (B), and an interaction (SB). Throughout this thesis, the system Hamiltonian has the typical form of a sum of kinetic and potential part

$$\hat{\mathcal{H}}_{\text{S}} = \hat{T} + \hat{\mathcal{V}} = \frac{\hat{\mathbf{p}}_{\text{S}}^2}{2M} + \hat{\mathcal{V}}(\hat{\mathbf{s}}). \quad (2.2)$$

Since the position representation is the preferred one in this thesis, the position operator $\hat{\mathbf{s}}$ is replaced by its eigenvalue and therefore always written as a scalar or vector. Usually one is interested in the explicit dynamics of the open quantum system solely, which is why it henceforth will be referred to as the system of interest (SOI). Introducing the reduced density operator as the partial trace of the full density operator over all bath degrees of freedom (DOFs)

$$\hat{\rho}_{\text{S}}(t) = \text{tr}_{\text{B}}\{\hat{\rho}(t)\}, \quad (2.3)$$

yields a quantity, that is solely comprised of the DOFs of the SOI. With the density operator in position representation, i.e. $\rho(\mathbf{x}', \mathbf{x}; t)$, and the position vector of the overall system, $\mathbf{x} = (\mathbf{s}, \mathbf{y})$, splitted into a SOI (\mathbf{s}) and bath (\mathbf{y}) subvector, the corresponding reduced density matrix is given by

$$\rho_{\text{S}}(\mathbf{s}, \mathbf{s}'; t) = \int d^{N_{\text{B}}}y \rho[(\mathbf{s}, \mathbf{y}), (\mathbf{s}', \mathbf{y}); t], \quad (2.4)$$

for a general bath, which consists of N_{B} DOFs. This reduced density matrix in position representation is the starting point for all quantities of interest throughout this thesis.

In this chapter the particular system-bath model used most of the time in this thesis, the Caldeira-Leggett (CL) model, will be introduced first, followed by a discussion of a frequency shift in bound systems originating from its coupling to the environment, which is observed in some of the results presented in this work. Subsequently, the initial system-bath state will be declared and particularly the initial thermal bath density operator will be given in different representations, which are prerequisites for the development of the specific semiclassical method used in this thesis later on. Finally, a convenient measure for the coherence of an open system, the purity, will be presented.

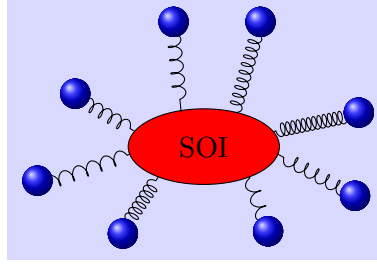


Figure 2.1: Sketch of the CL model showing an arbitrary SOI embedded in a bath consisting of harmonic oscillators (blue spheres and springs)

2.1 The Caldeira-Leggett Model

A frequently used model for the description of a reservoir and its interaction with the SOI traces back to Caldeira and Leggett [8, 29]. Here, the bath consists of a number of harmonic oscillators that are bilinearly coupled to the system, which, for this discussion (but not for all applications discussed later on), is restricted to one DOF (see also Fig. 2.1). Thus, the sum of interaction and bath Hamiltonian can be written in the form

$$\hat{\mathcal{H}}_{\text{SB}} + \hat{\mathcal{H}}_{\text{B}} = \sum_{i=1}^{N_{\text{B}}} c_i y_i s + \sum_{i=1}^{N_{\text{B}}} \left\{ \frac{\hat{p}_i^2}{2} + \frac{\omega_i^2}{2} y_i^2 \right\} + \sum_{i=1}^{N_{\text{B}}} \frac{c_i^2}{2\omega_i^2} s^2, \quad (2.5)$$

with the frequency ω_i , the momentum p_i , the mass-scaled position y_i of the respective harmonic bath mode and the coupling coefficients c_i . The bath consists of N_{B} harmonic oscillators of unit mass, while s is the position of the one-dimensional SOI. The last term in the equation is not included in the original CL Hamiltonian but is necessary as a counter-term to avoid an unphysical renormalization of the potential. This, for instance, ensures the translational invariance of a free particle SOI [5]. Thus the Hamiltonian of the overall system reads

$$\hat{\mathcal{H}} = \hat{\mathcal{H}}_{\text{s}} + \sum_{i=1}^{N_{\text{B}}} \left\{ \frac{\hat{p}_i^2}{2} + \frac{1}{2} \left(\omega_i y_i + \frac{c_i}{\omega_i} s \right)^2 \right\}. \quad (2.6)$$

The coefficients c_i denote the coupling to the bath and can be summarized in form of the spectral density [58], which in its general discretized form is given by

$$J(\omega) = \frac{\pi}{2} \sum_i \frac{c_i^2}{\omega_i} \delta(\omega - \omega_i). \quad (2.7)$$

Any given continuous spectral density J_{c} can be approximated by the original discretized form using a finite number of individual oscillators with the coupling coefficients

$$c_i^2 = \frac{2}{\pi} \frac{J_{\text{c}}(\omega_i)}{\rho_{\text{f}}(\omega_i)} \omega_i. \quad (2.8)$$

The individual frequencies are taken from a distribution of frequencies $\rho_{\text{f}}(\omega)$, which is normalized according to

$$\int_0^{\omega_{\max}} d\omega \rho_f(\omega) = N_B, \quad (2.9)$$

with the maximum considered bath frequency, ω_{\max} . Similarly, every frequency can be determined via

$$\int_0^{\omega_j} d\omega \rho_f(\omega) = j, \quad (2.10)$$

where j is the index of the particular bath mode and therefore an integer number. From Chapter 4 on, when numerical results will be presented, specific forms of the frequency distribution will be given. For more details on the sampling of the frequencies see also Appendix A.

2.2 Frequency Shift

When we treat *bound* systems coupled to a harmonic bath, it is of interest to investigate the effect of the bath on the frequency of the system. In the following the resulting frequency shift will be discussed for the harmonic oscillator, since an analytical treatment of this system is possible. Subsequently, the effect will be examined for the more realistic anharmonic Morse oscillator, which is one of the model systems used for the numerical calculations later in the main part of this thesis.

2.2.1 Harmonic Oscillator

In the case of a SOI with the harmonic potential

$$\mathcal{V}(s) = \frac{M\omega_s^2}{2}s^2 \quad (2.11)$$

it was shown via normal mode analysis (see e.g. [59]), that its vibrational frequency is changed due to the presence of the bath. The new frequency is then implicitly given by [17]

$$\lambda_s^2 = \frac{\omega_s^2}{1 + \frac{2}{\pi M} \int_0^\infty \frac{d\omega J(\omega)}{\omega(\omega^2 - \lambda_s^2)}}. \quad (2.12)$$

In order to allow for an analytical calculation of the integral in the denominator, the spectral density is chosen to be Ohmic with an abrupt cutoff

$$J_a(\omega) = \eta\omega\theta(\omega_c - \omega), \quad (2.13)$$

with the coupling strength η . Thus the integral in Eq. (2.12) becomes

$$\int_0^\infty \frac{d\omega J_a(\omega)}{\omega(\omega^2 - \lambda_s^2)} = -\eta \int_0^{\omega_c} \frac{d\omega}{\lambda_s^2 - \omega^2}. \quad (2.14)$$

Depending on the relative size of λ_s and ω_c , two qualitatively different solutions for the integral exist. For $\lambda_s > \omega_c$ we find

$$\int_0^{\omega_c} \frac{d\omega}{\lambda_s^2 - \omega^2} = \frac{1}{\lambda_s} \operatorname{artanh} \left(\frac{\omega_c}{\lambda_s} \right), \quad (2.15)$$

whereas for $\lambda_s < \omega_c$ we obtain

$$\begin{aligned} \int_0^{\omega_c} \frac{d\omega}{\lambda_s^2 - \omega^2} &= \lim_{\varepsilon \rightarrow 0} \left[\int_0^{\lambda_s - \varepsilon} \frac{d\omega}{\lambda_s^2 - \omega^2} + \int_{\lambda_s + \varepsilon}^{\omega_c} \frac{d\omega}{\lambda_s^2 - \omega^2} \right] \\ &= \lim_{\varepsilon \rightarrow 0} \frac{1}{2\lambda_s} \underbrace{\left[\ln \left(\frac{2\lambda_s - \varepsilon}{\varepsilon} \right) - \ln \left(\frac{2\lambda_s + \varepsilon}{\varepsilon} \right) \right]}_{=\ln \left(\frac{2\lambda_s + \varepsilon}{2\lambda_s - \varepsilon} \right) \rightarrow 0} + \frac{1}{\lambda_s} \operatorname{arcoth} \left(\frac{\omega_c}{\lambda_s} \right). \end{aligned} \quad (2.16)$$

Using the results above, Eq. (2.12) can be reorganized to a nonlinear equation

$$\lambda_s^2 - \frac{2\eta}{\pi M} f(\lambda_s) \lambda_s - \omega_s^2 = 0 \quad (2.17)$$

with the function

$$f(\lambda_s) = \begin{cases} \operatorname{arcoth} \left(\frac{\omega_c}{\lambda_s} \right) & \text{if } \lambda_s < \omega_c \\ \operatorname{artanh} \left(\frac{\omega_c}{\lambda_s} \right) & \text{if } \lambda_s > \omega_c. \end{cases} \quad (2.18)$$

This equation can be solved numerically using a Newton-Raphson root search scheme [60]. For the numerical root search, $\lambda_s = \omega_s$ turned out to be a good initial guess. Here, the harmonic system frequency and the mass are chosen to be $\omega_s = 0.001$ atomic units (a.u.) and $M = 1.165 \times 10^5$ a.u., respectively, which are parameters of I_2 that will be studied later on.

In Fig. 2.2 the dependence of the new frequency λ_s on the cutoff frequency of the bath is shown for two different dimensionless effective coupling strengths $\eta_{\text{eff}} = \eta/(M\omega_s)$, which are the mass-scaled coupling strengths. In the case of a finite coupling, λ_s equals the original unperturbed system frequency ω_s only in the case $\omega_c = 0$, which trivially means the absence of a bath, and in the rather unphysical case, where $\omega_c \rightarrow \infty$. For all other values of the cutoff frequency the perturbed frequency is larger than the unperturbed one, i.e. it is blue-shifted. As a remark, there is a singularity of $f(\lambda_s)$ at $\omega_c = \lambda_s$, which is not shown in Fig. 2.2. Also, a strictly monotonic increase of this blue-shift with increasing effective coupling strength is indicated, which is confirmed in Fig. 2.3. There, the dependence of the relative perturbed frequency on the effective coupling strength is shown.

Remarkably, the qualitative behavior of the function $\lambda_s(\eta_{\text{eff}})$ depends on the relative size of the cutoff frequency with respect to the system frequency. That is, for $\omega_c < \omega_s$ it is convex, whereas for $\omega_c > \omega_s$ it is concave. It should be stressed, that this frequency shift is a result of the normal mode analysis of the coupled system-bath supersystem, solely.

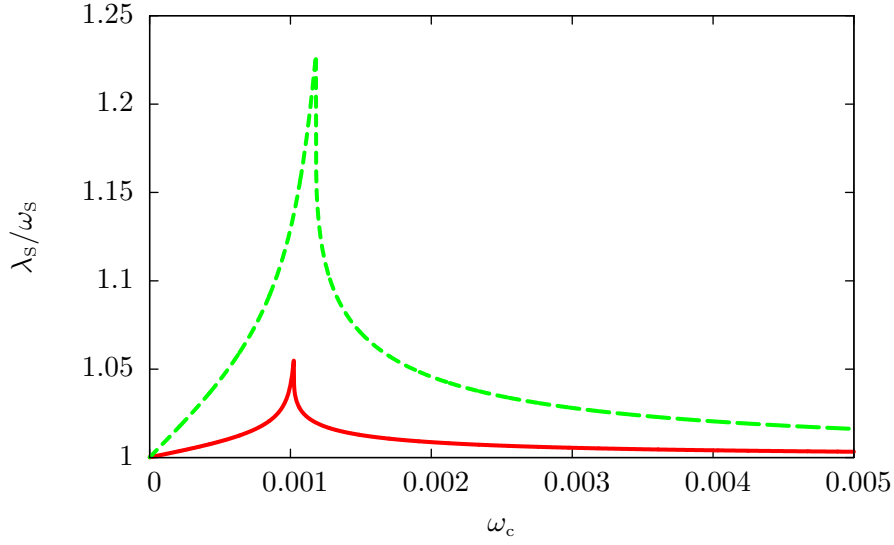


Figure 2.2: The relative frequency shift of a harmonic oscillator with $\omega_s = 0.001$ a.u. coupled to a harmonic bath vs the cutoff frequency for two different effective coupling strengths: $\eta_{\text{eff}} = \eta/(M\omega_s)$; solid line: $\eta_{\text{eff}} = 0.05$, dashed line: $\eta_{\text{eff}} = 0.25$

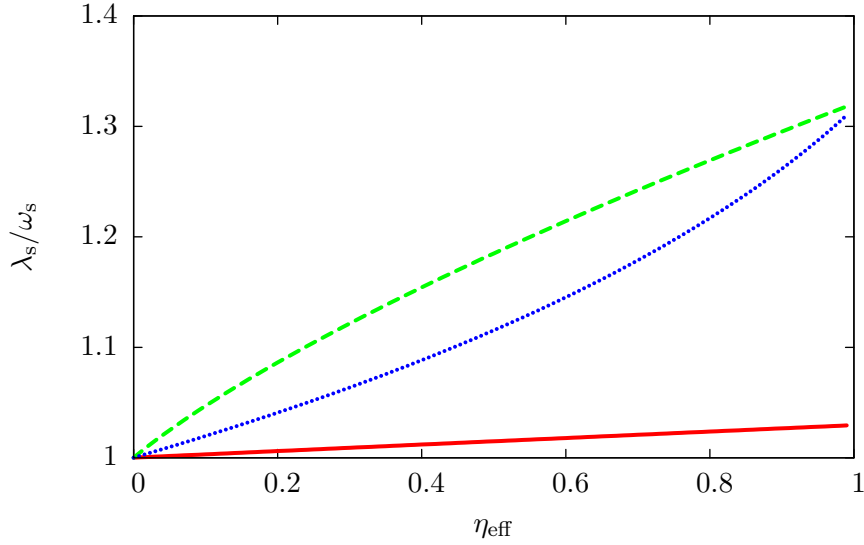


Figure 2.3: The relative frequency shift of a harmonic oscillator with $\omega_s = 0.001$ a.u. coupled to a harmonic bath vs the effective coupling strengths: $\eta_{\text{eff}} = \eta/(M\omega_s)$ for different cutoff frequencies; solid line: $\omega_c = 9.1 \times 10^5$ a.u., dashed line: $\omega_c = 9.0 \times 10^4$ a.u., dotted line: $\omega_c = 1.8 \times 10^3$ a.u.

2.2.2 Anharmonic Molecular Oscillator

A prominent and widely used potential in molecular physics is the anharmonic oscillator introduced by Morse in 1929 [61]. Since then, it has frequently been used as a model for the description of the vibration of diatomic molecules on a single electronic bound surface [62]. With the bond distance s the corresponding potential reads

$$\mathcal{V}(s) = D \left[1 - e^{-\alpha(s-s_e)} \right]^2, \quad (2.19)$$

where the parameters are the dissociation threshold D , the equilibrium bond distance s_e and the range parameter α . This potential, as sketched in Fig. 2.4, is strongly repulsive for bond distances below the equilibrium bond distance and weakly attractive with an asymptotic limit D for large distances of the nuclei from each other. Besides the fact, that the anharmonicity of the nuclear vibration is well captured, the Morse oscillator also comprises the effect of bond breaking and hence molecular dissociation, i.e. trajectories with energies above D move towards arbitrarily large bond distances for $t \rightarrow \infty$. Furthermore, atom-surface interactions can be described with the help of the Morse potential [63, 64]. Also, this is one of the few analytic potentials, for which an analytic expression for the spectrum is known [61]

$$E_n = \hbar\omega_s \left(n + \frac{1}{2} \right) - \hbar\nu_s \left(n + \frac{1}{2} \right)^2, \quad (2.20)$$

where $\omega_s = \alpha\sqrt{2D/M}$ is the harmonic frequency and $\nu_s = \hbar\alpha^2/(2M)$ is the anharmonicity parameter with the reduced mass of the diatomic molecule M . Also the bound energy eigenstates were found approximately [61, 65]

$$\psi_n(s) = \sqrt{\frac{n!\alpha(\lambda - 2n - 1)}{\Gamma(\lambda - n)}} e^{-\xi(s)/2} \xi(s)^{\lambda-2n-1} L_n^{\lambda-2n-1}(\xi(s)), \quad (2.21)$$

where $L_n^{\lambda-2n-1}$ are Laguerre polynomials [66] and

$$\begin{aligned} \lambda &= \frac{\omega_s}{\nu_s} = \frac{2\sqrt{DM}}{\hbar\alpha} \\ \xi(s) &= \lambda e^{-\alpha(s-s_e)}. \end{aligned} \quad (2.22)$$

For molecules this is a very good approximation [67].

In the past decades the Morse potential has been an object of thorough research, e.g. chaos [68] and the generation of harmonics [69] have been investigated in the driven oscillator. Moreover, this potential has been used for calculations of molecules beyond diatomics, e.g. water, HCN and DNA [70, 71, 72]. Calculations with the Morse oscillator using the semiclassical HK method have yielded results, that are in a very good agreement with quantum ones [73]. Thus, this system is suited for further semiclassical investigations.

Turning towards the frequency shift, further investigations are necessary regarding the Morse potential, since the harmonic approximation and the associated analytic prediction is only valid in the vicinity of the potential minimum. To this end, it is helpful to introduce the concept of a local frequency of a trajectory with a certain energy. For the uncoupled Morse oscillator this energy dependence of the local frequency is given by [74]

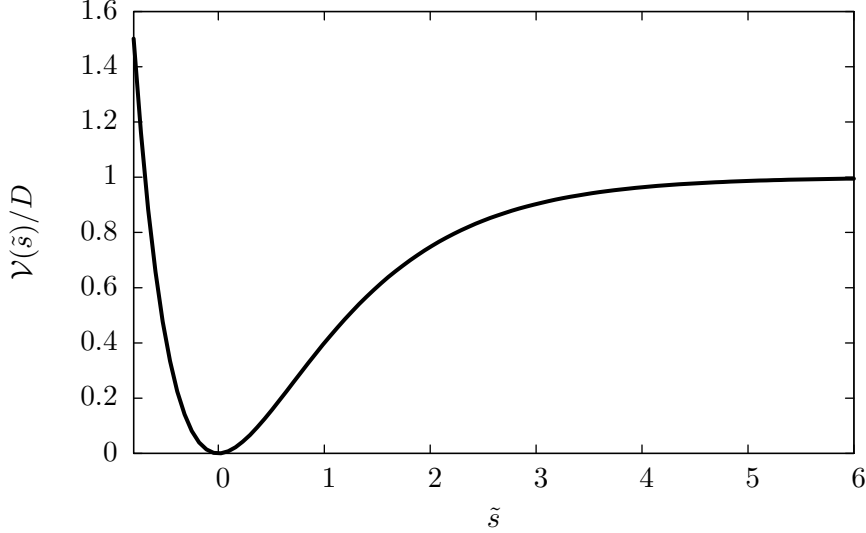


Figure 2.4: (Normalized) Morse potential versus a dimensionless bond distance

$$\tilde{s} \equiv (s - s_e)/s_e$$

$$\omega_{\text{loc}}(E) = \omega_s \sqrt{1 - \frac{E}{D}}. \quad (2.23)$$

In Fig. 2.5 the energy dependence of the coupled oscillator's local frequency λ_s^{loc} is shown using the potential parameters $D = 0.057$ a.u., $\alpha = 0.983$ a.u. and the bath cutoff frequency $\omega_c = 9.1 \times 10^{-5}$ a.u. (taken from Ref. [51]). The mass is the same as in the harmonic oscillator case above. Thus the harmonic frequency for small oscillations also equals the one in the harmonic oscillator case, that is

$$\omega_s = \alpha \sqrt{2 \frac{D}{M}} \approx 0.001 \text{ a.u.} \quad (2.24)$$

The solid and dashed curves are obtained “numerically” for different coupling strengths by running trajectories with a specific energy connected to a bath of 20 (initially relaxed) modes and reading off the period of oscillation. The dotted curve depicts the analytically determined energy-dependent local frequency of the coupled Morse oscillator. Here, the harmonic frequency from Eq. (2.24) is used to obtain the shifted result according to Eq. (2.17). Subsequently the results is then inserted into the analog of Eq. (2.23), that is

$$\lambda_s^{\text{loc}}(E) = \lambda_s \sqrt{1 - \frac{E}{D}}. \quad (2.25)$$

This “analytic” result is depicted by the dotted line in Fig. 2.5 for the coupling strength $\eta_{\text{eff}} = 0.25$.

However, comparison with the numerically obtained curve shows that obviously, this naive assumption of a coupled local frequency with the same energy dependence as the uncoupled one but with a global shift from ω_s to λ_s is only valid for low energies in the vicinity of the potential minimum. For higher energies the anharmonicity of the SOI significantly influences the energy dependence of the local frequency.

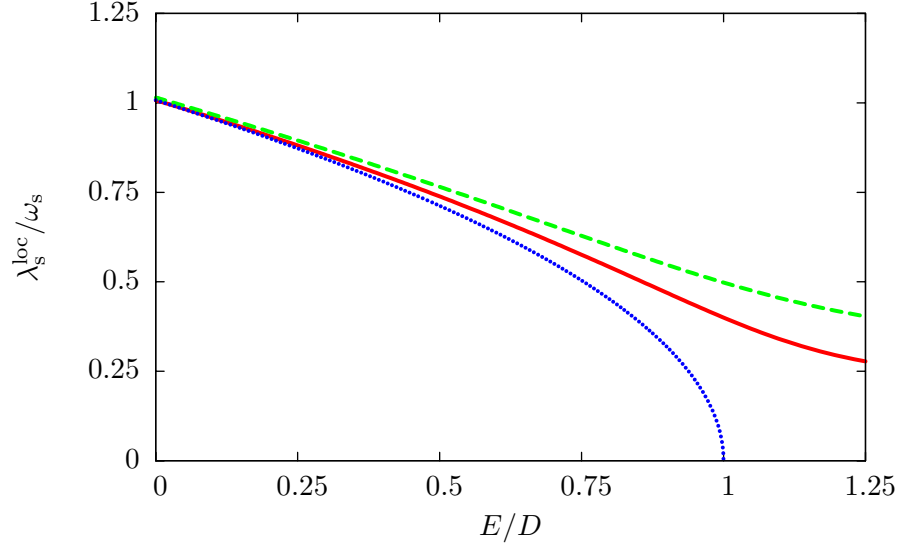


Figure 2.5: The coupled local frequency vs energy in the anharmonic Morse oscillator; solid line: numerical result for $\eta_{\text{eff}} = 0.25$, dashed line: numerical result for $\eta_{\text{eff}} = 0.5$, dotted line: coupled local frequency according to Eq. (2.25) for $\eta_{\text{eff}} = 0.25$

We note in passing, that the numerically evaluated graphs, i.e. the solid and the dashed line ($\eta_{\text{eff}} = 0.5$), show nonzero values even above the dissociation threshold D . These frequencies correspond to residual, bath induced oscillations of the asymptotically unbound trajectories.

2.3 The Initial State

In this work the initial state for the dynamics is assumed to be a product of the system and bath density operator [7]

$$\hat{\rho}(0) = \hat{\rho}_S(0)\hat{\rho}_B(0) \equiv \hat{\rho}_S\hat{\rho}_B = \hat{\rho}_S \frac{e^{-\beta\hat{\mathcal{H}}_B}}{Z_B}, \quad (2.26)$$

describing a bath in a thermal equilibrium, where $Z_B = \text{tr}(e^{-\beta\hat{\mathcal{H}}_B})$ is the partition function of the thermal density operator. Furthermore, the initial state contains the inverse temperature $\beta = 1/(kT)$ with the Boltzmann constant k and the temperature T . In the following, the position and coherent state representation of the initial bath density operator will be reviewed as they will be required later on in this work.

2.3.1 Thermal Bath Density Operator in Position Representation

Our starting point is the well-known harmonic oscillator propagator, which for instance can be derived using a path integral approach (see e.g. [75]). Considering a single harmonic oscillator with the Hamiltonian \hat{H}_b , frequency ω and unit mass, the associated propagator reads

$$\langle y'' | e^{-i\hat{\mathcal{H}}_b t/\hbar} | y' \rangle = \sqrt{\frac{\omega}{2\pi i \hbar \sin(\omega t)}} \exp \left\{ \frac{i\omega}{2\hbar \sin(\omega t)} [(y'^2 + y''^2) \cos(\omega t) - 2y'y''] \right\}. \quad (2.27)$$

From this, the aim is to find the thermal density matrix $\langle y'' | e^{-\beta \hat{\mathcal{H}}_b} | y' \rangle$ of the harmonic oscillator. By comparing the exponents in both the thermal and the time evolution operator, we find that this can be achieved by an adequate replacement of the time variable in the propagator, i.e. $t \rightarrow -i\hbar\beta$. Hence, this yields

$$\langle y'' | e^{-\beta \hat{\mathcal{H}}_b} | y' \rangle = \sqrt{\frac{\omega}{2\pi \hbar \sinh(\omega\beta\hbar)}} \exp \left\{ -\frac{\omega}{2\hbar \sinh(\omega\beta\hbar)} [(y'^2 + y''^2) \cosh(\omega\beta\hbar) - 2y'y''] \right\} \quad (2.28)$$

and the corresponding partition function, which can be gained by tracing the thermal density operator, reads

$$Z_b = \int dy' \langle y' | e^{-\beta \hat{\mathcal{H}}_b} | y' \rangle = \left[2 \sinh(\omega\beta\hbar) \tanh\left(\frac{\omega\beta\hbar}{2}\right) \right]^{-1/2}. \quad (2.29)$$

Assuming that the initial bath density matrix is a product of the individual harmonic mode densities, the former therefore results in

$$\begin{aligned} \left\langle \mathbf{y}'' \left| \frac{e^{-\beta \hat{\mathcal{H}}_B}}{Z_B} \right| \mathbf{y}' \right\rangle &= \prod_{i=1}^{N_B} \left\langle y_i'' \left| \frac{e^{-\beta \hat{\mathcal{H}}_b^{(i)}}}{Z_b^{(i)}} \right| y_i' \right\rangle \\ &= \prod_{i=1}^{N_B} \sqrt{\frac{\omega_i}{\pi \hbar} \tanh\left(\frac{\omega_i \beta \hbar}{2}\right)} \exp \left\{ -\frac{\omega_i}{2\hbar \sinh(\omega_i \beta \hbar)} [-2y_i'' y_i' \right. \\ &\quad \left. + (y_i''^2 + y_i'^2) \cosh(\omega_i \beta \hbar)] \right\}, \quad (2.30) \end{aligned}$$

where the index i denotes the particular bath mode.

2.3.2 Thermal Bath Density Operator in Coherent State Representation

A prerequisite for the derivation of the SCHD later on is the coherent state representation of the thermal density operator. It can be obtained by taking the operator in position representation and inserting the unit operator twice via the completeness relation of the position eigenfunctions

$$\begin{aligned} &\left\langle g_\gamma(q, p) \left| \frac{e^{-\beta \hat{\mathcal{H}}_b}}{Z_b} \right| g_\gamma(q', p') \right\rangle \\ &= \left\langle g_\gamma(q, p) \left| \underbrace{\left(\int dy'' |y''\rangle \langle y''| \right)}_1 \frac{e^{-\beta \hat{\mathcal{H}}_b}}{Z_b} \underbrace{\left(\int dy' |y'\rangle \langle y'| \right)}_1 \right| g_\gamma(q', p') \right\rangle. \quad (2.31) \end{aligned}$$

By making use of the coherent state in position representation

$$\langle y | g_\gamma(q, p) \rangle = \left(\frac{\gamma}{\pi} \right)^{1/4} \exp \left\{ -\frac{\gamma}{2} (y - q)^2 + \frac{i}{\hbar} p (y - q) \right\}, \quad (2.32)$$

Eq. (2.31) becomes a Gaussian integral with a linear term in the exponent

$$\begin{aligned} & \left\langle g_\gamma(q, p) \left| \frac{e^{-\beta \hat{\mathcal{H}}_b}}{Z_b} \right| g_\gamma(q', p') \right\rangle \\ &= \int dy'' dy' \langle g_\gamma(q, p) | y'' \rangle \left\langle y'' \left| \frac{e^{-\beta \hat{\mathcal{H}}_b}}{Z_b} \right| y' \right\rangle \langle y' | g_\gamma(q', p') \rangle \\ &= \sqrt{\frac{\gamma \omega}{\pi^2 \hbar} \tanh \left(\frac{\omega \beta \hbar}{2} \right)} \int dy'' dy' \\ & \quad \times \exp \left\{ -\frac{\gamma}{2} (y'' - q)^2 - \frac{i}{\hbar} p (y'' - q) - \frac{\gamma}{2} (y' - q')^2 + \frac{i}{\hbar} p' (y' - q') \right. \\ & \quad \left. - \frac{\omega}{2 \hbar \sinh(\omega \beta \hbar)} [-2y'' y' + (y''^2 + y'^2) \cosh(\omega \beta \hbar)] \right\} \\ &= \sqrt{\frac{\gamma \omega}{\pi^2 \hbar} \tanh \left(\frac{\omega \beta \hbar}{2} \right)} \int dy'' dy' \\ & \quad \times \exp \left\{ - \begin{pmatrix} y'' & y' \end{pmatrix} \mathbf{E} \begin{pmatrix} y'' \\ y' \end{pmatrix} + \mathbf{f}^T \begin{pmatrix} y'' \\ y' \end{pmatrix} - \frac{\gamma}{2} (q^2 + q'^2) + \frac{i}{\hbar} (pq - p'q') \right\}, \end{aligned} \quad (2.33)$$

where the matrix

$$\mathbf{E} = \frac{1}{2} \begin{pmatrix} \frac{\omega}{\hbar \tanh(\omega \beta \hbar)} + \gamma & -\frac{\omega}{\hbar \sinh(\omega \beta \hbar)} \\ -\frac{\omega}{\hbar \sinh(\omega \beta \hbar)} & \frac{\omega}{\hbar \tanh(\omega \beta \hbar)} + \gamma \end{pmatrix} \quad (2.34)$$

and vector

$$\mathbf{f}^T = (\gamma q - \frac{i}{\hbar} p \quad \gamma q' + \frac{i}{\hbar} p') \quad (2.35)$$

have been introduced. This Gaussian integral can be evaluated analytically by making use of the general formula

$$\int d^d y \exp \{ -\mathbf{y}^T \mathbf{E} \mathbf{y} + \mathbf{f}^T \mathbf{y} \} = \sqrt{\frac{\pi^d}{\det(\mathbf{E})}} \exp \left\{ \frac{1}{4} \mathbf{f}^T \mathbf{E}^{-1} \mathbf{f} \right\}, \quad (2.36)$$

where \mathbf{E} has to be a positive definite, symmetric matrix and d is the number of dimensions. The inverse and determinant of the matrix \mathbf{E} as defined in Eq. (2.35) are

$$\begin{aligned} \mathbf{E}^{-1} &= \frac{1}{2 \det(\mathbf{E})} \begin{pmatrix} \frac{\omega}{\hbar \tanh(\omega \beta \hbar)} + \gamma & \frac{\omega}{\hbar \sinh(\omega \beta \hbar)} \\ \frac{\omega}{\hbar \sinh(\omega \beta \hbar)} & \frac{\omega}{\hbar \tanh(\omega \beta \hbar)} + \gamma \end{pmatrix} \\ \det(\mathbf{E}) &= \frac{1}{4} \left(\frac{\omega^2}{\hbar^2} + \gamma^2 + \frac{2\gamma\omega}{\hbar \tanh(\omega \beta \hbar)} \right), \end{aligned} \quad (2.37)$$

respectively. Consequently, Eq. (2.33) results in

$$\begin{aligned}
 & \left\langle g_\gamma(q, p) \left| \frac{e^{-\beta \hat{\mathcal{H}}_b}}{Z_b} \right| g_\gamma(q', p') \right\rangle \\
 &= Z \exp \left\{ \frac{1}{4 \det(\mathbf{E})} \left[\left(\frac{\omega}{\hbar \tanh(\omega \beta \hbar)} + \gamma \right) \left(\frac{\gamma^2}{2} (q^2 + q'^2) - \frac{1}{2 \hbar^2} (p^2 + p'^2) + \frac{i \gamma}{\hbar} (p' q' - p q) \right) \right. \right. \\
 & \quad \left. \left. + \frac{i \gamma}{\hbar^2} \frac{\omega}{\sinh(\omega \beta \hbar)} (p' q - p q') + \gamma^2 \frac{\omega}{\hbar \sinh(\omega \beta \hbar)} q q' + \frac{1}{\hbar^3} \frac{\omega}{\sinh(\omega \beta \hbar)} p p' \right] \right. \\
 & \quad \left. - \frac{\gamma}{2} (q^2 + q'^2) + \frac{i}{\hbar} (p q - p' q') \right\}, \tag{2.38}
 \end{aligned}$$

which can be converted into a clearer form by setting $\gamma = \omega/\hbar$. From the normalization condition the prefactor then yields

$$\begin{aligned}
 Z &= \sqrt{\frac{2 \tanh(\omega \beta \hbar/2)}{1 + 1/\tanh(\omega \beta \hbar)}} \\
 &= e^{-\omega \beta \hbar/2} \sqrt{2 \tanh(\omega \beta \hbar/2) \sinh(\omega \beta \hbar)} \\
 &= e^{-\omega \beta \hbar/2} \sqrt{4 \tanh(\omega \beta \hbar/2) \sinh(\omega \beta \hbar/2) \cosh(\omega \beta \hbar/2)} \\
 &= 1 - e^{-\omega \beta \hbar} \tag{2.39}
 \end{aligned}$$

and the thermal density operator in coherent state representation for N_B harmonic bath modes finally reads

$$\begin{aligned}
 & \left\langle g_\gamma(\mathbf{q}, \mathbf{p}) \left| \frac{e^{-\beta \hat{\mathcal{H}}_B}}{Z_B} \right| g_\gamma(\mathbf{q}', \mathbf{p}') \right\rangle \\
 &= \prod_{i=1}^{N_B} \left\langle g_{\gamma_i}(q_i, p_i) \left| \frac{e^{-\beta \hat{\mathcal{H}}_b^{(i)}}}{Z_b^{(i)}} \right| g_{\gamma_i}(q'_i, p'_i) \right\rangle \\
 &= \prod_{i=0}^{N_B} (1 - e^{-\beta \omega_i \hbar}) \exp \left\{ -\frac{1}{4} (\mathbf{q}^T \boldsymbol{\gamma} \mathbf{q} + \mathbf{q}'^T \boldsymbol{\gamma} \mathbf{q}') - \frac{1}{4 \hbar^2} (\mathbf{p}^T \boldsymbol{\gamma}^{-1} \mathbf{p} + \mathbf{p}'^T \boldsymbol{\gamma}^{-1} \mathbf{p}') \right. \\
 & \quad \left. + \frac{i}{2 \hbar} (\mathbf{p}^T \mathbf{q} - \mathbf{p}'^T \mathbf{q}') + \frac{1}{2} \left(\boldsymbol{\gamma} \mathbf{q}_y - \frac{i}{\hbar} \mathbf{p}_y \right)^T e^{-\beta \boldsymbol{\gamma} \hbar^2} \left(\mathbf{q}'_y + \frac{i}{\hbar} \boldsymbol{\gamma}^{-1} \mathbf{p}'_y \right) \right\}, \tag{2.40}
 \end{aligned}$$

where $\boldsymbol{\gamma}$ is a diagonal matrix containing the individual harmonic frequencies.

2.4 Quantifying the Coherence of a System - The Purity

Incoherence, or, reversely, coherence, are important concepts in the theory of open quantum systems. Starting from the earlier developed von Neumann entropy the purity will be introduced in this section as an appropriate measure of a system's coherence (more on this can be found in [76]).

One of the effects of decoherence is the mixing of a system, i.e. the transition of a pure state into a mixed state density matrix. The former one is a quantum state $|\psi\rangle$ describing the regarded physical system and the corresponding density operator can thus be written as

$$\hat{\rho} = |\psi\rangle\langle\psi|, \quad (2.41)$$

which simply represents a projection operator on the quantum state $|\psi\rangle$. A mixed state is represented by a density operator of the form

$$\hat{\rho} = \sum_i p_i |\psi_i\rangle\langle\psi_i|, \quad (2.42)$$

which is a sum of pure states $|\psi_i\rangle$, each contained in the mixture with a statistical probability p_i , where at least two of the p_i are nonzero. Assuming that, for reasons of simplicity, $\{|\psi_i\rangle\}$ is an orthonormal basis (in general this is not necessarily the case), it is easy to see that Eq. 2.42 is an incoherent superposition of pure states, since interference terms proportional to $|\psi_i\rangle\langle\psi_j|$ ($j \neq i$) are not included. Thus the corresponding mixed density can be regarded as a purely classical distribution of pure state densities. Here, state mixing and the quantum-to-classical transition of a state as a consequence of decoherence becomes apparent, again.

Historically, the first measure for the “mixedness”, and thus the degree of incoherence of a state, is the von Neumann entropy [77]

$$\mathcal{S}(\hat{\rho}) = -\text{tr}(\hat{\rho} \log_2 \hat{\rho}) = -\sum_i \lambda_i \log_2 \lambda_i \quad (2.43)$$

with the eigenvalues λ_i of the density operator, where $\sum_i \lambda_i = 1$. This is an extension of the Gibbs entropy to the case of quantum states. In case of a pure state, all eigenvalues except for one are zero and thus $\mathcal{S} = 0$ (with $0 \log_2 0 \equiv 0$). For a fully mixed state $\lambda_i = 1/N_H$ in a N_H -dimensional Hilbert space, where all pure states have equal weights in the mixed ensemble, the von Neumann entropy has its maximum value $\mathcal{S} = \log_2(N_H)$. In this case, we have the least information about the system.

However, for numerical computations, the von Neumann entropy is rather inconvenient, since one always has to diagonalize the density matrix in order to determine the logarithm. In order to find an alternative measure, the logarithm can be expanded around the unit operator to the first order term [78]

$$\mathcal{S}(\hat{\rho}) = -\text{tr}(\hat{\rho} \log_2 \hat{\rho}) \approx -\text{tr}[\hat{\rho}(\hat{\rho} - \mathbf{1})] = 1 - \text{tr}(\hat{\rho}^2) \equiv 1 - \mathcal{P}(\hat{\rho}), \quad (2.44)$$

where $\mathcal{P}(\hat{\rho})$ is the purity, which - as the name suggests - now quantifies, how pure, or equivalently, how coherent a state is. Using Eq. (2.42), it can be written as

$$\mathcal{P}(\hat{\rho}) = \text{tr}(\hat{\rho}^2) = \sum_{i=1}^{N_H} p_i^2 \quad (2.45)$$

with the number of dimensions of the Hilbert space N_H . In the case of a pure state, the purity equals one, which is its maximum value. In turn, it has its minimum value in the case of a fully mixed state, where all $p_i = 1/N_H$ and consequently $\mathcal{P} = 1/N_H$. It should be

stressed that in contrast to the von Neumann entropy, the computational effort reduces to the squaring of the density matrix and the subsequent calculation of the trace.

So far, theoretical prerequisites from the field of open quantum system have been given, which are essential for the remainder of this thesis. In the next chapter some particular SC-IVRs are sketched first, which are origins of the subsequent derivation of the SCHD.

3 Semiclassical Propagators

In order to obtain a solution for the time-dependent Schrödinger equation in position representation, its corresponding Green's function, which is the propagator $K(\mathbf{x}, t; \mathbf{x}', t_0)$, is applied to an initial wave function $\Psi(\mathbf{x}, 0)$ according to

$$\Psi(\mathbf{x}, t) = \int d^N x' K(\mathbf{x}, t; \mathbf{x}', t_0 = 0) \Psi(\mathbf{x}', t_0 = 0), \quad (3.1)$$

with the number of DOFs N and the initial time being set to zero. Several approaches for the numerical propagation of the wave function exist, among which the most famous one probably is the split-operator method (SPO) [30]. It has become a standard procedure for a number of systems with few DOFs (e.g. [79]). However, as soon as the observed system becomes larger with several DOFs, the SPO fails due to an exponential scaling of the computational effort with the number of DOFs.

For larger quantum systems, i.e. many-body systems, one has to resort to well-known approaches, like the multi-configuration time-dependent Hartree(-Fock) method [31, 80, 81] as well as the time-dependent density functional theory [82]. Nevertheless, in both approaches approximations have to be made. In the former method, one has to make assumptions for the wave function. The latter method is based on an effective, so-called Kohn-Sham, potential, which consists of some external, a Coulomb and an exchange-correlation potential. The exchange-correlation potential is unknown and thus has to be approximated.

In contrast, semiclassical approximations are in a different spirit in the sense that the approximation consists in a truncation of an \hbar -expansion of the propagator. Besides their capability of treating quantum systems with a large number of DOFs, semiclassical methods can help to obtain a better understanding of quantum dynamics in terms of classical mechanics, since the underlying physics is based on classically propagated trajectories. However, in contrast to purely classical methods, these classical trajectories carry phase information and can thus interfere with each other. Hence, semiclassical methods contain so-called soft quantum effects, i.e. wave mechanics including interferences. Indeed, hard quantum effects, like tunneling, are not fully included, but there are attempts to approach this issue via multiple-spawning of trajectories [83] or propagation in imaginary time [84]. However, since in this work no tunneling problems are considered, the focus is on real-time propagation without trajectory-spawning.

In this chapter, first some well-established semiclassical initial value methods will be presented, that are widely used for numerical computations. They are the starting points for the new approach discussed in the second section: an extension of the SCHD to the density matrix propagation in the case of finite temperatures.

3.1 Semiclassical Initial Value Representations

A semiclassical approximation of the quantum mechanical propagator was first found by Van Vleck [32] and extended by Gutzwiller [33]

$$K^{\text{VVG}}(\mathbf{x}, t; \mathbf{x}', 0) = (2\pi\hbar)^{-N/2} \sum_k \left\{ \det \left[\frac{\partial \mathbf{x}}{\partial \mathbf{p}'_k} \right] \right\}^{-1/2} \exp \left\{ \frac{i}{\hbar} S_k(\mathbf{x}, \mathbf{x}', t) - i\pi \frac{\nu_k}{2} \right\}, \quad (3.2)$$

where the sum runs over all *classical* trajectories going from \mathbf{x}' to \mathbf{x} in time t . The propagator contains the classical action S_k and the so called Maslov index ν_k which counts the number of caustics of every trajectory, i.e., the points, where $\det |\partial \mathbf{x} / \partial \mathbf{p}'_k| = 0$. A typical derivation of this Van Vleck-Gutzwiller (VVG) propagator is based on the expansion of the action functional in the exponent of the Feynman path integral to second order within a stationary phase approximation (see e.g. [85]).

However, besides the problem of the singularity of the VVG propagator at a caustic, another numerical challenge comes along, which is the root search in order to solve the boundary value problem in Eq. (3.2). In particular the latter issue is avoided by semiclassical initial value representations (SC-IVRs) making them convenient tools for practical numerical applications.

In this section, two SC-IVRs, the well-established Herman-Kluk (HK) propagator and the thawed Gaussian wave packet dynamics (TGWD), will be reviewed, since both methods are basis of SCHD. Furthermore the linearized semiclassical initial value representation (LSC-IVR) will be discussed, which later on will be used for the numerical calculations of the classical results for reasons of comparison.

3.1.1 Herman-Kluk Propagator

Being a prominent representative of SC-IVRs, the HK approach is now going to be presented. Based on the VVG propagator and on the propagation of multiple Gaussians with fixed width (so called “Frozen Gaussians”), originally developed by Heller [36], the HK propagator has first been derived by Herman and Kluk [38] in 1984 but fell into oblivion afterwards. Then in 1994 the HK SC-IVR was rediscovered, when it was found to be a very efficient special case of a general SC-IVR formalism developed by Kay [37], and since then it has become a widely accepted method.

For a system with N DOFs the corresponding propagator is given by

$$K^{\text{HK}}(\mathbf{x}, t; \mathbf{x}', 0) = \int \frac{d^N q d^N p}{(2\pi\hbar)^N} \langle \mathbf{x} | g_\gamma(\mathbf{q}_t, \mathbf{p}_t) \rangle \sqrt{\det[\mathbf{h}(\mathbf{q}, \mathbf{p}, t)]} e^{iS/\hbar} \langle g_\gamma(\mathbf{q}, \mathbf{p}) | \mathbf{x}' \rangle. \quad (3.3)$$

Its main ingredients are coherent states, which are normalized Gaussian wave packets in position representation

$$\langle \mathbf{x} | g_\gamma(\mathbf{q}, \mathbf{p}) \rangle = \left(\frac{\det(\gamma)}{\pi^N} \right)^{1/4} \exp \left\{ -\frac{1}{2} (\mathbf{x} - \mathbf{q})^T \gamma (\mathbf{x} - \mathbf{q}) + \frac{i}{\hbar} \mathbf{p}^T \cdot (\mathbf{x} - \mathbf{q}) \right\}, \quad (3.4)$$

with a constant, real, positive definite and diagonal width parameter matrix γ . The integration is performed over phase space points which serve as initial conditions of classical trajectories ($\mathbf{p}_t = \mathbf{p}(\mathbf{q}, \mathbf{p}, t)$, $\mathbf{q}_t = \mathbf{q}(\mathbf{q}, \mathbf{p}, t)$). Furthermore classical mechanics comes into play via the classical action

$$S = S(\mathbf{q}, \mathbf{p}, t) = \int_0^t \mathcal{L} dt', \quad (3.5)$$

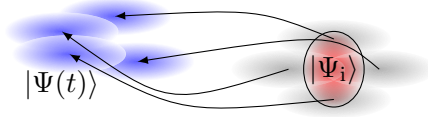


Figure 3.1: Sketch of the semiclassical propagation according to Herman and Kluk; **Red**: initial wave packet $|\Psi_i\rangle$, **Black**: coherent states at initial phase space points, **Blue**: coherent states at final phase space points forming the final wave function $|\Psi(t)\rangle$

with the Lagrangian $\mathcal{L} = \mathcal{T} - \mathcal{V}$.

The matrix in the determinantal prefactor, which goes back to the original work of Herman and Kluk, is given in a slightly generalized form by [52, 51]

$$\mathbf{h}(\mathbf{q}, \mathbf{p}, t) = \frac{1}{2} \left(\mathbf{m}_{11} + \gamma \mathbf{m}_{22} \gamma^{-1} - i\hbar \gamma \mathbf{m}_{21} + \frac{i}{\hbar} \mathbf{m}_{12} \gamma^{-1} \right). \quad (3.6)$$

It ensures the propagator's unitarity in the stationary phase sense [86] and consists of elements of the so-called monodromy (or stability) matrix,

$$\mathbf{M} = \begin{pmatrix} \mathbf{m}_{11} & \mathbf{m}_{12} \\ \mathbf{m}_{21} & \mathbf{m}_{22} \end{pmatrix} = \begin{pmatrix} \frac{\partial \mathbf{p}_t}{\partial \mathbf{p}} & \frac{\partial \mathbf{p}_t}{\partial \mathbf{q}} \\ \frac{\partial \mathbf{q}_t}{\partial \mathbf{p}} & \frac{\partial \mathbf{q}_t}{\partial \mathbf{q}} \end{pmatrix}. \quad (3.7)$$

This matrix describes the time evolution of the dependence of a classical trajectory on its initial conditions and can be obtained by solving linearized Hamilton equations as explained in Appendix B. An even more general expression for the prefactor in Eq. (3.6) can be found in [87]. In principle, a wave function propagated with the semiclassical propagator described by Eq. (3.3) can be regarded as a sum of Gaussians centered around the final points of classically propagated trajectories. Each of these Gaussians is weighted by the overlap of the initial wave function and Gaussians located at the corresponding initial phase space points. Furthermore, they carry a phase governed by the classical action (see also Fig. 3.1).

Indeed the propagator in Eq. (3.3) is semiclassical insofar, as it is related to the original VVG propagator [32, 33] via stationary phase approximation [88]. Moreover, the HK expression is more accurate, since it is uniform, i.e. it becomes exact as $\hbar \rightarrow 0$ uniformly. This goes along with the advantage that one does not have to struggle with caustics as it is the case for the VVG approximation. As an aside, the problem of counting these caustics in order to obtain the right Maslov index in the VVG propagator is replaced by ensuring the continuity of the determinantal complex square root of Eq. (3.6) by switching between both Riemann surfaces appropriately while propagating each trajectory.

So far the theory is formulated in terms of wave functions. In density formalism the corresponding semiclassical approximation to the general solution of the von-Neumann equation is

$$\rho(\mathbf{x}, \mathbf{x}'; t) = \int d\mathbf{x}'' d\mathbf{x}''' K(\mathbf{x}, t; \mathbf{x}'', 0) \rho(\mathbf{x}'', \mathbf{x}'''; 0) K^*(\mathbf{x}', t; \mathbf{x}''', 0). \quad (3.8)$$

However, since in this thesis the focus is on typical system-environment setups, the appropriate quantity to consider henceforth is the reduced density matrix, where only the

explicit dynamics of the SOI (with the coordinate vector \mathbf{s}) is left. Using Eq. (2.4) together with (3.8) and (3.3) and considering the circumstance that the Gaussian form of the HK propagator allows for an analytic calculation of the partial trace, we finally obtain a semiclassical expression for the reduced density matrix of a N -dimensional overall system

$$\begin{aligned} \rho_S(\mathbf{s}, \mathbf{s}'; t) = & \int \frac{d^N p d^N q d^N p' d^N q'}{(2\pi\hbar)^{2N}} \sqrt{\det[\mathbf{h}^*(\mathbf{q}', \mathbf{p}', t) \mathbf{h}(\mathbf{q}, \mathbf{p}, t)]} e^{i(S-S')/\hbar} \\ & \times \langle g_{\gamma_B}(\mathbf{q}'_{B,t}, \mathbf{p}'_{B,t}) | g_{\gamma_B}(\mathbf{q}_{B,t}, \mathbf{p}_{B,t}) \rangle \langle g_{\gamma_S}(\mathbf{q}'_{S,t}, \mathbf{p}'_{S,t}) | \mathbf{s}' \rangle \\ & \times \langle \mathbf{s} | g_{\gamma_S}(\mathbf{q}_{S,t}, \mathbf{p}_{S,t}) \rangle \langle g_{\gamma}(\mathbf{q}, \mathbf{p}) | \hat{\rho}(0) | g_{\gamma}(\mathbf{q}', \mathbf{p}') \rangle, \end{aligned} \quad (3.9)$$

with the initial density operator $\hat{\rho}(0)$ and the width parameter matrix divided into system and bath related submatrices γ_S and γ_B , respectively. We note, that S and S' is the action of the overall system. Also, the labels “S” and “B” denote the subvectors for the system and the environmental DOFs. Furthermore we note in passing, that the overlap of two coherent states $\langle g_{\gamma_B}(\mathbf{q}'_{B,t}, \mathbf{p}'_{B,t}) | g_{\gamma_B}(\mathbf{q}_{B,t}, \mathbf{p}_{B,t}) \rangle$ can be calculated analytically (see next subsection). Although the integration over phase space is usually performed by a Monte-Carlo procedure [89], the computational effort for the calculation of the $4N$ -dimensional integral in Eq. (3.9) is still formidable.

3.1.2 Thawed Gaussian Wave Packet Dynamics

Knowing that the multi-trajectory approach can become computationally enormously costly, another semiclassical method, based on the propagation of only a single trajectory and thus involving a smaller computational effort, is now going to be sketched in this section. This single-trajectory approach, known as TGWD, was introduced by Heller [35, 56] and can directly be derived from the HK wave function. If the initial wave function in Eq. (3.1) is a Gaussian wave packet (GWP), a distinct advantage of the HK propagator becomes manifest. Let $\Psi_\alpha(\mathbf{x}, 0)$ be a Gaussian centered around $(\mathbf{q}_\alpha, \mathbf{p}_\alpha)$ with the width parameter matrix γ_α . Then the integration over \mathbf{x}' in Eq. (3.1) can be performed analytically and the overlap of $\Psi_\alpha(\mathbf{x}, 0)$ with the coherent state centered around (\mathbf{q}, \mathbf{p}) in Eq. (3.3) reads

$$\begin{aligned} & \langle g_{\gamma}(\mathbf{q}, \mathbf{p}) | \Psi_\alpha(0) \rangle \\ &= \int d^N \mathbf{x}' \langle g_{\gamma}(\mathbf{q}, \mathbf{p}) | \mathbf{x}' \rangle \langle \mathbf{x}' | \Psi_\alpha(0) \rangle \\ &= 4^{N/4} \frac{\det(\gamma\gamma_\alpha)^{1/4}}{\sqrt{\det(\gamma + \gamma_\alpha)}} \exp \left\{ -\frac{\gamma\gamma_\alpha}{2} (\gamma + \gamma_\alpha)^{-1} (\mathbf{q} - \mathbf{q}_\alpha)^2 \right. \\ & \quad \left. - \frac{1}{2\hbar^2} (\gamma + \gamma_\alpha)^{-1} (\mathbf{p} - \mathbf{p}_\alpha)^2 + \frac{i}{\hbar} (\gamma + \gamma_\alpha)^{-1} (\mathbf{q} - \mathbf{q}_\alpha) (\gamma_\alpha \mathbf{p} + \gamma \mathbf{p}_\alpha) \right\} \\ &= \exp \left\{ -\frac{1}{4} (\mathbf{q} - \mathbf{q}_\alpha)^T \gamma (\mathbf{q} - \mathbf{q}_\alpha) - \frac{1}{4\hbar^2} (\mathbf{p} - \mathbf{p}_\alpha)^T \gamma^{-1} (\mathbf{p} - \mathbf{p}_\alpha) \right. \\ & \quad \left. + \frac{i}{2\hbar} (\mathbf{q} - \mathbf{q}_\alpha)^T \cdot (\mathbf{p} + \mathbf{p}_\alpha) \right\}, \end{aligned} \quad (3.10)$$

assuming that both Gaussians have the same width parameter matrix, i.e. $\gamma = \gamma_\alpha$. The more general case can also be dealt with analytically but leads to a less transparent final result. Now the HK propagator as applied to a Gaussian wave packet can be approximated

in a simple fashion by expanding the exponent in the resulting phase space integral around the initial wave packet center $(\mathbf{q}_\alpha, \mathbf{p}_\alpha)$ up to second order. The integration in Eq. (3.3) can then be performed analytically via Gaussian integration [55], yielding

$$\begin{aligned} \Psi_\alpha(\mathbf{x}, t) = & \left(\frac{\det(\gamma)}{\pi^N} \right)^{1/4} \det(\mathbf{m}_{22} + i\hbar \mathbf{m}_{21} \gamma)^{-1/2} \\ & \times \exp \left\{ -\frac{1}{2} (\mathbf{x} - \mathbf{q}_{\alpha,t})^T (\mathbf{m}_{11} \gamma + \frac{1}{i\hbar} \mathbf{m}_{12}) (\mathbf{m}_{22} + i\hbar \mathbf{m}_{21} \gamma)^{-1} (\mathbf{x} - \mathbf{q}_{\alpha,t}) \right. \\ & \left. + \frac{i}{\hbar} \mathbf{p}_{\alpha,t}^T \cdot (\mathbf{x} - \mathbf{q}_{\alpha,t}) + \frac{i}{\hbar} S(\mathbf{p}_\alpha, \mathbf{q}_\alpha, t) \right\}, \end{aligned} \quad (3.11)$$

where $\mathbf{p}_{\alpha,t} = \mathbf{p}(\mathbf{q}_\alpha, \mathbf{p}_\alpha, t)$ and $\mathbf{q}_{\alpha,t} = \mathbf{q}(\mathbf{q}_\alpha, \mathbf{p}_\alpha, t)$.

A full and more detailed derivation of the TGWD from the HK propagator than in [55] is given in Appendix C. It should be emphasized that, in contrast to the HK-expression (3.3), this expression is given in terms of just one single trajectory with initial conditions according to the mean position of the initial Gaussian. The Gaussian form of the wave packet is retained throughout the propagation, only the position and the width change in time. In addition, it is exact for potentials that are at most quadratic [56]. However, due to the additional approximation which was applied to obtain Eq. (3.11), the TGWD is obviously less accurate than the HK approximation applied to an initial GWP.

3.1.3 Linearized Semiclassical Initial Value Representation

In order to be able to compare the semiclassical results with a classical counterpart, the LSC-IVR will now be briefly introduced and appropriately adapted for the purpose of this work. The starting point is a general time-correlation function of the form

$$C_{AB}(t) = \text{tr} \left[\hat{A} e^{i\hat{\mathcal{H}}t/\hbar} \hat{B} e^{-i\hat{\mathcal{H}}t/\hbar} \right]. \quad (3.12)$$

The operator \hat{A} represents the initial state, whereas the projection operator \hat{B} defines the measure of interest.

By using a form of the semiclassical evolution operator different from the HK expression [90], expanding the exponent to second order and integrating over the difference variables of the forward and backward trajectories, one obtains an expression for the LSC-IVR of the time-correlation function [91]

$$\tilde{C}_{AB}(t) = \iint \frac{d^N q d^N p}{(2\pi\hbar)^N} A^w(\mathbf{p}, \mathbf{q}) B^w(\mathbf{p}_t, \mathbf{q}_t), \quad (3.13)$$

with the Wigner transform A^w and B^w . Since the Wigner transforms are real functions, the expression for the time-correlation function in Eq. (3.13) does not contain any phases and thus no interference terms. Hence, this method can be regarded as a classical Wigner method.

As stated before, the interesting observable is the reduced density, here for a one-dimensional SOI, with the initial state being a product of a Gaussian state for the SOI (centered around (q_α, p_α)) and a thermal state for the bath DOFs. Consequently the operators in Eq. (3.12) are chosen to be

$$\hat{A} = \rho(0) = |\Psi_\alpha\rangle\langle\Psi_\alpha| \frac{e^{-\beta\hat{\mathcal{H}}_B}}{Z_B} \quad (3.14)$$

$$\hat{B} = |s\rangle\langle s|, \quad (3.15)$$

where $|s\rangle$ is the eigenvector of the SOI coordinate.

For \hat{A} this yields the corresponding Wigner transform

$$\begin{aligned} A^w &= \int d^N \zeta \, e^{-i\mathbf{p} \cdot \boldsymbol{\zeta} / \hbar} \left\langle \mathbf{q} + \frac{\boldsymbol{\zeta}}{2} \left| \hat{A} \right| \mathbf{q} - \frac{\boldsymbol{\zeta}}{2} \right\rangle \\ &= \int d\zeta_s \, e^{-ip_s \zeta_s / \hbar} \left\langle q_s + \frac{\zeta_s}{2} \left| \Psi_\alpha \right\rangle \left\langle \Psi_\alpha \right| q_s - \frac{\zeta_s}{2} \right\rangle \\ &\quad \times \prod_{i=1}^{N_B} \int d\zeta_i \, e^{-ip_i \zeta_i} \left\langle q_i + \frac{\zeta_i}{2} \left| \frac{e^{-\beta\hat{\mathcal{H}}_b^{(i)}}}{Z_b^{(i)}} \right| q_i - \frac{\zeta_i}{2} \right\rangle \\ &= \int d\zeta_s \, \sqrt{\frac{\gamma_s}{\pi}} \exp \left\{ -\frac{\gamma_s}{4} \left(\zeta_s + \frac{2i}{\hbar} (p_\alpha - p_s) \right)^2 - \gamma_s (q_\alpha - q_s)^2 - \frac{1}{\gamma_s \hbar^2} (p_\alpha - p_s)^2 \right\} \\ &\quad \times \prod_{i=1}^{N_B} \int d\zeta_i \, \exp \left\{ -\frac{\omega_i}{4\hbar \tanh(\frac{\omega_i \beta \hbar}{2})} \zeta_i^2 \right. \\ &\quad \left. - \frac{i}{\hbar} p_i \zeta_i - \frac{\omega_i}{\hbar} \tanh \left(\frac{\omega_i \beta \hbar}{2} \right) q_i^2 \right\} \sqrt{\frac{\omega_i}{\pi \hbar} \tanh \left(\frac{\omega_i \beta \hbar}{2} \right)} \\ &= 2^N \exp \left\{ -\frac{1}{\gamma_s \hbar^2} (p_s - p_\alpha)^2 - \gamma_s (q_s - q_\alpha)^2 \right\} \\ &\quad \times \prod_{i=1}^{N_B} \tanh \left(\frac{\omega_i \beta \hbar}{2} \right) \exp \left\{ -\tanh \left(\frac{\omega_i \beta \hbar}{2} \right) \left[\frac{1}{\hbar \omega_i} p_i^2 + \frac{\omega_i}{\hbar} q_i^2 \right] \right\}, \end{aligned} \quad (3.16)$$

where the thermal density matrix for a harmonic oscillator from Eq. (2.30) has been used. The second Wigner transform for \hat{B} reads

$$\begin{aligned} B^w &= \int d^N \zeta \, e^{-i\mathbf{p} \cdot \boldsymbol{\zeta} / \hbar} \left\langle \mathbf{q}_t + \frac{\boldsymbol{\zeta}}{2} \left| \hat{B} \right| \mathbf{q}_t - \frac{\boldsymbol{\zeta}}{2} \right\rangle = \int d^N \zeta \, e^{-i\mathbf{p} \cdot \boldsymbol{\zeta} / \hbar} \left\langle \mathbf{q}_t + \frac{\boldsymbol{\zeta}}{2} \left| s \right\rangle \left\langle s \right| \mathbf{q}_t - \frac{\boldsymbol{\zeta}}{2} \right\rangle \\ &= \int d\zeta_s \, e^{-ip_{s,t} \zeta_s / \hbar} \left\langle q_{s,t} + \frac{\zeta_s}{2} \left| s \right\rangle \left\langle s \right| q_{s,t} - \frac{\zeta_s}{2} \right\rangle \prod_{i=1}^{N_B} \int d\zeta_i \, e^{-ip_{i,t} \zeta_i / \hbar} \underbrace{\left\langle q_{i,t} + \frac{\zeta_i}{2} \left| q_{i,t} - \frac{\zeta_i}{2} \right\rangle}_{\delta(\zeta_i)} \\ &= \int d\zeta_s \, e^{-ip_{s,t} \zeta_s / \hbar} \delta \left(q_{s,t} + \frac{\zeta_s}{2} - s \right) \delta \left(q_{s,t} - \frac{\zeta_s}{2} - s \right) \\ &= \lim_{\epsilon \rightarrow 0} \frac{1}{2\pi\epsilon} \int d\zeta_s \, e^{-ip_{s,t} \zeta_s / \hbar} \exp \left\{ -\frac{1}{2\epsilon} \left[\frac{\zeta_s}{2} - (s - q_{s,t}) \right]^2 \right\} \exp \left\{ -\frac{1}{2\epsilon} \left[\frac{\zeta_s}{2} + (s - q_{s,t}) \right]^2 \right\} \\ &= \lim_{\epsilon \rightarrow 0} \sqrt{\frac{1}{\pi\epsilon}} \exp \left\{ -\frac{(q_{s,t} - s)^2}{\epsilon} - \frac{\epsilon p_{s,t}^2}{\hbar} \right\} = \delta(q_{s,t} - s), \end{aligned} \quad (3.17)$$

with the SOI position of the classically propagated trajectory.

Hence we obtain a LSC-IVR expression for the reduced density

$$\begin{aligned} \tilde{C}_{AB}(t) = \rho(s; t) = & \frac{1}{(\pi\hbar)^N} \prod_{i=1}^{N_B} \tanh\left(\frac{\omega_i\beta\hbar}{2}\right) \int d^N p d^N q \delta(q_{S,t} - s) \\ & \times e^{-1/(\gamma_S\hbar^2)(p_S-p_\alpha)^2 - \gamma_S(q_S-q_\alpha)^2} \prod_{i=1}^{N_B} e^{-\tanh(\omega_i\beta\hbar/2)/\hbar[(1/\omega_i)p_i^2 + \omega_i q_i^2]}. \end{aligned} \quad (3.18)$$

Indeed, the $2N$ -dimensional phase space integral still needs to be performed numerically. However, the integral in the LSC-IVR integral converges faster than the one in the HK expression. The main reason for this is not the lower dimensionality of the integral but rather the fact that this expression does not convey any phase information and thus the integrand is non-oscillating. Basically, it is a classical time evolution of a probability distribution, which, however, does not capture any interference effects as will be seen later. As an aside, for the numerical computation of the phase space integral, the delta distribution in Eq. (3.18) has to be approximated by a sufficiently narrow Gaussian, such that the result is independent on the Gaussian width parameter.

3.2 Semiclassical Hybrid Dynamics for Systems in a Thermal Bath

Based on the semiclassical approximations presented in the previous section, i.e. the HK method and the TGWD, the SCHD for the density matrix propagation can now be derived. Originally this was done for wave functions [55]. Here, within a reduced density matrix formalism, the SCHD is extended in such a way that systems interacting with thermal CL baths are considered.

We start with the initial density operator, which is assumed to be factorizable into a system ($\hat{\rho}_S$) and a bath part ($\hat{\rho}_B$) as introduced in Eq. (2.26). As a generalization, which will be needed later in this thesis, the initial density operator contribution $\hat{I}_{\alpha,\alpha'}^S = |\Psi_\alpha\rangle\langle\Psi_{\alpha'}|$ for the SOI is an outer product of two Gaussians generally located at two different phase space points labeled with the indices α and α' .

Thus, using Eq. (3.8) together with Eq. (3.3), the HK expression for the full density matrix contribution can be written as

$$\begin{aligned} I_{\alpha,\alpha'}(\mathbf{x}, \mathbf{x}'; t) = & \int \frac{d^N p d^N q d^N p' d^N q'}{(2\pi\hbar)^{2N}} \sqrt{\det[\mathbf{h}(\mathbf{h}')^*]} e^{i(S-S')/\hbar} \langle \mathbf{x} | g_\gamma(\mathbf{q}_t, \mathbf{p}_t) \rangle \langle g_\gamma(\mathbf{q}'_t, \mathbf{p}'_t) | \mathbf{x}' \rangle \\ & \times \langle g_{\gamma_S}(\mathbf{q}_S, \mathbf{p}_S) | \Psi_\alpha \rangle \langle \Psi_{\alpha'} | g_{\gamma_S}(\mathbf{q}'_S, \mathbf{p}'_S) \rangle \left\langle g_{\gamma_B}(\mathbf{q}_B, \mathbf{p}_B) \left| \frac{e^{-\beta\hat{H}_B}}{Z_B} \right| g_{\gamma_B}(\mathbf{q}'_B, \mathbf{p}'_B) \right\rangle, \end{aligned} \quad (3.19)$$

where again “S” and “B” denote the SOI and the bath subvectors, respectively, and the width parameter matrix is sub-divided

$$\gamma = \begin{pmatrix} \gamma_S & \mathbf{0} \\ \mathbf{0} & \gamma_B \end{pmatrix} \quad (3.20)$$

into a $N_S \times N_S$ system and $N_B \times N_B$ bath submatrix, γ_S and γ_B . The thermal density operator in coherent state representation, as derived in Section 2.3.2, reads

$$\begin{aligned}
 & \left\langle g_{\gamma_B}(\mathbf{q}_B, \mathbf{p}_B) \left| \frac{e^{-\beta \hat{H}_B}}{Z_B} \right| g_{\gamma_B}(\mathbf{q}'_B, \mathbf{p}'_B) \right\rangle \\
 &= \tilde{Z} \exp \left\{ -\frac{1}{4}(\mathbf{q}_B^T \gamma_B \mathbf{q}_B + \mathbf{q}'_B^T \gamma_B \mathbf{q}'_B) - \frac{1}{4\hbar^2}(\mathbf{p}_B^T \gamma_B^{-1} \mathbf{p}_B + \mathbf{p}'_B^T \gamma_B^{-1} \mathbf{p}'_B) + \frac{i}{2\hbar}(\mathbf{p}_B \mathbf{q}_B - \mathbf{p}'_B \mathbf{q}'_B) \right. \\
 &\quad \left. + \frac{1}{2} \left(\gamma_B \mathbf{q}_B - \frac{i}{\hbar} \mathbf{p}_B \right)^T e^{-\beta \gamma_B \hbar^2} \left(\mathbf{q}'_B + \frac{i}{\hbar} \gamma_B^{-1} \mathbf{p}'_B \right) \right\} \\
 &\equiv \tilde{Z} K(\mathbf{p}_B, \mathbf{q}_B, \mathbf{p}'_B, \mathbf{q}'_B) \equiv \tilde{Z} K_B
 \end{aligned} \tag{3.21}$$

with the prefactor $\tilde{Z} \equiv \prod_{i=1}^{N_B} (1 - e^{-\beta \omega_i \hbar})$ and the choice $\gamma_B = \boldsymbol{\omega}_B / \hbar$, where $\boldsymbol{\omega}_B$ is a diagonal matrix consisting of all bath mode frequencies.

The central idea of the derivation of the hybrid approximation now arises. Instead of expanding the exponent in Eq. (3.21) to second order for *all* DOFs as it is done in the derivation of the TGWD from the HK approximation (see Appendix C), the expansion is performed only for a part, i.e. N_{tg} DOFs. The corresponding expansion of the action is then

$$\begin{aligned}
 S(\mathbf{q}, \mathbf{p}, t) = & S[(\mathbf{q}_{\text{hk}}, \mathbf{0}), (\mathbf{p}_{\text{hk}}, \mathbf{0}), t] + \mathbf{p}_{\alpha,t}^T \tilde{\mathbf{m}}_{21} \mathbf{p}_{\text{tg}} + \mathbf{p}_{\alpha,t}^T \tilde{\mathbf{m}}_{22} \mathbf{q}_{\text{tg}} + \frac{1}{2} \mathbf{p}_{\text{tg}}^T \tilde{\mathbf{m}}_{11}^T \tilde{\mathbf{m}}_{21} \mathbf{p}_{\text{tg}} \\
 & + \frac{1}{2} \mathbf{q}_{\text{tg}}^T \tilde{\mathbf{m}}_{12}^T \tilde{\mathbf{m}}_{22} \mathbf{q}_{\text{tg}} + \frac{1}{2} \mathbf{p}_{\text{tg}}^T \tilde{\mathbf{m}}_{21}^T \tilde{\mathbf{m}}_{12} \mathbf{q}_{\text{tg}},
 \end{aligned} \tag{3.22}$$

where $\tilde{\mathbf{m}}_{ij}$ are now $N \times N_{\text{tg}}$ matrices consisting of the derivatives with respect to variables carrying the label “tg” only, assuming that these DOFs are part of the bath DOFs solely. On the other hand, the label “hk” denotes the DOFs that are excluded from this expansion. Additionally, the final phase space points are expanded, yielding

$$\begin{aligned}
 \mathbf{p}_t &\approx \mathbf{p}_{\alpha,t} + \delta \mathbf{p}_t \\
 &= \mathbf{p}_{\alpha,t} + \tilde{\mathbf{m}}_{11} \mathbf{p}_{\text{tg}} + \tilde{\mathbf{m}}_{12} \mathbf{q}_{\text{tg}}
 \end{aligned} \tag{3.23}$$

$$\begin{aligned}
 \mathbf{q}_t &\approx \mathbf{q}_{\alpha,t} + \delta \mathbf{q}_t \\
 &= \mathbf{q}_{\alpha,t} + \tilde{\mathbf{m}}_{21} \mathbf{p}_{\text{tg}} + \tilde{\mathbf{m}}_{22} \mathbf{q}_{\text{tg}},
 \end{aligned} \tag{3.24}$$

with $\mathbf{q}_{\alpha,t} = \mathbf{q}[(\mathbf{q}_{\text{hk}}, \mathbf{0}), (\mathbf{p}_{\text{hk}}, \mathbf{0}), t]$ and $\mathbf{p}_{\alpha,t} = \mathbf{p}[(\mathbf{q}_{\text{hk}}, \mathbf{0}), (\mathbf{p}_{\text{hk}}, \mathbf{0}), t]$.

Within this expansion, the part of the phase space integral carrying the label “tg” in Eq. (3.19) becomes a multidimensional Gaussian integral, which can be performed analytically using the general formula in Eq. (2.36). In doing so, we obtain the hybrid density matrix

contribution

$$\begin{aligned}
 I_{\alpha,\alpha'}(\mathbf{x}, \mathbf{x}'; t) &= \int \frac{d^N p d^N q d^N p' d^N q'}{(2\pi\hbar)^{2N}} \sqrt{\det[\mathbf{h}(\mathbf{h}')^*]} \tilde{Z} \\
 &\quad \times \langle g_{\gamma_S}(\mathbf{q}_S, \mathbf{p}_S) | \Psi_\alpha \rangle \langle \Psi_{\alpha'} | g_{\gamma_S}(\mathbf{q}'_S, \mathbf{p}'_S) \rangle K_{\text{hb}} \\
 &\quad \times \exp \left\{ -(\mathbf{p}_{\text{tg}}, \mathbf{q}_{\text{tg}}, \mathbf{p}'_{\text{tg}}, \mathbf{q}'_{\text{tg}}) \mathbf{A} (\mathbf{p}_{\text{tg}}, \mathbf{q}_{\text{tg}}, \mathbf{p}'_{\text{tg}}, \mathbf{q}'_{\text{tg}})^T + \mathbf{b}^T \cdot (\mathbf{p}_{\text{tg}}, \mathbf{q}_{\text{tg}}, \mathbf{p}'_{\text{tg}}, \mathbf{q}'_{\text{tg}})^T \right. \\
 &\quad \left. + \frac{i}{\hbar} (S - S') \right\} \langle g_{\gamma}(\mathbf{q}'_{\alpha',t}, \mathbf{p}'_{\alpha',t}) | \mathbf{x}' \rangle \langle \mathbf{x} | g_{\gamma}(\mathbf{q}_{\alpha,t}, \mathbf{p}_{\alpha,t}) \rangle \\
 &= \int \frac{d^{N_{\text{hk}}} p_{\text{hk}} d^{N_{\text{hk}}} q_{\text{hk}} d^{N_{\text{hk}}} p'_{\text{hk}} d^{N_{\text{hk}}} q'_{\text{hk}}}{(2\hbar)^{2N} \pi^{2N_{\text{hk}}}} \tilde{Z} \sqrt{\frac{\det[\mathbf{h}(\mathbf{h}')^*]}{\det(\mathbf{A})}} \\
 &\quad \times \langle g_{\gamma_S}(\mathbf{q}_S, \mathbf{p}_S) | \Psi_\alpha \rangle \langle \Psi_{\alpha'} | g_{\gamma_S}(\mathbf{q}'_S, \mathbf{p}'_S) \rangle \exp \left\{ \frac{1}{4} \mathbf{b}^T \mathbf{A}^{-1} \mathbf{b} + \frac{i}{\hbar} (S - S') \right\} K_{\text{hb}} \\
 &\quad \langle g_{\gamma}(\mathbf{q}'_{\alpha',t}, \mathbf{p}'_{\alpha',t}) | \mathbf{x}' \rangle \langle \mathbf{x} | g_{\gamma}(\mathbf{q}_{\alpha,t}, \mathbf{p}_{\alpha,t}) \rangle,
 \end{aligned} \tag{3.25}$$

$$\begin{aligned}
 &= \int \frac{d^{N_{\text{hk}}} p_{\text{hk}} d^{N_{\text{hk}}} q_{\text{hk}} d^{N_{\text{hk}}} p'_{\text{hk}} d^{N_{\text{hk}}} q'_{\text{hk}}}{(2\hbar)^{2N} \pi^{2N_{\text{hk}}}} \tilde{Z} \sqrt{\frac{\det[\mathbf{h}(\mathbf{h}')^*]}{\det(\mathbf{A})}} \\
 &\quad \times \langle g_{\gamma_S}(\mathbf{q}_S, \mathbf{p}_S) | \Psi_\alpha \rangle \langle \Psi_{\alpha'} | g_{\gamma_S}(\mathbf{q}'_S, \mathbf{p}'_S) \rangle \exp \left\{ \frac{1}{4} \mathbf{b}^T \mathbf{A}^{-1} \mathbf{b} + \frac{i}{\hbar} (S - S') \right\} K_{\text{hb}} \\
 &\quad \langle g_{\gamma}(\mathbf{q}'_{\alpha',t}, \mathbf{p}'_{\alpha',t}) | \mathbf{x}' \rangle \langle \mathbf{x} | g_{\gamma}(\mathbf{q}_{\alpha,t}, \mathbf{p}_{\alpha,t}) \rangle,
 \end{aligned} \tag{3.26}$$

with the notation $S \equiv S[(\mathbf{q}_{\text{hk}}, \mathbf{0}), (\mathbf{p}_{\text{hk}}, \mathbf{0}), t]$ and $S' \equiv S[(\mathbf{q}'_{\text{hk}}, \mathbf{0}), (\mathbf{p}'_{\text{hk}}, \mathbf{0}), t]$. Here, for reasons of readability, vectors are written in form of row vectors $(\mathbf{p}_{\text{tg}}, \mathbf{q}_{\text{tg}}, \mathbf{p}'_{\text{tg}}, \mathbf{q}'_{\text{tg}})$. The label “hb” denotes the DOFs of the bath which are still treated on the level of the full HK approximation, i.e. $N_{\text{B}} = N_{\text{hb}} + N_{\text{tg}}$. The term K_{hb} is defined as in Eq. (3.21) except that here only the HK bath modes are considered. Further abbreviations in Eq. (3.26) are the symmetric $4N_{\text{tg}} \times 4N_{\text{tg}}$ matrix¹

$$\mathbf{A} = \begin{pmatrix} \mathbf{A}_1 & \mathbf{A}_2 \\ \mathbf{A}_2^T & (\mathbf{A}_1')^* \end{pmatrix}, \tag{3.27}$$

where

$$\mathbf{A}_1 = \begin{pmatrix} \frac{\gamma_{\text{tg}}^{-1}}{4\hbar^2} + \frac{\tilde{\mathbf{u}}\tilde{\mathbf{m}}_{21}}{2} & \frac{i}{4\hbar} + \frac{\tilde{\mathbf{m}}_{21}^T \tilde{\mathbf{v}}^T}{2} \\ \frac{i}{4\hbar} + \frac{\tilde{\mathbf{v}}\tilde{\mathbf{m}}_{21}}{2} & \frac{\gamma_{\text{tg}}}{4} + \frac{\tilde{\mathbf{v}}\tilde{\mathbf{m}}_{22}}{2} \end{pmatrix} \quad \mathbf{A}_2 = \begin{pmatrix} -\frac{\gamma_{\text{tg}}^{-1}}{4\hbar^2} e^{-\beta\gamma_{\text{tg}}\hbar} & \frac{i}{4\hbar} e^{-\beta\gamma_{\text{tg}}\hbar} \\ -\frac{i}{4\hbar} e^{-\beta\gamma_{\text{tg}}\hbar} & -\frac{\gamma_{\text{tg}}}{4} e^{-\beta\gamma_{\text{tg}}\hbar} \end{pmatrix} \tag{3.28}$$

are $2N_{\text{tg}} \times 2N_{\text{tg}}$ matrices. The matrix \mathbf{A}_1' in Eq. (3.27) corresponds to the phase space part with variables carrying a prime, i.e. $(\mathbf{q}', \mathbf{p}')$. Furthermore the matrices

$$\tilde{\mathbf{u}} = \tilde{\mathbf{m}}_{21}^T \gamma + \frac{i}{\hbar} \tilde{\mathbf{m}}_{11}^T \quad \tilde{\mathbf{v}} = \tilde{\mathbf{m}}_{22}^T \gamma + \frac{i}{\hbar} \tilde{\mathbf{m}}_{12}^T \tag{3.29}$$

are included as well as

$$\mathbf{b}^T = \begin{pmatrix} \mathbf{x} - \mathbf{q}_{\alpha,t} \\ \mathbf{x}' - \mathbf{q}'_{\alpha',t} \end{pmatrix}^T \begin{pmatrix} [\tilde{\mathbf{u}}^T & \tilde{\mathbf{v}}^T] \\ \mathbf{0} & [(\tilde{\mathbf{u}}')^T & (\tilde{\mathbf{v}}')^T] \end{pmatrix}, \tag{3.30}$$

which is a $4N_{\text{tg}}$ -dimensional vector.

¹For reasons of clarity, it should be stressed that here the Symbol “*” in Eq. (3.27) does not denote the adjoint of a matrix but rather its complex conjugate.

Next, we have to trace over all bath modes in Eq. (3.26) in order to obtain the reduced density matrix contribution for the SOI. To begin with, the first term in the exponent in Eq. (3.26) is considered

$$\frac{1}{4}\mathbf{b}^T\mathbf{A}^{-1}\mathbf{b}\equiv\frac{1}{4}\mathbf{b}^T\begin{pmatrix}\mathbf{D}_1 & \mathbf{D}_2 \\ \mathbf{D}_2^T & \mathbf{D}_3\end{pmatrix}\mathbf{b}=\begin{pmatrix}\mathbf{x}-\mathbf{q}_{\alpha,t} \\ \mathbf{x}'-\mathbf{q}'_{\alpha',t}\end{pmatrix}^T\begin{pmatrix}\mathbf{K} & \mathbf{L} \\ \mathbf{L}^T & \mathbf{K}'\end{pmatrix}\begin{pmatrix}\mathbf{x}-\mathbf{q}_{\alpha,t} \\ \mathbf{x}'-\mathbf{q}'_{\alpha',t}\end{pmatrix}, \quad (3.31)$$

where in the last step the definition of the vector \mathbf{b} from Eq. (3.30) was used. Therefore the submatrices in the last term read

$$\begin{aligned}\mathbf{K} &\equiv \frac{1}{4}[\tilde{\mathbf{u}}^T & \tilde{\mathbf{v}}^T]\mathbf{D}_1[\tilde{\mathbf{u}}^T & \tilde{\mathbf{v}}^T]^T \\ \mathbf{L} &\equiv \frac{1}{4}[\tilde{\mathbf{u}}^T & \tilde{\mathbf{v}}^T]\mathbf{D}_2[(\tilde{\mathbf{u}}'^*)^T & (\tilde{\mathbf{v}}'^*)^T]^T \\ \mathbf{K}' &\equiv \frac{1}{4}[(\tilde{\mathbf{u}}'^*)^T & (\tilde{\mathbf{v}}'^*)^T]\mathbf{D}_3[(\tilde{\mathbf{u}}'^*)^T & (\tilde{\mathbf{v}}'^*)^T]^T.\end{aligned} \quad (3.32)$$

We emphasize that the forward and backward trajectories are coupled only via the matrix \mathbf{L} and its transpose. Also note, that \mathbf{K} is symmetric, whereas \mathbf{L} is not, except for the trivial case $\beta \rightarrow \infty$. Now in turn, these newly introduced $N \times N$ matrices are divided into submatrices

$$\mathbf{K} \equiv \begin{pmatrix} \mathbf{K}_{SS} & \mathbf{K}_{SB} \\ \mathbf{K}_{BS} & \mathbf{K}_{BB} \end{pmatrix} \quad \mathbf{L} \equiv \begin{pmatrix} \mathbf{L}_{SS} & \mathbf{L}_{SB} \\ \mathbf{L}_{BS} & \mathbf{L}_{BB} \end{pmatrix}, \quad (3.33)$$

coupling the different classes of DOFs (system and bath), e.g.

$$\begin{aligned}(\mathbf{x}-\mathbf{q}_{\alpha,t})^T\mathbf{K}(\mathbf{x}-\mathbf{q}_{\alpha,t}) &= (\mathbf{s}-\mathbf{q}_{\alpha,S,t})^T\mathbf{K}_{SS}(\mathbf{s}-\mathbf{q}_{\alpha,S,t}) + (\mathbf{y}-\mathbf{q}_{\alpha,B,t})^T\mathbf{K}_{BS}(\mathbf{s}-\mathbf{q}_{\alpha,S,t}) \\ &\quad + (\mathbf{s}-\mathbf{q}_{\alpha,S,t})^T\mathbf{K}_{SB}(\mathbf{y}-\mathbf{q}_{\alpha,B,t}) + (\mathbf{y}-\mathbf{q}_{\alpha,B,t})^T\mathbf{K}_{BB}(\mathbf{y}-\mathbf{q}_{\alpha,B,t}),\end{aligned} \quad (3.34)$$

where again, the additional indices “S” and “B” denote the subvectors for the system and bath DOFs, i.e. $\mathbf{q}_{\alpha,t} = (\mathbf{q}_{\alpha,S,t}, \mathbf{q}_{\alpha,B,t})$. After rearranging the exponent in Eq. (3.26) to a quadratic form in \mathbf{y} with a linear term, i.e. the form $\mathbf{y}^T\mathbf{H}\mathbf{y} + \mathbf{e}^T\mathbf{y} + f$, the integral over \mathbf{y} and therefore the trace over all bath modes can be performed analytically using Eq. (2.36) again. This yields an expression for the hybrid reduced density matrix contribution for a N_S -dimensional SOI

$$\begin{aligned}I_{\alpha,\alpha'}^S(\mathbf{s}, \mathbf{s}'; t) &= \int \frac{d^{N_{hk}}p_{hk} d^{N_{hk}}q_{hk} d^{N_{hk}}p'_{hk} d^{N_{hk}}q'_{hk}}{(2\hbar)^{2N} \pi^{2N_{hk}} \pi^{N_S/2}} \left(\prod_{i=1}^{N_B} (1 - e^{-\beta\omega_i\hbar}) \right) \sqrt{\frac{\det(\boldsymbol{\gamma}) \det[\mathbf{h}(\mathbf{h}')^*]}{\det(\mathbf{A}) \det(\mathbf{H})}} \\ &\quad \times \exp \left\{ \begin{pmatrix} \mathbf{s}-\mathbf{q}_{\alpha,S,t} \\ \mathbf{s}'-\mathbf{q}'_{\alpha',S,t} \end{pmatrix}^T \boldsymbol{\Lambda} \begin{pmatrix} \mathbf{s}-\mathbf{q}_{\alpha,S,t} \\ \mathbf{s}'-\mathbf{q}'_{\alpha',S,t} \end{pmatrix} + \boldsymbol{\sigma}^T \begin{pmatrix} \mathbf{s}-\mathbf{q}_{\alpha,S,t} \\ \mathbf{s}'-\mathbf{q}'_{\alpha',S,t} \end{pmatrix} + h + \frac{i}{\hbar}(S-S') \right\} \\ &\quad \times \langle g_{\gamma_S}(\mathbf{q}_S, \mathbf{p}_S) | \Psi_{\alpha} \rangle \langle \Psi_{\alpha'} | g_{\gamma_S}(\mathbf{q}'_S, \mathbf{p}'_S) \rangle K_{hb}.\end{aligned} \quad (3.35)$$

The expression consists of the $N_B \times N_B$ matrix

$$\mathbf{H} = -(\mathbf{K}_{BB} + \mathbf{K}'_{BB} + \mathbf{L}_{BB} + \mathbf{L}_{BB}^T - \boldsymbol{\gamma}_B) \quad (3.36)$$

and the symmetric $2N_s \times 2N_s$ matrix

$$\Lambda = \begin{pmatrix} \Lambda_{11} & \Lambda_{12} \\ \Lambda_{12}^T & \Lambda_{22} \end{pmatrix} = \begin{pmatrix} \mathbf{F}_{SB} \mathbf{H}^{-1} \mathbf{F}_{SB}^T - \frac{\gamma_S}{2} + \mathbf{K}_{SS} & \mathbf{F}_{SB} \mathbf{H}^{-1} \mathbf{F}_{SB}'^T + \mathbf{L}_{SS} \\ \mathbf{F}_{SB}'^T \mathbf{H}^{-1} \mathbf{F}_{SB}^T + \mathbf{L}_{SS}^T & \mathbf{F}_{SB}'^T \mathbf{H}^{-1} \mathbf{F}_{SB}'^T - \frac{\gamma_S}{2} + \mathbf{K}_{SS}' \end{pmatrix}, \quad (3.37)$$

with the abbreviations

$$\mathbf{F}_{SB} = \mathbf{K}_{SB} + \mathbf{L}_{SB} \quad \mathbf{F}_{SB}' = \mathbf{K}_{SB}' + \mathbf{L}_{BS}'^T. \quad (3.38)$$

Furthermore it contains the $2N_s$ -dimensional vector

$$\boldsymbol{\sigma} = \begin{pmatrix} \sigma_1 \\ \sigma_2 \end{pmatrix} = \begin{pmatrix} \mathbf{F}_{SB} \mathbf{H}^{-1} \mathbf{d} - 2\mathbf{K}_{BS}^T \mathbf{q}_{\alpha,B,t} - 2\mathbf{L}_{SB} \mathbf{q}'_{\alpha',B,t} + \frac{i}{\hbar} \mathbf{p}_{\alpha,S,t} \\ \mathbf{F}_{SB}'^T \mathbf{H}^{-1} \mathbf{d} - 2\mathbf{K}_{BS}'^T \mathbf{q}'_{\alpha',B,t} - 2\mathbf{L}_{BS}^T \mathbf{q}_{\alpha,B,t} - \frac{i}{\hbar} \mathbf{p}'_{\alpha',S,t} \end{pmatrix} \quad (3.39)$$

where the vector

$$\mathbf{d} = (\gamma_B - 2\mathbf{K}_{BB} - 2\mathbf{L}_{BB})^T \mathbf{q}_{\alpha,B,t} + (\gamma_B - 2\mathbf{K}_{BB}' - 2\mathbf{L}_{BB}'^T)^T \mathbf{q}'_{\alpha',B,t} + \frac{i}{\hbar} (\mathbf{p}_{\alpha,B,t} - \mathbf{p}'_{\alpha',B,t}) \quad (3.40)$$

is included. The last abbreviation is the scalar

$$\begin{aligned} h = & - \left(\mathbf{q}_{\alpha,B,t}^T \frac{\gamma_B - 2\mathbf{K}_{BB}}{2} + \frac{i}{\hbar} \mathbf{p}_{\alpha,B,t}^T \right) \cdot \mathbf{q}_{\alpha,B,t} - \left(\mathbf{q}'_{\alpha',B,t}^T \frac{\gamma_B - 2\mathbf{K}_{BB}'}{2} - \frac{i}{\hbar} \mathbf{p}'_{\alpha',B,t}^T \right) \cdot \mathbf{q}'_{\alpha',B,t} \\ & + 2\mathbf{q}_{\alpha,B,t}^T \mathbf{L}_{BB} \mathbf{q}'_{\alpha',B,t} + \frac{1}{4} \mathbf{d}^T \mathbf{H}^{-1} \mathbf{d}. \end{aligned} \quad (3.41)$$

We stress that in contrast to the full HK reduced density matrix expression in Eq. (3.9), the present one is just a $4N_{hk}$ -dimensional phase space integral. Also, the dynamics of the bath DOFs is still fully included in its expression, although they are not part of the reduced density matrix contribution. The SCHD expression in Eq. (3.35) is the method of choice for the numerical computations, whose results are presented in the next chapters.

4 Pure Decoherence

With the theoretical prerequisites in place, the SCHD will now be applied in numerical studies of various open quantum systems. Decoherence, which is also called dephasing, will be investigated first. It is a pure quantum consequence of the SOI-bath interaction. While dissipation, which may also occur in open quantum systems, changes the energy of the SOI, decoherence influences its quantum state in the sense, that it blurs the phase relations within the states. This plays an important (and usually unwanted) role in several fields of quantum theory, in particular in quantum computation, which has become a topic of high interest in the past 20 years [2, 92, 1, 93]. The fact, that the coherence of a quantum system is highly sensitive to influences from outside, makes the control and suppression of decoherence a challenging endeavor and hence a deeper understanding of this process is necessary. Dissipation, in turn, will be the topic of the next chapter and thus is ignored here in order to study the consequences of pure decoherence solely, unaltered by the effect of energetic transitions. To achieve such negligible dissipation, the bath mode frequencies have to be much smaller than the typical system frequency, so that resonant and thus effective energetic coupling is not possible.

At the beginning of this chapter decoherence in an anharmonic oscillator coupled to a finite bath is studied using the SCHD. In particular, the influence of bath and interaction parameters on the loss of coherence is investigated qualitatively as well as quantitatively. Subsequently, we focus on the long time dynamics of the anharmonic molecular oscillator resulting in a quantum phenomenon known as wave packet revivals. There, the semiclassical treatment of quantum revivals in the isolated system as well as the bath-influence on the revival dynamics will be studied. The final section of this chapter discusses dephasing in a fundamental quantum mechanics textbook experiment, namely a quantum particle propagating through a double slit. Here the coupling to the bath is slightly modified from the one in the original CL model to ensure a system-bath coupling only in the vicinity of the slit.

4.1 Vibrational Dynamics of Diatomics

The first system used for the investigation of pure decoherence effects is the Morse oscillator, whose potential is given in Eq. (2.19). Here, the parameters for the diatomic Iodine in its electronic ground state are used, i.e. $D = 0.057$ a.u., $\alpha = 0.983$ a.u., the equilibrium bond distance $s_e = 5.04$ a.u. and the reduced mass of this system $M = 1.165 \times 10^5$ a.u. (taken from Ref. [51]). Thus the frequency of the harmonic approximation is $\omega_s = \alpha \sqrt{2D/M} \approx 0.001$ a.u. implying a harmonic vibrational system period of $\tau_s \approx 156$ fs for small oscillations around the minimum. For the numerical calculations, the initial wave function is a GWP centered around $s_i = 4.53$ a.u., i.e. on the steep side of the potential, with zero momentum and the width parameter $\gamma_s = M\omega_s$ as shown in Fig. 4.1(a). Hence the initial energy expectation value is $\langle E \rangle = 0.426 D$, which is well away from the potential minimum and therefore from the area of validity of the harmonic approximation. Further snapshots of

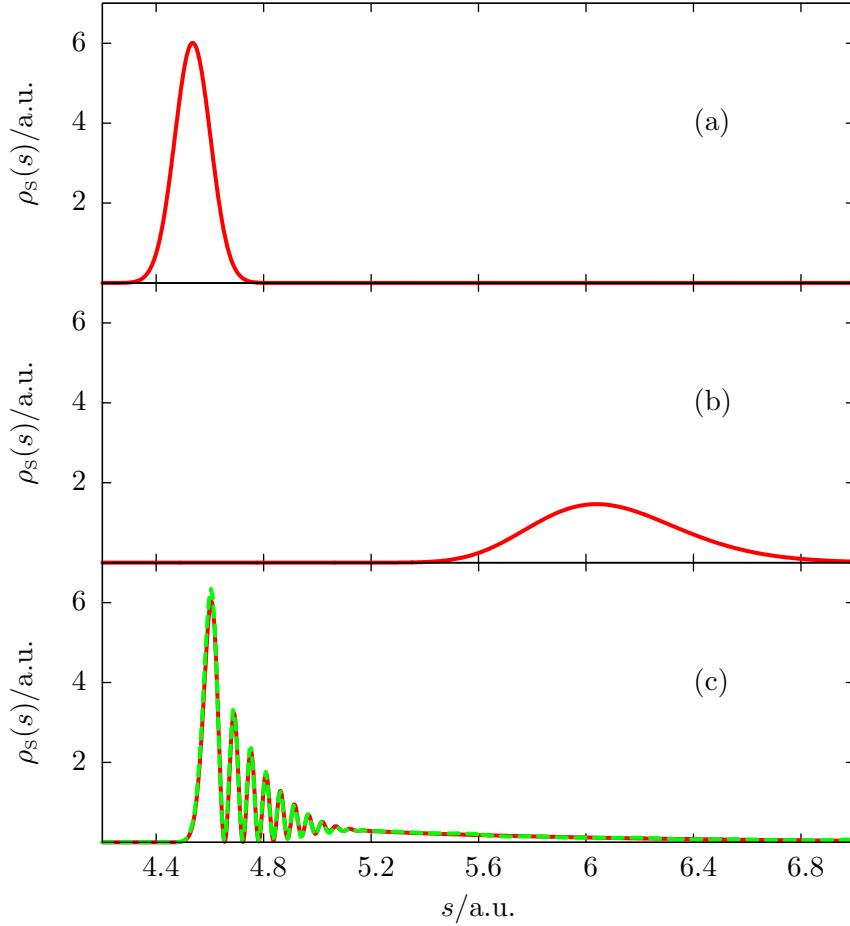


Figure 4.1: Density of a wave packet in a Morse potential at different times (full quantum results unless stated explicitly otherwise)

(a) initial GWP at time $t = 0$; (b) at time $t = 96$ fs

(c) solid (red) line: shortly before the end of the first period at time $t = 192$ fs, all quantum results; dash-dotted (green) line: semiclassical HK result at time $t = 192$ fs with 5×10^4 trajectories

the density of the wave packet are shown in Fig. 4.1 within the first vibrational period: at $t = 96$ fs, when the wave packet is softly reflected at the flat side of the potential (Fig. 4.1(b)), and at $t = 192$ fs, where an interference pattern becomes visible while a part of the wave packet is reflected (Fig. 4.1(c)). The latter time is shortly before the end of the first vibrational period since the local energy-dependent period for the given energy expectation value is

$$\tau_{\text{loc}}(\langle E \rangle) = \frac{\tau_s}{1 - \langle E \rangle / D} \approx 206 \text{ fs}. \quad (4.1)$$

All the results depicted with solid lines in Fig. 4.1 are obtained with the SPO-method [30] and thus are full quantum results. Additionally, the semiclassical HK result is plotted at $t = 192$ fs with 5×10^4 trajectories, confirming the excellent agreement with the quantum one, such that both results can hardly be distinguished. Also, this is the time, at which snapshots of the density will be considered in the next two subsections for the case of the

anharmonic oscillator coupled to a bath.

4.1.1 SCHD vs Various Semiclassical Approximations for $T=0$

So far the free Morse oscillator was investigated. Now we turn to the system coupled to a finite bath at temperature $T=0$ with a continuous spectral density, which is Ohmic with an exponential cutoff

$$J_e(\omega) = \eta\omega e^{-\omega/\omega_c}, \quad (4.2)$$

where ω_c is the cutoff frequency and η the coupling strength. The frequencies of the bath are drawn from the density of frequencies, which is chosen to be

$$\rho_f(\omega) = a \frac{J_e(\omega)}{\omega}, \quad (4.3)$$

with the normalization coefficient

$$a = \frac{N_B}{\eta\omega_c} \frac{1}{1 - e^{-\omega_{\max}/\omega_c}} \quad (4.4)$$

which is determined utilizing the normalization condition in Eq. (2.9).

The cutoff frequency is set to $\omega_c = 9.1 \times 10^{-5}$ a.u. as in Ref. [51], which is much smaller than the local system frequency $\omega_{\text{loc}}(\langle E \rangle) = 7.3 \times 10^{-4}$ a.u.. Since the maximum frequency is chosen to be $\omega_{\max} = 5\omega_c$, no resonant coupling will occur and thus dissipation will be negligible.

For the coupled system, the HK result is assumed to be in a very good agreement with the full quantum result, since the former method works excellent for every separate DOF, i.e. the Morse and harmonic oscillator, and the linear coupling between those DOFs does not significantly increase the semiclassical errors.

Therefore, it is sufficient to check the accuracy of the SCHD by comparing it with the more accurate full HK method for this coupled system. To this end, we consider a bath with only three modes. This already involves a 16-dimensional phase space integral in the HK case [see Eq. (3.9)] which has to be computed numerically. In contrast, with the SCHD only a four-dimensional integral needs to be evaluated, since the (non-resonant) bath DOFs are treated on the level of the single-trajectory approach [see Eq. (3.35)]. In Fig. 4.2 the reduced densities at time $t = 192$ fs obtained with the HK method and the SCHD are plotted for a system-bath coupling strength $\eta_{\text{eff}} = \eta/(M\omega_s) = 0.25$. Obviously, the agreement between both approximations is excellent, a difference is hardly visible. Regarding the computational effort, however, the difference is significant since 3×10^6 trajectories are necessary to obtain the HK result, whereas 2×10^4 trajectories are needed to obtain the SCHD result. In other words, the computation takes 6 h on a modern workstation in the first case and 20 minutes in the second case.

In Fig. 4.3 the SCHD is compared with two other computationally less costly classical respectively semiclassical methods, that, on the other hand, are also less accurate: the LSC-IVR, which was introduced in Section 3.1.3, and the single-trajectory pure TGWD. Still the bath consists of three bath modes and now the effective coupling strength is $\eta_{\text{eff}} = 0.05$. We stress that TGWD as well as the LSC-IVR highlight different aspects of the observed system. The TGWD contains information about the harmonicity of a bound system, since it is valid only in the harmonic regime. On the one hand the reduced density's shape is restricted to be Gaussian for all times and on the other hand the wave packet's initial

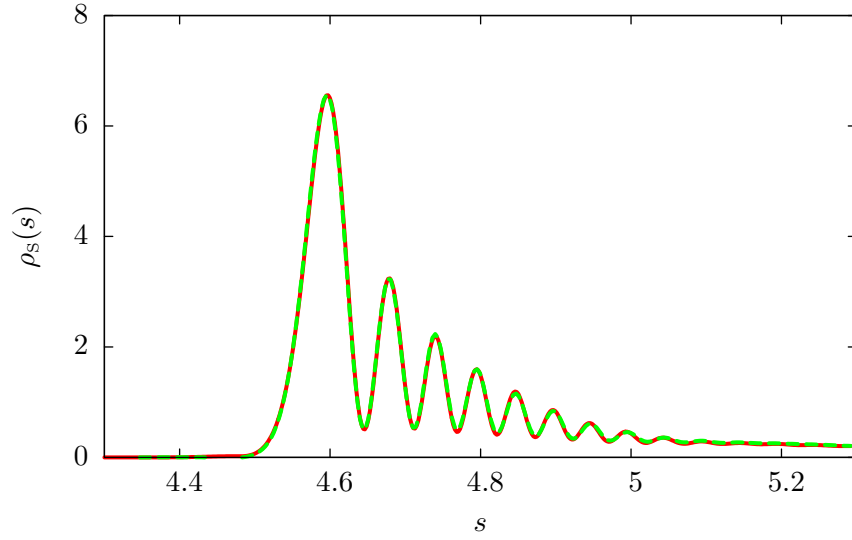


Figure 4.2: Reduced density at time $t = 192$ fs for a Morse oscillator coupled to a bath consisting of 3 modes with $\eta_{\text{eff}} = 0.25$; solid line: HK result with 3×10^6 trajectories; dashed line: SCHD result with 10^5 trajectories

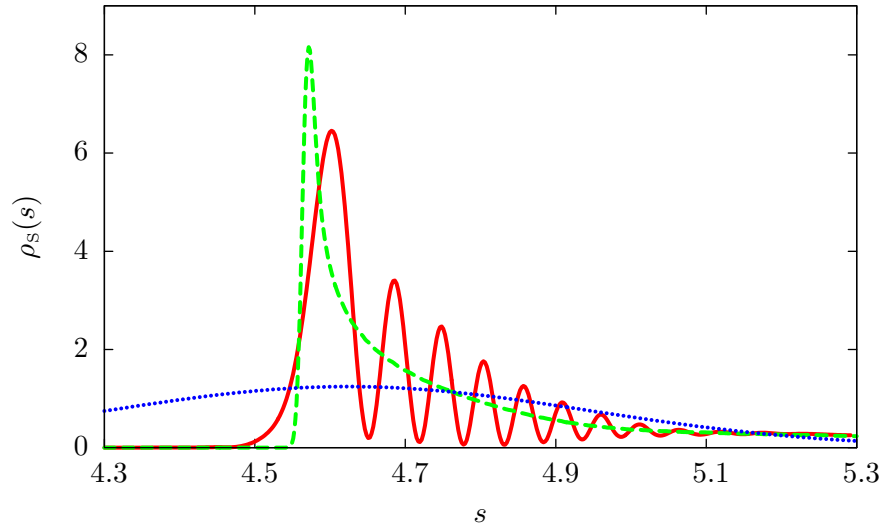


Figure 4.3: Reduced density at time $t = 192$ fs for a Morse oscillator coupled to a bath consisting of 3 modes with $\eta_{\text{eff}} = 0.05$ obtained with three different semiclassical approximations; solid line: SCHD; dashed line: LSC-IVR; dotted line: pure TGWD

position is away from the harmonic regime, as mentioned above. Thus, although it is the method with the least computational effort, it is obviously completely incapable of showing a similar behavior on the observed time scale as the SCHD result. The LSC-IVR, in turn, is a classical Wigner method revealing information about the classical nature of a system. As it does not contain any phase information, it is incapable of reproducing the interference pattern that occurs at the observed time. But in contrast to the TGWD, the LSC-IVR result is closer to the hybrid one in the sense that the mean shapes of the reduced densities are similar.

4.1.2 From the Quantum to the Classical Regime at $T=0$

The previous comparison demonstrated the capability of the SCHD for treating the SOI in a finite, non-resonant bath with three bath oscillators. Now we study the influence of the bath on the time evolution of the system in more detail. To this end, we need to increase the number of bath modes to 20 in order to mimic the continuous spectral density better than in the three-mode case, as indicated by the different results in Fig. 4.4. All other bath parameters are the same as introduced before and at first the bath has zero temperature.

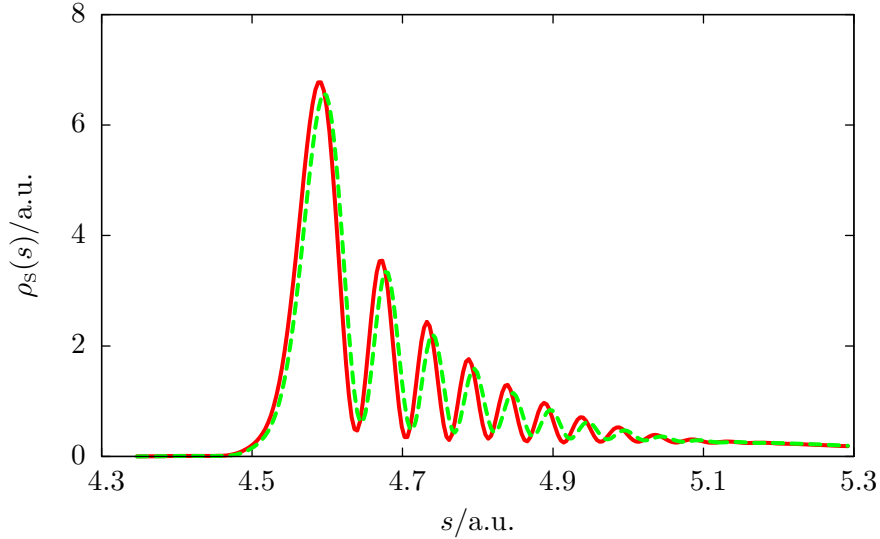


Figure 4.4: Reduced density at time $t = 192$ fs for zero bath temperature and with coupling strength $\eta_{\text{eff}} = 0.25$ with different numbers of bath modes; solid line: 20 bath modes; dashed line: three bath modes

For the given parameters, the reduced density at $t = 192$ fs is shown in Fig. 4.5 for three different coupling strengths with zero initial bath temperature. In each subfigure the corresponding SCHD and LSC-IVR result for the open system as well as the exact quantum density for the free Morse oscillator are plotted. The number of trajectories used in the SCHD computation is 2×10^4 . In turn, considering that a 22-dimensional phase-space integral has to be solved numerically, 10^6 trajectories were taken into account for the LSC-IVR result in order to obtain a sufficient convergence of the integral. However, in the case of the LSC-IVR the integrand is easily determined, whereas in the case of the SCHD two matrices in the order of $N_B \times N_B$ (with the number of bath modes N_B) need to

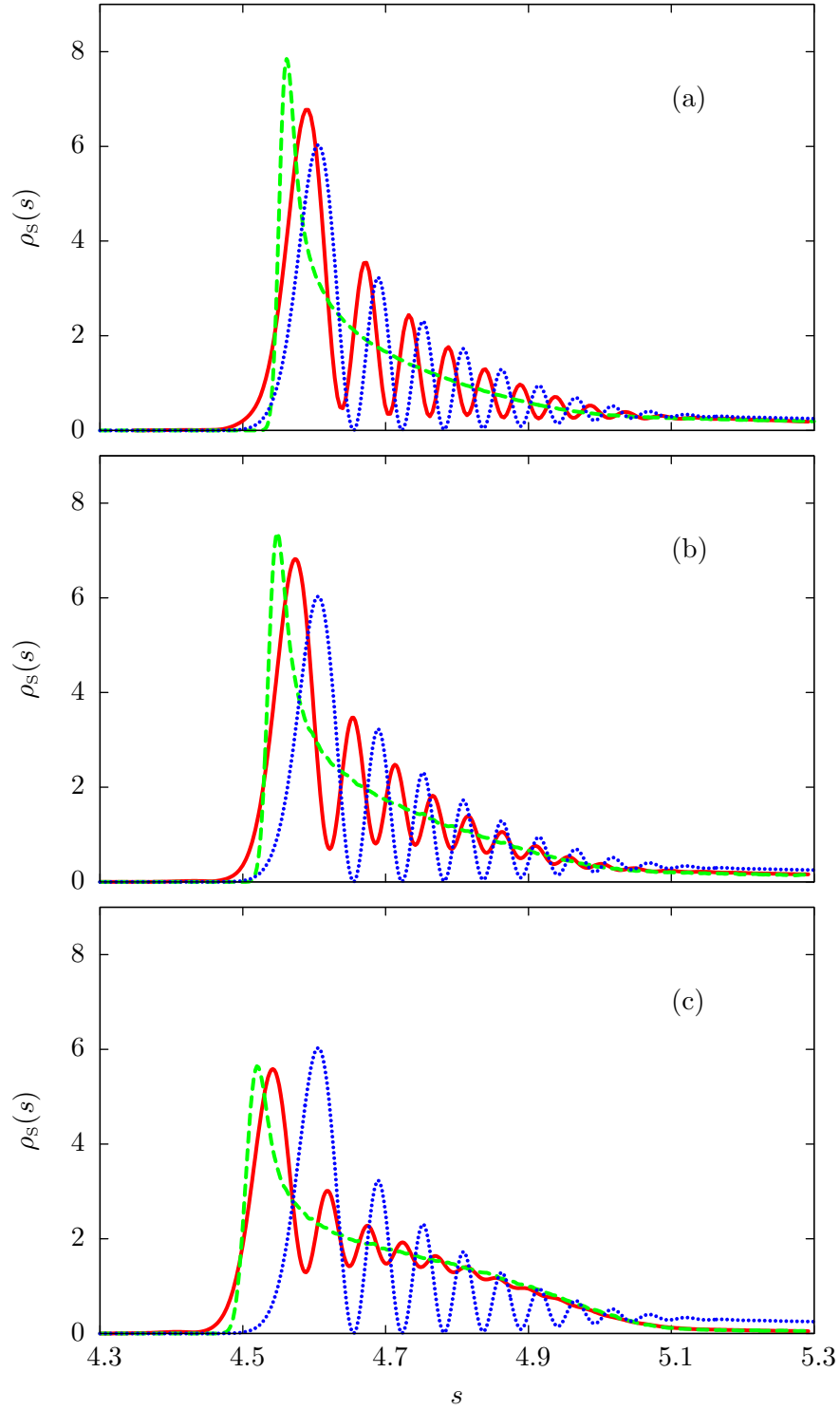


Figure 4.5: Reduced density at time $t = 192$ fs for a Morse oscillator coupled to a bath consisting of 20 modes for different effective coupling strengths: (a) $\eta_{\text{eff}} = 0.25$, (b) $\eta_{\text{eff}} = 0.5$, (c) $\eta_{\text{eff}} = 1.0$; solid line: SCHD result, dashed line: LSC-IVR result, dotted line: full quantum result for the free oscillator; the initial bath temperature is $T = 0$

be inverted for every Monte-Carlo sampling point. For this reason, in both cases, SCHD and LSC-IVR, the computational time was in the same order of a few hours on a modern workstation.

Focusing on the difference of the results in Fig. 4.5, two peculiarities become apparent. First, the system frequency shift is observed to become stronger with increasing coupling strength. This blue shift was elucidated in section 2.2 for single trajectories. In the reduced density formalism this is indicated by the circumstance that the reduced density in Fig. 4.5, for both the SCHD and LSC-IVR result, is shifted to the left relative to the free system's density (note that the first vibrational period is not completely over yet). A quantitative estimate of this shift can be made by considering the frequency of a single "coupled" trajectory (see Fig. 2.5) that has the same energy as the energy expectation value of the initial state used here, i.e. $\langle E \rangle = 0.426 D$. Again we stress that this is reasonable under the assumption that dissipation, i.e. loss of energy, is negligible due to the specific nature of the bath. This assumption yields a reduction of the local period of $\tau_{\text{loc}} = 206$ fs to $\tau_{\text{loc}}^c = 199.5$ fs when the SOI is coupled to the bath with $\eta_{\text{eff}} = 0.25$. This is corroborated by looking at the position expectation value of the system, which can be derived from the reduced density (see also Appendix D).

The second conspicuity is the smoothing of the interference pattern in the SCHD reduced density, i.e. the oscillatory structure, while being very prominent in the free oscillator case, is getting smeared with increasing coupling (see Fig. 4.5(c)). This smoothing becomes more distinct with increasing influence of the bath on the SOI. This effect, which has also been termed quenching of quantum coherence [51], originates from the coupling to the environment that leads to a loss of phase coherence in the system dynamics. At the same time, the SCHD approaches the LSC-IVR result with increasing coupling strength, which indicates the transition from quantum to classical behavior.

4.1.3 From the Quantum to the Classical Regime at Finite Temperature

So far, a zero temperature bath was considered. However, the SCHD as derived in Section 3.2 also allows for the investigation of systems in baths that have a finite temperature. Therefore, now the influence of the bath temperature on the dynamics of the density will be investigated. For this, the same bath parameters are used as before and the coupling strength is fixed, while the temperature is varied from 0 to 300 K.

In Fig. 4.6, again the free density as well as the SCHD and LSC-IVR results for the reduced density are plotted for different bath temperatures and an intermediate coupling strength $\eta_{\text{eff}} = 0.25$. Additionally, the SCHD Wigner function

$$W(s, \tilde{p}_s) = \frac{1}{\pi\hbar} \int d\zeta \langle s - \zeta | \hat{\rho}_s | s + \zeta \rangle e^{2i\tilde{p}_s\zeta/\hbar} \quad (4.5)$$

is shown in every subfigure. The momentum in the Wigner representation \tilde{p}_s is different from the momentum p_s being part of the phase space integral in the SCHD. An explicit SCHD expression of the Wigner function is derived in Appendix D.

Looking at the reduced density, we find that again the interference pattern is increasingly smeared with temperature going from 0 to 300 K, which goes along with the SCHD and LSC-IVR results approaching each other. At the highest considered temperature in Fig. 4.6(c), i.e. $T = 300$ K, both results are virtually equal suggesting the assumption that the transition from the quantum to the classical regime is nearly performed. Of course,

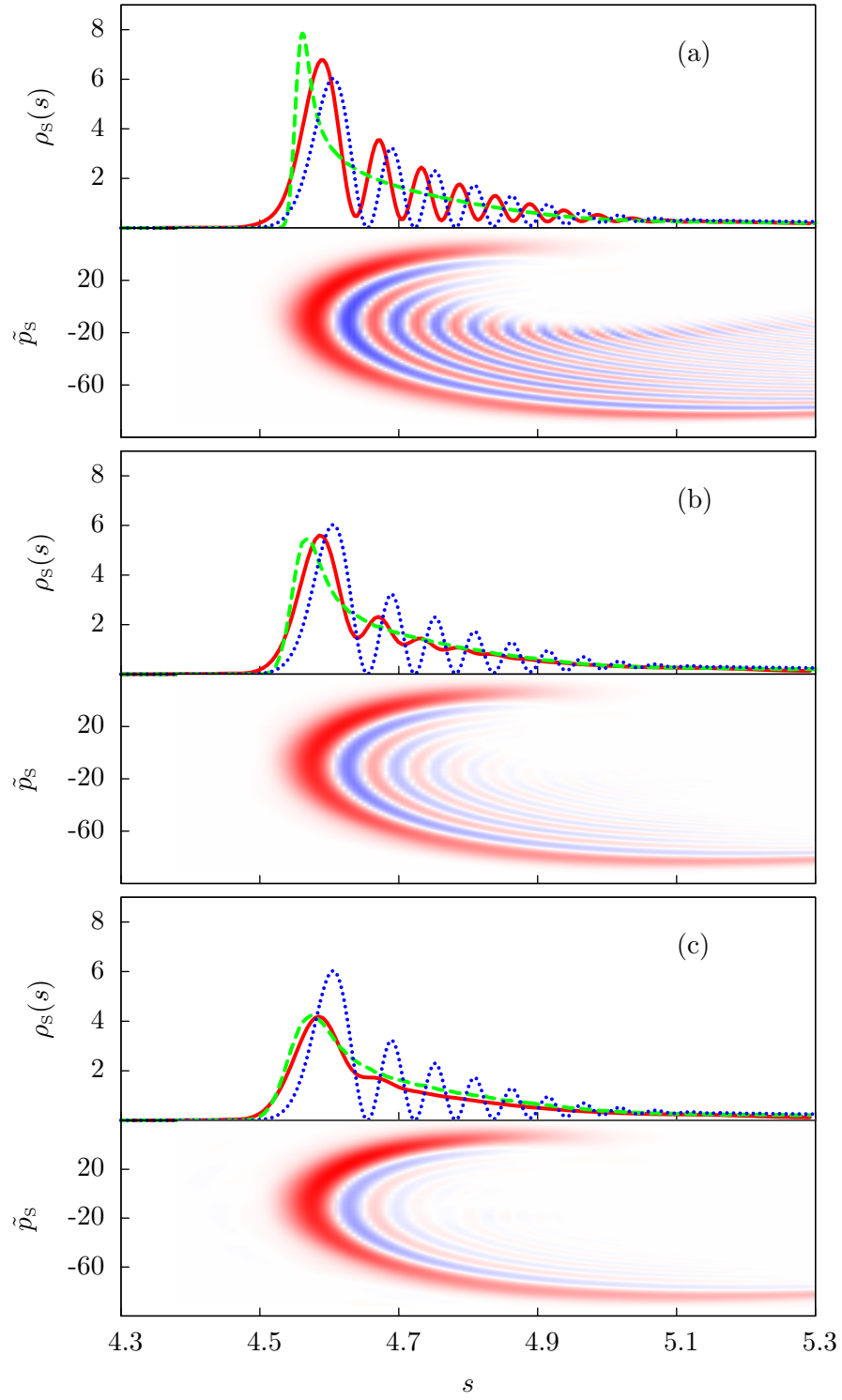


Figure 4.6: Reduced density (in each case upper subfigure) and Wigner function (lower subfigure) at time $t = 192$ fs for $\eta_{\text{eff}} = 0.25$, 20 bath modes and different bath temperatures: (a) $T = 0$, (b) $T = 100$ K, (c) $T = 300$ K; solid line: SCHD result, dashed line: LSC-IVR result, dotted line: full quantum result for the free oscillator; the Wigner function is the SCHD result, where the red color indicates positive and the blue color negative values

since the coupling to the bath is constant, so is the blue shift of the system frequency. However, even without a classical reference method, such as the LSC-IVR, the quantum-to-classical transition can be observed by looking at the Wigner function. We can utilize the circumstance that it can adopt negative values identifying non-classical states. Thus, the existence and intensity of these negative regions gives a qualitative estimate of what can be called the quantumness [94] of a particular wave function [95, 96]. In the Wigner function shown here, the region with rapid oscillations between negative and positive parts vanishes more and more with increasing temperature. Finally the Wigner function consists mainly of a weakly negative and a prominent positive region corroborating the nearly completed transition to a classical state.

4.1.4 Purity Dynamics and Decoherence

By looking at the reduced density and the Wigner function, the quantum-to-classical transition can be observed clearly, as was the case above. However, this is just one manifestation of decoherence among several others. A convenient quantity for the time evolution of decoherence, i.e. the mixing of a quantum state, is the purity $\mathcal{P}(t) = \text{tr}(\rho^2)$, which was introduced in Section 2.4. For the numerical computations, the bath parameters are still the same as above and the initial state for the SOI part has not changed either. As an aside, in principle the structure of the hybrid reduced density expression allows for the analytical performance of the trace of the squared density operator such that eventually, only the phase space integral needs to be calculated numerically in order to obtain the SCHD purity. However, this is a $8N_s$ -dimensional integral, whose calculation turns out to be computationally much more costly than the computation of the reduced density matrix on a grid and its subsequent numerical squaring and tracing. The number of trajectories used to obtain the following purity results is in the range 2×10^4 to 4×10^4 .

In Fig. 4.7 the purity is plotted for different coupling strengths and zero temperature. Note that the initial increase above unity is due to numerical reasons, which could be diminished by an increased number of trajectories. Obviously the purity is very sensitive to decoherence processes since a decrease becomes already visible after one vibrational period, although smaller coupling strengths are used than in the density calculations. A stronger decrease of the purity with increasing coupling strength is apparent. On the other hand, the coupling strength is fixed in Fig. 4.8, while the bath temperature is varied.

Another frequently used type of states for the investigation of decoherence is a coherent superposition of two locally separated Gaussians, a so-called cat state

$$|\Psi_{\text{cat}}\rangle = \sqrt{\frac{1}{2}} \left(1 + e^{-(\gamma_s/4)(s_{i,a} - s_{i,b})^2} \right)^{-1/2} (|\Psi_a\rangle + |\Psi_b\rangle), \quad (4.6)$$

with the respective centers, which are chosen to be $s_{i,a} = 4.91$ and $s_{i,b} = 5.67$ here. Such a state could, for instance, represent a particle in a superposition of locations in a Stern-Gerlach experiment [94] or a situation of a diatomic molecule “simultaneously” stretched and compressed as studied in Chapter 6 later on.

The results for this initial state in a Morse oscillator are shown in Fig. 4.9. For both coupling coefficients, the decoherence rate is obviously smaller than in the case of a single Gaussian with a higher energy expectation value placed at $s_i = 4.54$ as shown in Fig. 4.7. This observation is consistent with the assumption that the decoherence rate is correlated with the highest occupied vibrational state [27]. However, this is not the only criterion

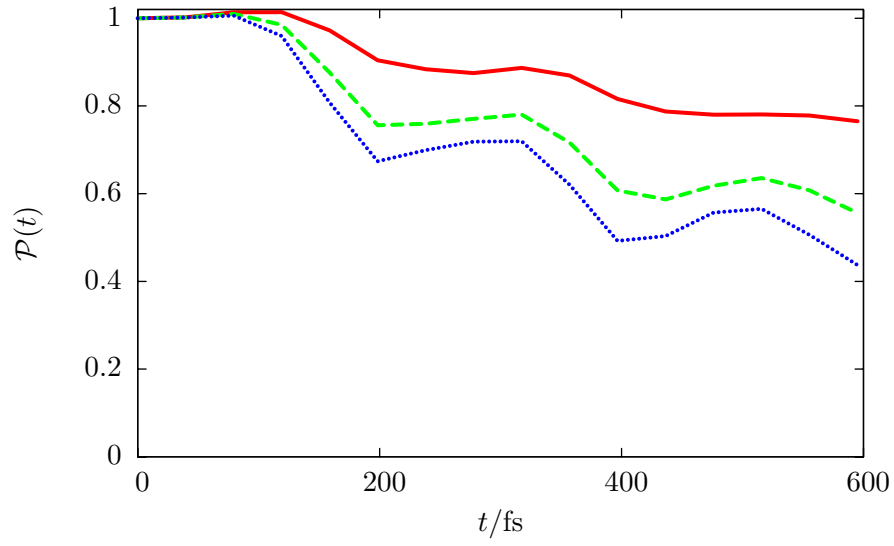


Figure 4.7: Time-evolution of the purity at zero temperature for different coupling strengths; solid line: $\eta_{\text{eff}} = 0.05$, dashed line: $\eta_{\text{eff}} = 0.15$, dotted line: $\eta_{\text{eff}} = 0.25$

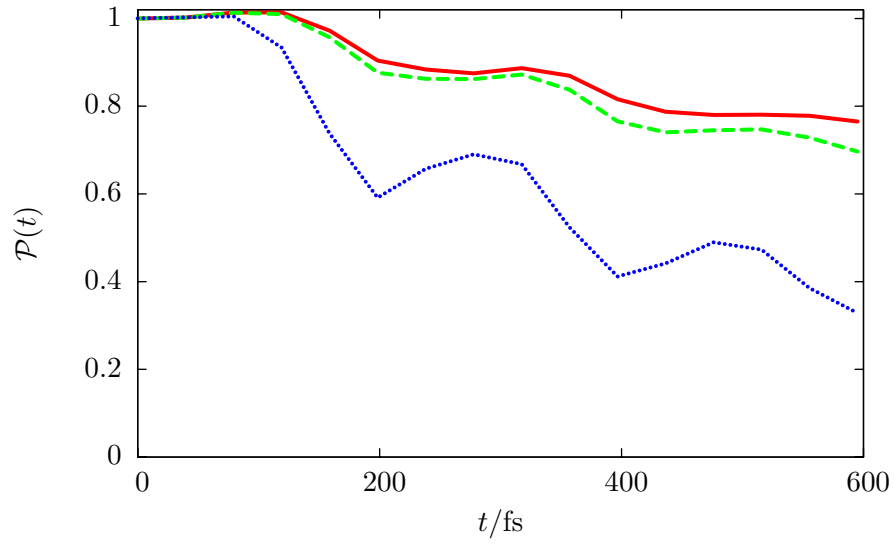


Figure 4.8: Time-evolution of the purity for a fixed coupling strength $\eta_{\text{eff}} = 0.05$ at various bath temperatures; solid line: $T = 0$, dashed line: $T = 10$ K, dotted line: $T = 100$ K

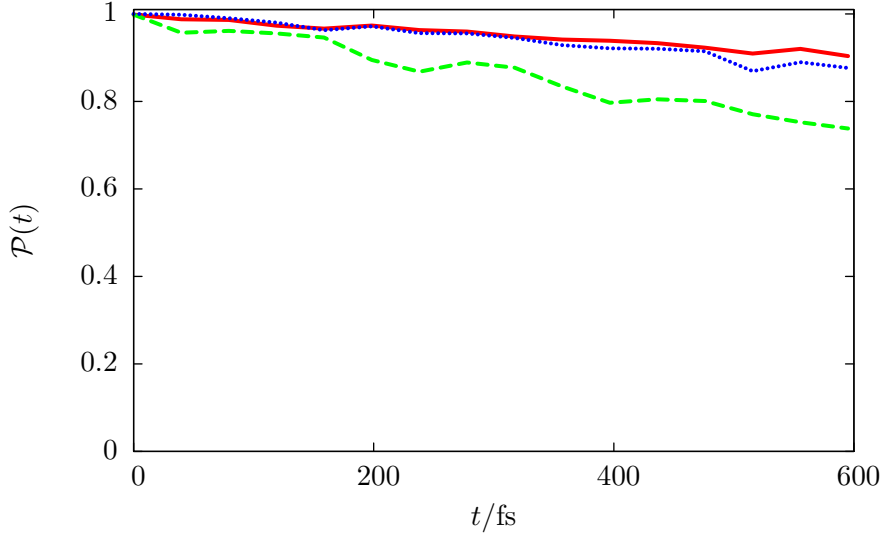


Figure 4.9: Time-evolution of the purity for different initial states at zero temperature; solid line: cat state consisting of two Gaussians centered around $s_{i,a} = 4.91$ and $s_{i,b} = 5.67$ with coupling strength $\eta_{\text{eff}} = 0.05$, dashed line: the same cat state with $\eta_{\text{eff}} = 0.25$, dotted line: single Gaussian centered around $s_i = 5.67$ with $\eta_{\text{eff}} = 0.25$

for the decrease of the purity. In Fig. 4.9 we present the time evolution of the purity for an initial Gaussian centered around $s_i = 5.67$ and thus occupying the same highest vibrational state as the cat state. Nevertheless, in the Gaussian case the decoherence rate is lower than in the cat case. This is in agreement with the statement by Elran and Brumer that interference between the two Gaussians is suppressed which again increases the decoherence rate [27]. Thus the decrease of the purity in time depends on the initial state, as well. It should be stressed that in all the non-dissipative results shown above, the norm is preserved up to marginal deviations. In dissipative and long time dynamics this is not always the case, as will be seen later.

4.2 Long Time Quantum Dynamics - Wave Packet Revivals

Besides interference effects and tunneling, a quantum revival is another quantum phenomenon of interest occurring in the long time dynamics of wave packets of numerous bound systems. In 1986, quantum wave packet revivals had been theoretically predicted in Rydberg atoms [97] before they have been observed in experiments [98] a few years later. Moreover, theoretical studies have then been extended to Rydberg clusters [99]. However, in the past, revivals have been also observed in other systems besides Rydberg atoms. For instance, in optical lattices, oscillating wave packets of atoms undergo revivals [100] and even a chaotic system, i.e. the stadium billiard, can exhibit revival dynamics [101].

Here, however, we are interested in revivals in molecular systems. Since laser pulses had been used to prepare molecular wave packets, quantum revivals became highly relevant, e.g. in pump-probe experiments [102, 103]. Moreover, in a recent publication [104], a proposal

has been made for the exploitation of revivals for quantum control of molecules. Our focus is particularly on revivals of molecular vibrational wave packets in the presence of a bath. This is of high interest in recent research, where wave packet dynamics of diatomic rubidium molecules in superfluid helium nanodroplets were studied experimentally and theoretically [105]. However, in this study dissipation is present and the theoretical approach used there is Markovian, i.e. in the quantum optical limit for very weak coupling. In contrast we recall that our SCHD approach is non-Markovian and that again, here, we are interested in pure decoherence phenomena by using a non-resonant bath and thus neglecting dissipation.

Before we get into the semiclassical treatment in the anharmonic Morse oscillator, with and without a bath, however, we will review and discuss the theoretical background of revivals.

4.2.1 Quantum Revival Time Analysis

In position representation, a quantum revival is defined as the event that a wave function - or equivalently the corresponding density - adopts its initial form after some revival time τ_{rev} , that is

$$\Psi(x, \tau_{\text{rev}}) \simeq \Psi(x, 0). \quad (4.7)$$

To investigate τ_{rev} , we start out with the basis expansion of an arbitrary wave function

$$\Psi(x, t) = \sum_n c_n \psi_n(x) e^{-iE_n t/\hbar}, \quad (4.8)$$

with the energy eigenfunctions $\psi_n(x)$, the energy eigenvalues E_n and the coefficients c_n , where only the bound states of a system are considered. The particular considered potential is again the Morse potential introduced in Eq. (2.19).

A revival requires all phase factors to become unity, which is equivalent to the condition that

$$\frac{E_n \tau_{\text{rev}}}{\hbar} = \left[\omega_S \left(n + \frac{1}{2} \right) - \nu_S \left(n + \frac{1}{2} \right)^2 \right] \tau_{\text{rev}} \stackrel{!}{=} 2\pi L_n \quad L_n \in \mathbb{Z} \quad n \in \mathbb{N}, \quad (4.9)$$

where the eigenenergies of the Morse oscillator, given in Eq. (2.20), were used. Hence, the difference of two consecutive phases must be an n -dependent integer multiple of 2π , as well, yielding

$$\begin{aligned} [(E_{n+1} - E_n) - (E_n - E_{n-1})] \frac{\tau_{\text{rev}}}{\hbar} &= (E_{n+1} - 2E_n + E_{n-1}) \frac{\tau_{\text{rev}}}{\hbar} \\ &= \left[\omega_S \left(n + \frac{3}{2} \right) - \nu_S \left(n + \frac{3}{2} \right)^2 - 2\omega_S \left(n + \frac{1}{2} \right) \right. \\ &\quad \left. + 2\nu_S \left(n + \frac{1}{2} \right)^2 + \omega_S \left(n - \frac{1}{2} \right) - \nu_S \left(n - \frac{1}{2} \right)^2 \right] \tau_{\text{rev}} \\ &= -2\nu_S \tau_{\text{rev}} \stackrel{!}{=} 2\pi L, \end{aligned} \quad (4.10)$$

where L is some fixed positive integer. Thus the revival time is $\tau_{\text{rev}} = \pi/\nu_S L$, since the sign is irrelevant.

However, for a better understanding of the dynamics in the vicinity of the revival time of the specific system and to find the smallest integer L to obtain a unique revival time, we will examine the respective phase more thoroughly. Hence, assuming $L = 1$, we consider

$$E_n \frac{\tau_{\text{rev}} \pm \delta}{\hbar} = \left[\frac{\omega_s}{2} - \frac{\nu_s}{4} \right] \left(\frac{\pi}{\nu_s} \pm \delta \right) + [\omega_s n - \nu_s n(n+1)] \left(\frac{\pi}{\nu_s} \pm \delta \right) \quad (4.11)$$

$$= -\pi n(n+1) + \omega_s n \left(\frac{\pi}{\nu_s} \pm \delta \right) \mp \nu_s n(n+1) \delta, \quad (4.12)$$

where δ is some small deviation from the revival time. The first term on the right hand side of Eq. (4.11) is not considered in Eq. (4.12) any more, since it gives only a global phase not affecting the physics of the system. Regarding Eq. (4.12), we find that the first term is an even multiple of π . Thus the revival condition would be fulfilled at the revival time, that is for $\delta = 0$, if the second term also were an integer multiple of 2π , i.e. if $\omega_s/\nu_s = 2H_n/n$, where H_n is the n -dependent integer.

Indeed, in general this is not the case, but still we can obtain an excellent approximation to a full revival. The reason for this is the fact, that

$$\frac{\omega_s}{\nu_s} = \frac{\sqrt{8DM}}{\hbar\alpha} \gg 1, \quad (4.13)$$

since for realistic systems $\alpha \ll \sqrt{DM}$, with the system mass M . The second term in Eq. (4.12) becomes an even multiple of π , if

$$\frac{\pi}{\nu_s} \pm \delta = \frac{2\pi I_n}{\omega_s} \quad I_n \in \mathbb{Z}. \quad (4.14)$$

Since $\nu_s \ll \omega_s$, there is always a $\delta < 2\pi/\omega_s = \tau_s$, with τ_s the harmonic system period of oscillation, for which Eq. (4.14) is fulfilled. Under this condition, the third term in Eq. (4.12) is then much smaller compared to the sum of the other terms and the estimate for the revival time is $\tau_{\text{rev}} = \pi/\nu_s = 983.5$, if we work with unit mass and choose the dimensionless units as $D = 30$ and $\alpha = 0.08$.

Following this analysis it becomes clear, that the wave packet revival is a result of phase relations of the eigenstates and thus it does not have a classical analog. For further reading on wave packet revivals an elaborate summary can be found in [106].

4.2.2 Revivals in Semiclassics

The time scale of the dynamics in a bound quantum system can be separated into three regimes. The first and also shortest one is the initial part of the propagation, when the evolution of the initially localized wave packet is closely followed by the classical evolution of the corresponding probability distribution. This time scale is also denoted as the Ehrenfest time. Beyond this time, the wave packet spreads over the whole phase space region restricted by the particular energy. In general, a seemingly disordered interference pattern occurs and the classical evolution of the probability density becomes incapable of reproducing the quantum evolution. However, it is well-known, that semiclassical dynamics works satisfactorily on this time scale especially for systems evolving regularly and even for chaotic “long time” dynamics [107], as demonstrated already in this thesis and in numerous

publications. After a sufficiently long time, the wave packet relocates, reconstructing the form of the initial packet. This is the quantum revival regime, which is characterized by the revival time introduced above.

Here, the aim is to clarify, whether the semiclassical HK method is valid in the revival regime and thus reproduces quantum revivals. Indeed, quantum revivals have already been described semiclassically using Heller's cellular dynamics [108]. However, in contrast to the HK method, the cellular dynamics method is a non-uniform SC-IVR and thus potentially less accurate.

For the numerical treatment, we choose a GWP centered around $\tilde{s}_i = -3.0$ (dimensionless units) with zero momentum and a width parameter $\gamma = 2.0$ as the initial wave function. An appropriate quantity for the investigation of revivals is the autocorrelation function, which is the overlap of the propagated wave function with the initial one. In terms of densities a generalization of the autocorrelation function is the survival probability, which can be interpreted as the expectation value of the initial density $\hat{\rho}_i \equiv \hat{\rho}(0)$, and thus

$$C(t) \equiv \langle \hat{\rho}_i \rangle(t) = \text{tr}[\hat{\rho}_i \hat{\rho}(t)]. \quad (4.15)$$

In Fig. 4.10, this survival probability is plotted in time for three different methods of propagation. The quantum revival is indicated by the survival probability returning to unity after the revival time $\tau_{\text{rev}} = 983.5$, that is nearly 100 vibrational periods. This is confirmed by the numerical results, where the revival is apparent not only in the quantum but also in the semiclassical case and even the agreement in the time dependence of $C(t)$ between both cases is excellent. Thus, the HK method is still a valid approximation to quantum mechanics even on time scales, that are much longer than a typical system period. In principle, the HK expression in wave function formalism consisting of a *single* phase space integral would be sufficient for the calculation, since a one-dimensional system is considered. Here, however, the density expression of the HK method involving the *double* phase space integral is used for reasons of consistency with results for the system-bath case shown below. In doing so, 10^6 trajectories are necessary to obtain a sufficiently converged result. Further increasing the number of sampling points would only change minor details in the time dependence of the considered survival probability.

The LSC-IVR result, in turn, shows a good agreement with the other results only for short times in the order of only a few vibrational periods corresponding to the Ehrenfest regime. However, with proceeding time the deviation from the other results increases until the classical survival probability equilibrates at a constant value of nearly 0.2 not showing any revival at all.

Hence, obviously the phase relations of the trajectories in the HK expression are responsible for the occurrence of revivals. In order to see in detail how this leads to such a revival, we consider the distribution of trajectory (angular) phases in a phase space cut at the revival time, since the overall system's double phase space is a four-dimensional one. Here, the two-dimensional phase space cut at the time of revival is chosen, where the initial conditions of the trajectories are varied in one half of the double phase space and fixed at the maximum of the initial wave packet in the other half, i.e. $(q_{S,\tau_{\text{rev}}}(q_S, p_S), p_{S,\tau_{\text{rev}}}(q_S, p_S); q'_{S,\tau_{\text{rev}}}(q'_S = \tilde{s}_i, p'_S = 0), p'_{S,\tau_{\text{rev}}}(q'_S = \tilde{s}_i, p'_S = 0))$. In Fig. 4.11 this cut is shown in the topmost panel. Each final phase space point carries a phase, which is encoded by a color in a continuous way. Here, a certain clustering of similar colors and thus phases can be observed in the region of the initial wave function. This becomes distinct below in the Gaussian blurred

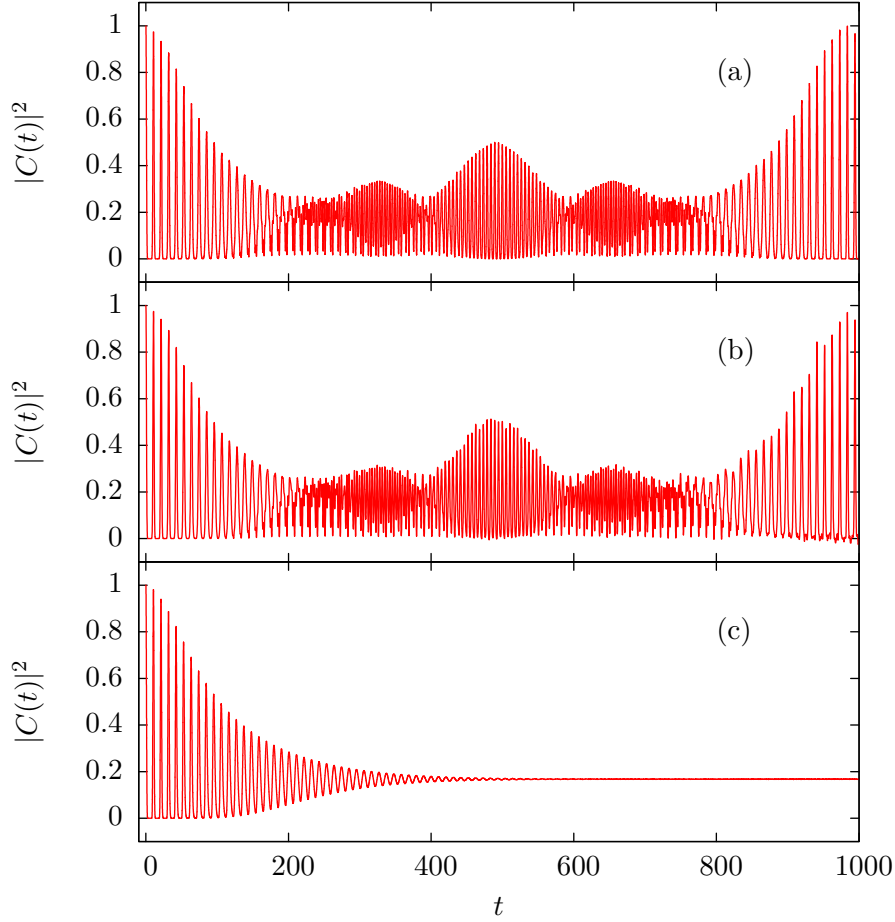


Figure 4.10: Survival probability vs time obtained with various propagation methods; (a) quantum result (with SPO), (b) semiclassical HK result, (c) classical Wigner (LSC-IVR) result; time is given in dimensionless units

version of this phase space distribution. The Gaussian blurring of a function in phase space $f(\tilde{s}, \tilde{p}_s)$ is achieved by centering a Gaussian window function around each phase space point and averaging over the phase space, so that the blurred function reads

$$\mathfrak{f}(\tilde{s}, \tilde{p}_s) = \int d\tilde{s}' d\tilde{p}'_s \exp \left[-\tilde{\gamma}_1(\tilde{s}' - \tilde{s})^2 - \tilde{\gamma}_2(\tilde{p}'_s - \tilde{p}_s)^2 \right] f(\tilde{s}', \tilde{p}'_s), \quad (4.16)$$

with the width parameters $\tilde{\gamma}_1$ and $\tilde{\gamma}_2$. Hence, the parts, that appear rather grey, indicate neighboring points with strongly varying phases, that eventually cancel their contributions mutually. The contributions of the trajectories only add up in regions with similar phases, which yields regions with identifiable colors. This is the case in those parts, where the revived wave packet is localized, as can be seen from the wave packet density in position space. The agreement with the initial wave function is outstanding and the small contributions outside this region of the initial wave packet will eventually vanish with increasing number of trajectories.

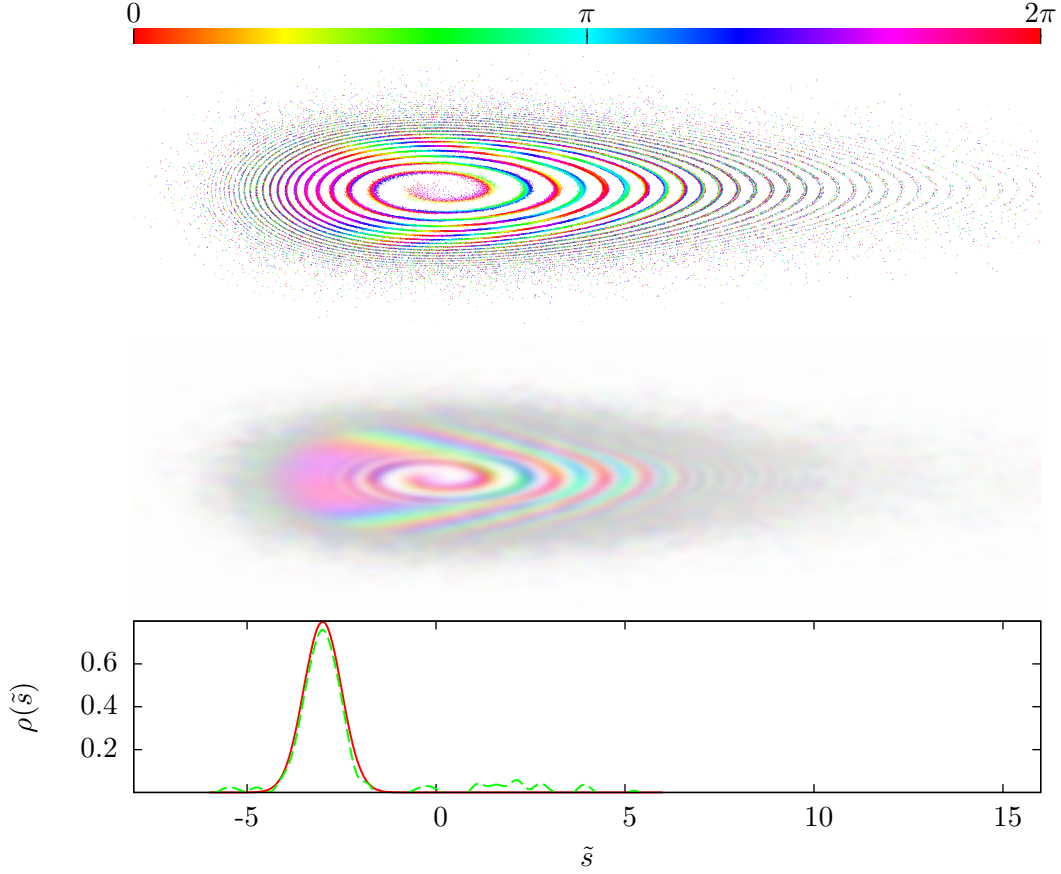


Figure 4.11: Topmost panel: Distribution of wave function phases in the $(q_{\text{S}}, \tau_{\text{rev}}(q_{\text{S}}, p_{\text{S}}), p_{\text{S}}, \tau_{\text{rev}}(q_{\text{S}}, p_{\text{S}}); q'_{\text{S}}, \tau_{\text{rev}}(q'_{\text{S}} = \tilde{s}_{\text{i}}, p'_{\text{S}} = 0), p'_{\text{S}}, \tau_{\text{rev}}(q'_{\text{S}} = \tilde{s}_{\text{i}}, p'_{\text{S}} = 0))$ phase space cut at the time of revival $\tau_{\text{rev}} = 983.5$ with color-coded phases for each point (the phases are taken mod 2π); Central panel: Gaussian blurred phase space distribution at the revival time; Lowermost panel: Initial (solid line) and revived (dashes) density in position space

4.2.3 Suppression of Revivals due to Decoherence

Based on the knowledge, that the semiclassical HK method is capable of describing quantum revivals, we know apply the SCHD to the anharmonic system coupled to a non-dissipative finite bath again, since we wish to investigate the revival dynamics in the presence of pure decoherence solely. For this, the cutoff frequency is $\omega_{\text{c}} = 0.05$ and the maximum frequency of the bath $\omega_{\text{max}} = 3\omega_{\text{c}}$.

The survival probability is plotted in Fig. 4.12 for different numbers of bath modes and varying initial bath temperatures. In all cases the coupling strength is $\eta = 0.05$. Trajectory numbers in the order of 10^5 are sufficient to obtain converged results with the semiclassical hybrid method. A further increase of the number of sampling points only changes minor details in the course of the time evolution of the survival probability. As an aside, the results shown here, are renormalized in the sense, that the survival probability is divided by its norm. The reason for this procedure is the fact that the SCHD fails to maintain norm conservation and hence the norm drop-off is between 60% and 80% on the regarded

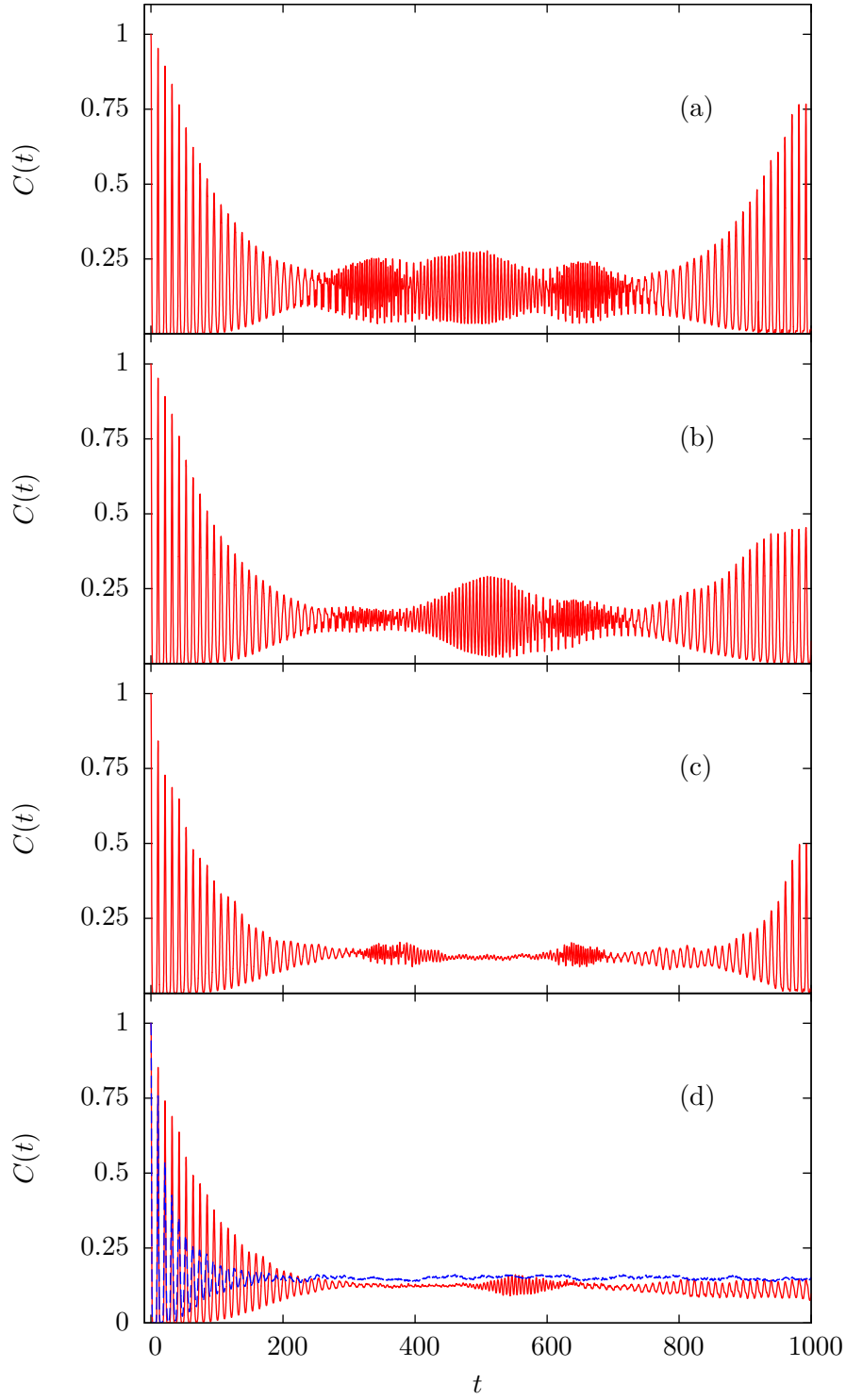


Figure 4.12: SCHD survival probability for fixed coupling $\eta = 0.05$ and various mode numbers and temperatures: (a) 3 bath modes, $\beta = 1.0$; (b) 5 bath modes, $\beta = 1.0$; (c) 3 bath modes, $\beta = 0.1$; (d) 5 bath modes, $\beta = 0.1$, the dashed line is the classical LSC-IVR result

time scale in the coupled case (in the uncoupled case the norm drop-off is negligible). Nonetheless, structures indicating decoherence are clearly visible even in the case of the weakest perturbation, where the bath consists of only 3 bath modes and has a rather low initial temperature of $\beta = 1/(kT) = 1.0$. Here, the damping of the coherent oscillations is clearly visible, although they never come to a full standstill. An increase of the number of modes as well as an increase of the temperature result in a stronger damping of the oscillation. For the largest considered bath with the highest regarded temperature, the revival is nearly fully suppressed, where the survival probability shows only small residual oscillations. For this case also the classical result is plotted as a reference, being in a good agreement with the SCHD result.

Indeed, we cannot be sure that this result is a consequence of pure dephasing, since the selected cutoff frequency could still be too close to the resonance frequency. Then, the damping of oscillations could also be due to dissipation, where finally thermal equilibrium is reached on this relatively long time scale. In Fig. 4.13 the energy expectation value of the SOI

$$\langle E \rangle(t) = \text{tr}(\mathcal{H}_s \rho_s) \quad (4.17)$$

is plotted (see more on the calculation of this energy expectation value in Appendix D.2.1). Here, the bath has a temperature of $\beta = 1.0$ and consists of 3 modes. Since the integrand of the energy expectation value is more strongly oscillating than in the case of the survival probability, far more trajectories are required to obtain a sufficiently converged result, i.e. 2×10^6 . This shows a nearly constant energy with very small deviations of about 5 % from the initial energy. Similar results for the time evolution of the energy are obtained with a larger bath at a higher temperature, which is not shown here.

Of course, the survival probability gives a compact impression about the time evolution of the density with respect to the initial one. However, just like in the case of the free oscillator, a more illustrative way to study revival dynamics is to regard the density at the expected revival time. Hence, in Fig. 4.14 these reduced densities are plotted for

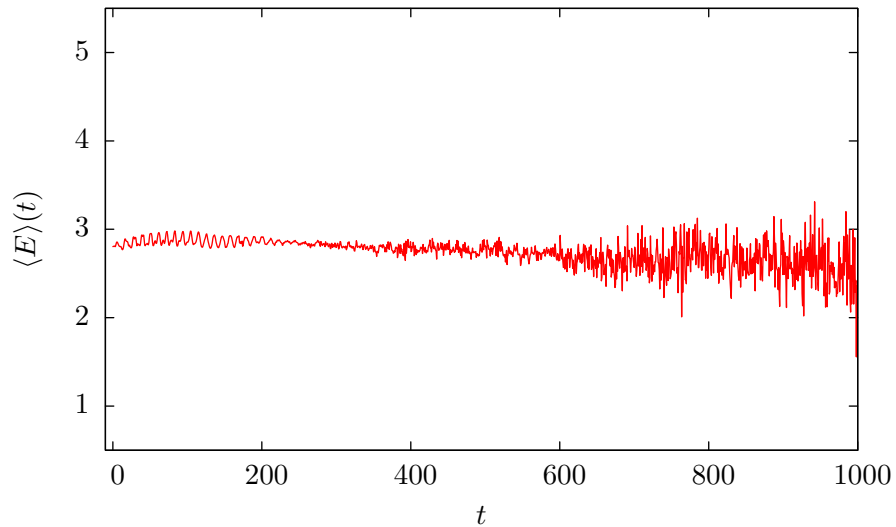


Figure 4.13: Energy expectation value with bath consisting of 3 modes and $\beta = 1.0$

different parameters and compositions of the bath. Due to the blue shift of the system frequency described in Section 2.2, the revival time is now expected to be earlier than in the free case, i.e. $\tau_{\text{rev}} = 981.5$, which is in agreement with the prediction. In the case of the weakest damping of oscillations, where $\beta = 1.0$ and the bath has 3 modes, the shape of the reduced density is similar to the initial one, albeit broader and not exactly Gaussian any more. Hence, the revival has become rather a partial revival with small and still negligible oscillatory contributions outside the revival region. Furthermore, the density is spread over the whole allowed region in position space according to the energy range covered by the initial wave packet as shown in Fig. 4.14(b). The quantum revival is maximally suppressed and the density is virtually identical with the classical result. Therefore, by varying the temperature of the bath as well as its size, one can systematically and continuously tune the revival dynamics from full revival to full suppression passing all grades of partial revivals.

A description of the semiclassical mechanism is not comprehensively possible, since only a part of the overall phase space can be captured. However, to get an idea of the in-

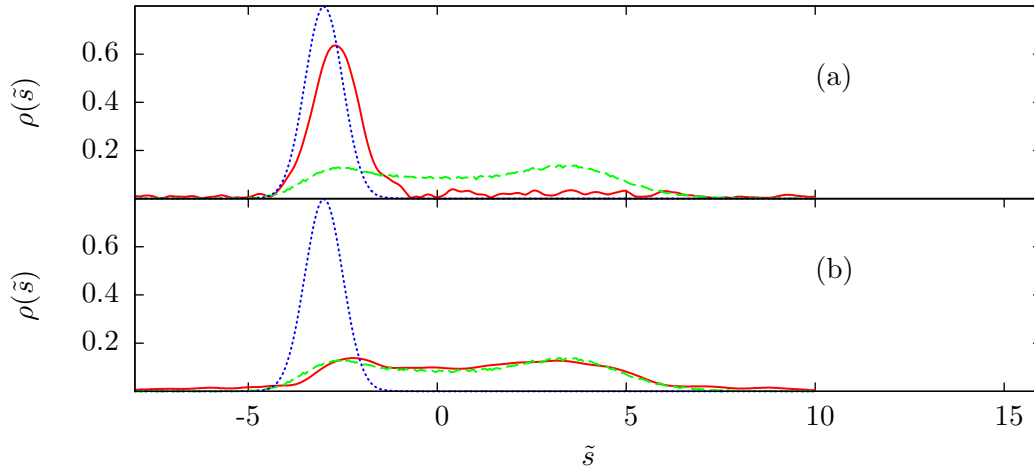


Figure 4.14: (a) Density in position space at the expected revival time (solid line) for a bath with 3 modes and temperature $\beta = 1.0$; (b) Density in position space at the expected revival time (solid line) for a bath with 5 modes and temperature $\beta = 0.1$ and LSC-IVR result (dashed line); in both panels, the dotted line is the initial density

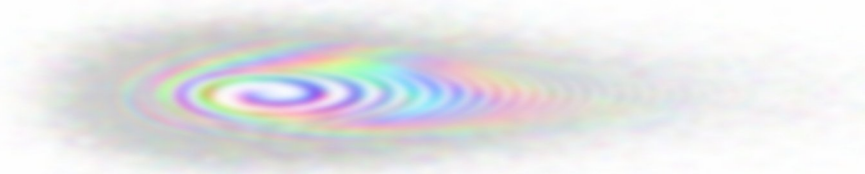


Figure 4.15: Gaussian blurred phase space distribution in the phase space cut $(q_S, \tau_{\text{rev}}(q_S, p_S), p_S, \tau_{\text{rev}}(q_S, p_S); q'_S, \tau_{\text{rev}}(q'_S = \tilde{s}_i, p'_S = 0), p'_S, \tau_{\text{rev}}(q'_S = \tilde{s}_i, p'_S = 0))$ at the expected revival time with a bath consisting of 3 modes with $\beta = 0.1$

fluence of the coupling and the temperature on the phases of the trajectories, again the blurred distribution of the phase space cut $(q_{S,\tau_{\text{rev}}}(q_S, p_S), p_{S,\tau_{\text{rev}}}(q_S, p_S); q'_{S,\tau_{\text{rev}}}(q'_S = \tilde{s}_i, p'_S = 0), p'_{S,\tau_{\text{rev}}}(q'_S = \tilde{s}_i, p'_S = 0))$ is shown in Fig. 4.15. In contrast to the phase space cut shown in Fig. 4.11, there is no such region of similar phases and therefore no homogeneous color in the vicinity of the revival region. The phases of the trajectories have rather become mixed showing only small “non-grey” regions with similar colors.

4.3 Diffraction at a Double Slit

Within the framework of non-dissipative system-bath problems, we are interested in the investigation of another SOI, which is of a different type than the anharmonic oscillator investigated above. Here, we consider a wave packet in the plane, e.g. an electron, propagating through a double slit. This refers to the typical experiment appearing in standard literature on quantum mechanics and is of interest in many respects. For instance, one makes use of the double slit in atom interferometry [109]. It also plays an important role regarding fundamental questions of quantum physics. In a very recent experiment the double slit was extended to a triple slit and as a result higher order interferences could be ruled out and thus Born’s interpretation confirmed [110]. Furthermore, the double slit-propagation of a wave packet exiting from a chaotic billiard, leads to chaos-induced, so-called dynamical, decoherence [111]. Here, we want to investigate decoherence by coupling the slit to a non-resonant bath. We will use a system-bath model, which will be given below and which is slightly different from the CL model to allow for the coupling to be effective only in the vicinity of the slit.

The considered double slit is described by the potential [52]

$$\mathcal{V}(s_1, s_2) = \left(V_0 - \frac{m\omega^2}{2}s_2^2 + \frac{m^2\omega^4}{16V_0}s_2^4 \right) e^{-(s_1/\alpha_d)^2}, \quad (4.18)$$

which is a superposition of a double well potential in the s_2 coordinate and a Gaussian potential in the s_1 coordinate, see also Fig. 4.16. The potential parameters used here are $\alpha_d = 50$ a.u., $\omega = 0.0027$ a.u. and the barrier height $V_0 = 0.036$ a.u.. Also, the particle is assumed to have mass $m = 1$ a.u.. Initially the state is a two-dimensional GWP located to the left side of the barrier at $s_1 = -300$ a.u. and $s_2 = 0$ a.u. with a positive momentum in the s_1 direction $p_{s,1} = 0.137$ a.u., yielding a kinetic energy of roughly 25% of the barrier height. Hence, the energy is sufficiently high, so that the particle can pass the barrier, except for tunneling. However, the barrier is sufficiently broad in the direction of propagation, so that tunneling processes will not dominate the dynamics. Finally, the widths of the incident Gaussian are $\gamma_{s,1} = 1/(2\alpha_d^2)$ and $\gamma_{s,2} = \omega^2/(8V_0)$.

4.3.1 Free Double Slit

Before the barrier is coupled to a thermal bath, we will study the free double slit first. To this end, the angular distribution of the transmitted part

$$P(\vartheta) = \int_0^\infty dR R \rho_S(R, \vartheta; t \rightarrow \infty) \quad (4.19)$$

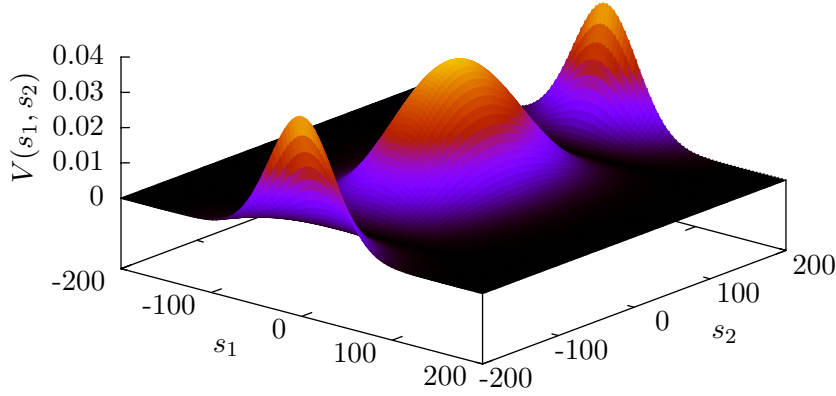


Figure 4.16: Energy surface plot of the double slit potential described by Eq. (4.18) with the parameters given in the text

is investigated. It is identical with the diffraction pattern that would appear on a concave screen arranged behind the double slit. Hence, the reduced density as a function of polar coordinates is needed at sufficiently long times, when the scattering process is assumed to be terminated and consequently the wave packet is split into two distinct parts, a reflected and a transmitted one.

Fig. 4.17 shows the quantum and the HK result of this distribution. In the quantum case the wave function is propagated with the SPO on a cartesian grid [30] and subsequently the distribution is calculated via interpolation. In contrast, the computation of the HK density on a polar grid is straightforward, since the cartesian coordinates only need to be written as functions of polar coordinates

$$\rho(s_1, s_2; t) = \rho[R \cos(\vartheta), R \sin(\vartheta); t] \rightarrow \rho(R, \vartheta; t). \quad (4.20)$$

Nonetheless, for the particular regarded system we encounter chaos, which occurs in the underlying classical dynamics and thus complicates the semiclassical computation. In principle, this can appear in all systems with a phase space that has more than two dimensions, which is the case here. In the semiclassical propagator, chaos involves a highly oscillating integrand and thus numerically the corresponding integral converges very slowly. In other words, it takes a very high number of sampling points to obtain a sufficiently converged result compared to integrable systems with the same dimensionality, since the phase space needs to be covered very densely in the chaotic case (more on semiclassical treatment of chaotic systems, see [49, 112]).

However, several approaches have been made to increase the convergence of the phase space integral, in particular for chaotic problems. A number of these approaches is based on the Filinov integral smoothing technique (a nice review on this can be found in [54]), where the phase space integral is additionally preaveraged.

In this work, we take a simpler but very efficient approach: a chaotic trajectory is

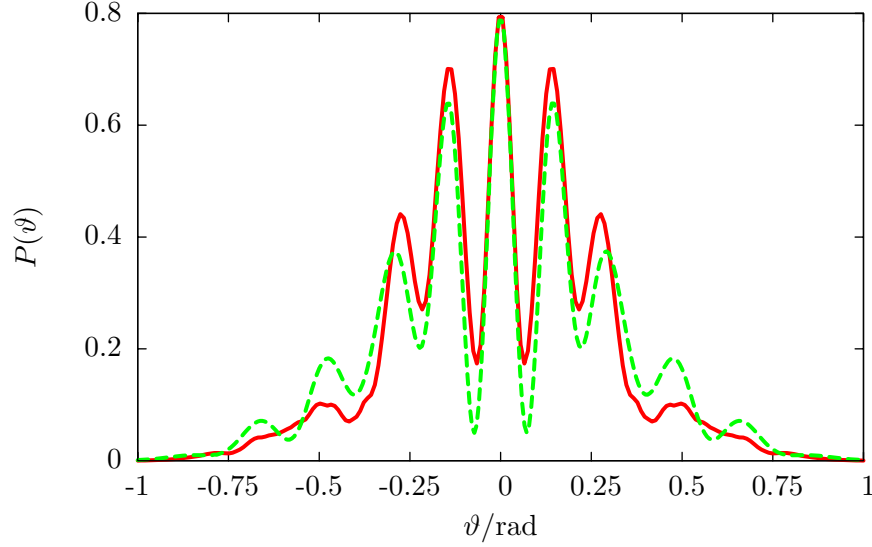


Figure 4.17: Angular distribution of the transmitted part of a wave packet propagating through a double slit; solid line: HK result with 10^7 trajectories, dashed line: quantum result; The propagation time of the wave packet is 9000 a.u.

discarded if the corresponding prefactor $|RR'^*|$ exceeds a certain threshold value according to a suggestion by Kay [113]. This idea is based on the assumption that the stability prefactor, discussed in Appendix B, governing the dependence of a trajectory on its initial conditions, is large in regions with a highly oscillating integrand, that averages to zero locally. Furthermore, the sudden cutoff of a trajectory was shown to be a special case of the Filinov preaveraging technique which is much easier to apply than other prevalent Filinov approaches [114]. At the same time, it has a comparable efficiency. Still, some care must be taken when choosing the appropriate cutoff value, since too many dismissed trajectories can entail a strong suppression of originally non-negligible parts of the density. Here, the cutoff value is chosen such that less than 4% of the trajectories are discarded at the final time.

Hence, the semiclassical result reproduces the quantum diffraction pattern very well up to minor deviations, particularly in the higher order diffraction peaks as shown in Fig. 4.17. Considering that the semiclassical calculation of the density involves the computation of an eight-dimensional phase space integral, which in addition shows partially chaotic behavior, it is not surprising that 10^7 trajectories are necessary to obtain a sufficiently converged result. We note, that for the semiclassical results, the symmetry of the regarded problem with respect to the axis of propagation (s_1 -axis) is exploited, and thus the reduced density is averaged over both quadrants of the positive position half-plane.

4.3.2 Damping of Diffraction

For the following discussion the barrier shall be coupled to a thermal low-frequency bath. To this end, the system-bath Hamiltonian is slightly modified as compared to the CL case in Eq. (2.5) and is given by

$$\hat{\mathcal{H}} = \hat{\mathcal{H}}_s + \sum_{i=1}^{N_B} \left\{ \frac{\hat{p}_i^2}{2} + \frac{\omega_i^2}{2} \left(y_i + \frac{c_i}{\omega_i^2} s_2 e^{-(s_1/v)^2} \right)^2 \right\}. \quad (4.21)$$

Now the coupling is linear along the barrier, i.e. in the s_2 direction, and of exponential form transverse to the slit. The latter kind of coupling restricts the bath-system interaction to the vicinity of the barrier continuously, governed by the range parameter v . Effectively, this implies a position-dependent coupling coefficient, which in principle is no restriction for the SCHD since it treats the system-bath Hamiltonian as a whole explicitly. The spectral density of the bath is again assumed to be of Ohmic form with an exponential cutoff as given in Eq. (4.2). Furthermore, the bath frequencies are distributed according to the exponential density of frequency in Eq. (4.3). The corresponding maximum frequency is $\omega_{\max} = 4\omega_c$ with the cutoff frequency $\omega_c = 4.56 \times 10^{-4}$ a.u., which again is smaller than the harmonic frequency of the bound DOF of the SOI, i.e. the frequency of the harmonic approximation of one of the wells in the s_2 direction. Hence, this bath is also non-dissipative and will lead to pure dephasing. Considering the system's short interaction time with the bath compared to the overall propagation time due to the restricted interaction region, five bath modes were found to be sufficient to mimic a continuous bath. At this point it should be stressed, that the numerical complexity, which is already high in the free case of the SOI, does not increase by the coupling to a bath. The number of sampling points for the numerical phase space integration is still 10^7 and thus the same as in the free case, since all bath modes are treated on the level of the TGWD here.

In Fig. 4.18 the angular distribution is shown for different range parameters v . The variation of this parameter changes the effective coupling nonlinearly. The loss of coherence manifests first distinctly in the decrease of the central diffraction peak, since it results from the strongest constructive interference of quantum paths and is thus most sensitive to

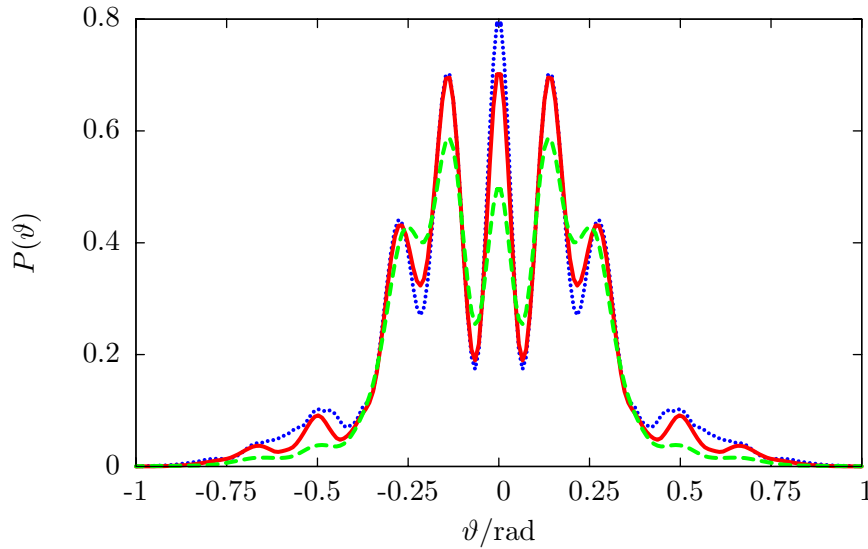


Figure 4.18: Angular distribution for a barrier coupled to a bath with 5 bath modes, $T = 0$ and $\eta = 4.56 \times 10^{-5}$ a.u. for different range parameters; solid line: $v = 100$ a.u., dashed line: $v = 1000$ a.u., dotted line: result for the uncoupled double slit

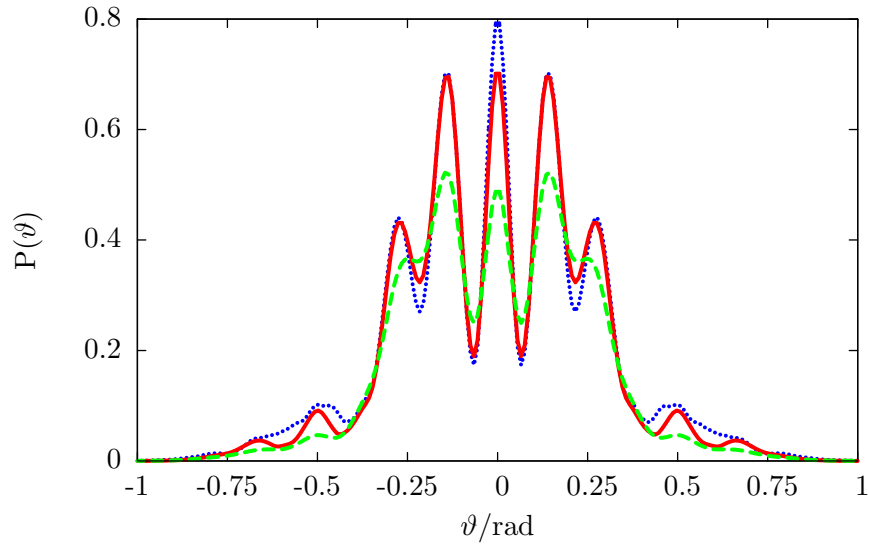


Figure 4.19: Angular distribution for a barrier coupled to a bath with 5 bath modes, $T = 0$ and a fixed range parameter $\nu = 100$ a.u. for different coupling strengths; solid line: $\eta = 4.56 \times 10^{-5}$ a.u., dashed line: $\eta = 2.27 \times 10^{-4}$ a.u., dotted line: result for the uncoupled double slit

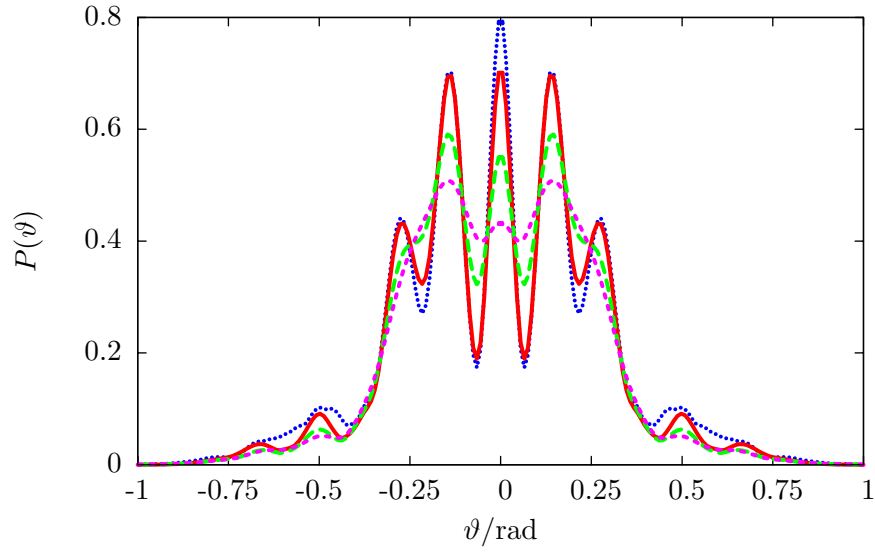


Figure 4.20: Angular distribution for a barrier coupled to a bath with 5 bath modes, $\eta = 4.56 \times 10^{-5}$ a.u. and a fixed range parameter $\nu = 100$ a.u. for various bath temperatures; solid line: $T = 0$, long dashes: $T = 400$ K, short dashes: $T = 1000$ K, dotted line: result for the uncoupled double slit

incoherent contributions. A further increase of the coupling range leads to a smearing of the diffraction pattern with less prominent peaks. Eventually, for the largest range parameter shown, the higher order peaks (4th and higher)) have virtually vanished. The same qualitative behavior can be seen in Fig. 4.19, where the coupling strength η is varied, still with a zero temperature bath. Finally, the alteration of the bath temperature, as presented in Fig. 4.20, is the physically most interesting case showing a similar change of the diffraction image as in the cases before. However, for the highest regarded temperature, even the lower order peaks are strongly smeared. Moreover, the central peak has almost vanished and two remaining broader ones are left, suggesting a virtually fully incoherent reduced density. This is equivalent to the statement, that the sum of partial amplitudes has turned into a sum of probabilities, i.e. the angular distribution is a sum of two partial distributions that can be related to particles passing the right or the left slit solely.

So far, systems coupled to low-frequency baths allowing only pure decoherence have been studied. In the next chapter we will discuss resonant baths allowing for energy transfer, i.e. dissipation.

5 Energy Dissipation

In addition to pure decoherence, the exchange and flux of SOI energy into the bath, i.e. dissipation, plays an important role in the theory of open quantum systems. Moreover, this phenomenon is already known in classical mechanics, where it turns out to be the only effect of the interaction between a SOI and a thermal bath. However, classical mechanics does not reproduce the correct transient dissipative dynamics [53] and does not lead to correct thermalization [115].

For the investigation of dissipation, the finite bath needs to have a cutoff frequency that is larger than a typical characteristic frequency of the SOI, e.g. the frequency of the harmonic approximation of a bound system. For this dissipative bath, we compare SCHD results to semiclassical Brownian motion (SCBM) ones. SCBM is a method that treats the bath as a reservoir, i.e. an infinitely large environment. At the heart of the SCBM is again the HK propagator applied to the system DOF. The main difference to the SCHD lies in the treatment of the bath, whose influence on the SOI is accounted for implicitly via a complex stochastic force [57, 116]. In the SCBM the averaging over a number of these complex force realizations goes along with the Monte-Carlo sampling within the computation of the HK phase-space integral. Comparing both methods we find, how many bath modes are necessary in the explicit scheme to obtain thermal equilibrium, and to check, which bath modes are responsible for dissipative effects. The SCBM results to be compared with have been provided by W. Koch.

In this chapter, two systems will be investigated: The dissipative harmonic oscillator, which is a convenient test system since we can refer to an analytic solution, and the more sophisticated and physically more relevant dissipative Morse oscillator that has been studied already in Chapter 4. In addition, the time scales of dissipation and decoherence, the two prominent processes in open quantum systems, will be compared for a finite bath.

5.1 Damped Harmonic Oscillator

The first test system for the investigation of dissipation effects is the harmonic oscillator, which is one of the simplest bound systems, with the potential given in Eq. (2.11). Moreover, there is an analytical solution available for the time evolution of the second momentum of position of a wave packet in a harmonic oscillator coupled to an infinite CL bath with a particular spectral density, which is reviewed in the next subsection. It will serve as the reference result in the subsequent part, where finite-bath SCHD results are compared with SCBM results for infinite baths.

5.1.1 Analytical Expectation Values

In the following, an analytical result for the time evolution of position's second moment of a wave packet in a one-dimensional dissipative harmonic oscillator will be presented,

following [117] together with [118]. The spectral density is assumed to be Ohmic with a Drude-Lorentz cutoff

$$J_D(\omega) = \frac{\eta\omega}{1 + \omega^2/\omega_c^2}, \quad (5.1)$$

where ω_c is the cutoff frequency. The time evolution of the second moment of position can then be described by

$$\begin{aligned} \langle s^2 \rangle_t = & \dot{G}^2(t) \langle s^2 \rangle_0 + \frac{1}{M^2} \dot{G}^2(t) \langle p_s^2 \rangle_0 + \frac{1}{M} G(t) \dot{G}(t) \langle p_s s + s p_s \rangle_0 \\ & + \left[1 - \frac{S^2(t)}{\langle s^2 \rangle_{\text{eq}}^2} \right] \langle s^2 \rangle_{\text{eq}} + 2G(t) \dot{S}(t) + \frac{1}{M^2} G^2(t) \langle p_s^2 \rangle_{\text{eq}}, \end{aligned} \quad (5.2)$$

with the initial expectation values given for a Gaussian at rest

$$\begin{aligned} \langle s^2 \rangle_0 &= \langle s \rangle_0^2 + \frac{1}{2\gamma_s} \\ \langle p_s^2 \rangle_0 &= \langle p_s \rangle_0^2 + \frac{\gamma_s}{2} \\ \langle p_s s + s p_s \rangle_0 &= 0, \end{aligned} \quad (5.3)$$

Eq. (5.2) also contains the equilibrium expectation values

$$\begin{aligned} \langle s^2 \rangle_{\text{eq}} &= \frac{1}{M\beta} \sum_{n=-\infty}^{\infty} \left[\omega_s^2 + \nu_n^2 + \frac{\eta|\nu_n|\omega_c}{M(\omega_c + |\nu_n|)} \right]^{-1} \\ \langle p_s^2 \rangle_{\text{eq}} &= \frac{M}{\beta} \sum_{n=-\infty}^{\infty} \frac{\omega_s^2 + \frac{\eta|\nu_n|\omega_c}{M(\omega_c + |\nu_n|)}}{\omega_s^2 + \nu_n^2 + \frac{\eta|\nu_n|\omega_c}{M(\omega_c + |\nu_n|)}}, \end{aligned} \quad (5.4)$$

with the inverse bath temperature β , the oscillator mass M and the Matsubara frequencies

$$\nu_n = \frac{2\pi n}{\hbar\beta}. \quad (5.5)$$

Furthermore, the equation for the second moment contains the Green's function

$$G(t) = c_1 e^{-\lambda_1 t} + c_2 e^{-\lambda_2 t} + c_3 e^{-\lambda_3 t}, \quad (5.6)$$

where $\lambda_{1,2,3}$ are the solutions of the cubic equation

$$\lambda^3 - \omega_c \lambda^2 + \left(\omega_s^2 + \frac{\eta}{M} \omega_c \right) \lambda - \omega_s^2 \omega_c = 0, \quad (5.7)$$

which can be solved by applying Cardano's method. The coefficients in Eq. (5.6) are

$$\begin{aligned} c_1 &= -\frac{\imath}{2\mu} \frac{\alpha - \imath\mu + \delta}{\alpha + \imath\mu - \delta} \\ c_2 &= \frac{\imath}{2\mu} \frac{\alpha + \imath\mu + \delta}{\alpha - \imath\mu - \delta} \\ c_3 &= \frac{2\alpha}{(\alpha - \imath\mu - \delta)(\alpha + \imath\mu - \delta)} \end{aligned} \quad (5.8)$$

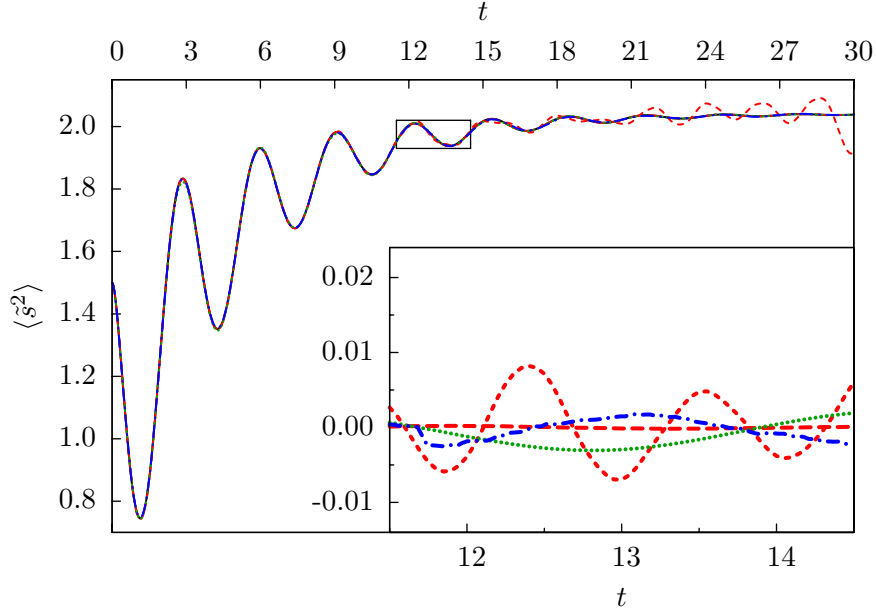


Figure 5.1: Second moment of position of the harmonic oscillator for $\eta = 0.2$, $\beta = 0.5$; solid line: analytical, short dashes: SCHD with frequency distribution (5.12) and 40 modes, long dashes: the same as before but with 100 modes, dotted line: SCHD with frequency distribution (5.13) and 300 modes, dash-dotted line: SCBM; Inset: Difference between the numerical results and the analytical expression

and the abbreviations can be extracted from the relations

$$\begin{aligned} \lambda_{1/2} &= \alpha \pm i\mu & \alpha, \mu &\in \mathbb{R} \\ \lambda_3 &= \delta & \delta &\in \mathbb{R}. \end{aligned} \quad (5.9)$$

Finally, the term

$$S(t) = d_1 e^{-\lambda_1 t} + d_2 e^{-\lambda_2 t} + d_3 e^{-\lambda_3 t} - \frac{2\eta}{\beta} \sum_{n=1}^{\infty} \frac{\omega_c^2 \nu_n e^{-\nu_n t}}{(\lambda_1^2 - \nu_n^2)(\lambda_2^2 - \nu_n^2)(\lambda_3^2 - \nu_n^2)} \quad (5.10)$$

is included in Eq. (5.2) as well as its time derivative. The corresponding coefficients read

$$d_i = c_i \frac{\hbar}{2M} \cot\left(\frac{\pi \lambda_i}{\nu_1}\right). \quad (5.11)$$

In principle the expression in Eq. (5.2) is exact given that enough terms are incorporated in the sums containing the Matsubara frequencies.

5.1.2 Comparison With an Infinite Bath

Now, results for the harmonic oscillator coupled to a finite bath, obtained with the SCHD, will be compared with infinite-bath results computed with the SCBM, while the analytical

result will be the reference. For the numerical calculations, dimensionless units are used. The frequency of the oscillator is chosen as $\omega_s = 1$ and the mass is set to unity. Initially the wave function is a Gaussian with displacement $s_i = 1$, width parameter $\gamma_s = 1$ and zero momentum. Consistently with the analytical result, the spectral density is Ohmic with a Drude-Lorentz cutoff as given in Eq. (5.1) with the cutoff frequency $\omega_c = 10$, such that resonant coupling and hence dissipation is possible. As mentioned before, the modes of the finite bath treated explicitly in the SCHD need to be chosen according to a particular density of frequencies which is not unique. In order to explore the influence of this choice on the final result, first, two different frequency distributions are chosen [23, 51]

$$\rho_f^{(1)}(\omega) = a_1 \omega^{-1/2} \quad (5.12)$$

$$\rho_f^{(2)}(\omega) = a_2 \frac{J_D(\omega)}{\omega} = a_2 \frac{\eta}{1 + \omega^2/\omega_c^2}, \quad (5.13)$$

where a_1 and a_2 are normalization coefficients determined from the normalization condition given in Eq. (2.9) with $\omega_{\max} = 2\omega_c$. More details can be found in Appendix A.

In Fig. 5.1 the second moment of position versus time is shown for the harmonic oscillator. The coupling strength is $\eta = 0.2$ and the inverse temperature $\beta = 0.5$. Besides the analytical result, two curves for the frequency distribution (5.12), one curve for the frequency density (5.13) and the SCBM result are plotted. Except for the result with 40 bath modes (for the sampling density (5.12)), all other results are converged towards the analytical one within line thickness and we had to plot the differences to the analytical result as an inset to unveil the deviations.

In the finite bath case, using only 40 modes is not enough to reach an equilibrium of the SOI on the observed time scale and coherent oscillations can be observed for longer times. Increasing the number of modes to 100 is sufficient to obtain a converged result showing almost no deviations from the analytical result even in the more detailed inset plot in Fig. 5.1.

The third SCHD graph represents the result obtained with the Lorentzian density (5.13). Although the threefold number of modes is used, the result does not achieve the same quality of agreement with the analytical graph, which highlights the importance of choosing an appropriate distribution of the bath modes. However, this dependence on the frequency distribution is manifest only for a finite number of modes and the choice of the sampling density becomes irrelevant in the limit of infinitely many bath oscillators. The density (5.12) places more emphasis on modes with lower frequency, i.e. modes below and near the system frequency $\omega_s = 1$ supporting resonant energy transfer.

In addition, to highlight the importance of resonant modes for dissipation, additionally a frequency distribution of Gaussian form is employed

$$\rho_f^{(3)}(\omega) = a_3 e^{-b(\omega - \omega_s)^2}, \quad (5.14)$$

again with the normalization coefficient a_3 . This distribution is peaked at the harmonic system frequency, so that mainly resonant and near-resonant bath modes are sampled depending on the width parameter, which is here chosen as $b = 0.125$. In Fig. 5.2, results for this frequency density and the one from (5.12) are compared. It is remarkable that the number of already 40 bath modes is sufficient to achieve thermal equilibrium with the Gaussian density. However, comparison of both frequency densities at 100 modes, where

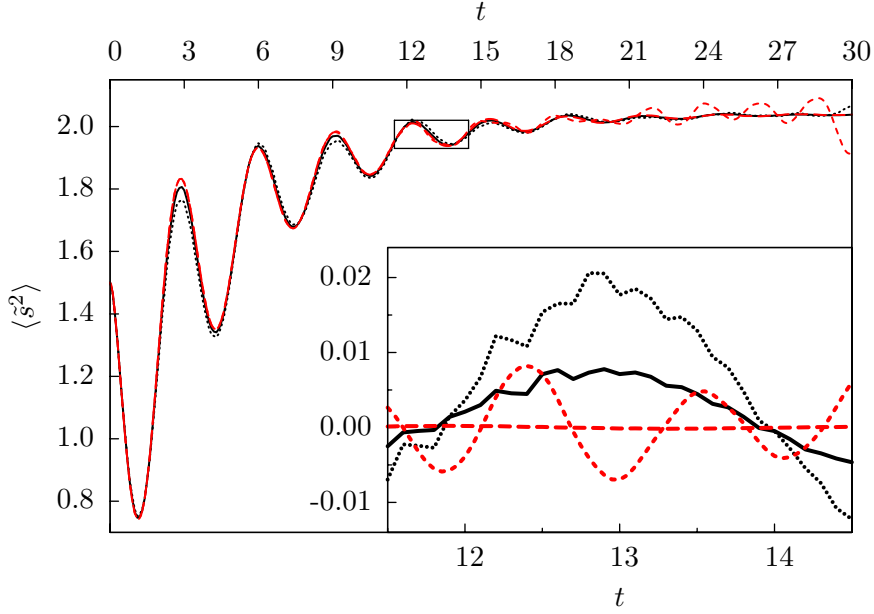


Figure 5.2: Second moment of position of the harmonic oscillator for $\eta = 0.2$, $\beta = 0.5$; dotted line: SCHD with frequency density (5.14) and 40 modes; solid line: the same as before but with 100 modes; short dashes: SCHD with frequency density (5.12) and 40 modes; long dashes: the same as before but with 100 modes; Inset: Difference between the numerical results and the analytical expression

both results are equilibrated, still reveals differences in the time evolution of the second moment of position. Thus we can conclude, that a sampling density of Gaussian form is appropriate in case equilibrium should be reached with as little bath modes as modes as possible. On the other hand, the convergence behavior for an increasing number of modes regarding the detailed time evolution is worse for the Gaussian distribution than in the case of the density (5.12). We point out that for the harmonic oscillator case, the SCHD method needs only a *single* trajectory for the dynamics of all modes, since all DOFs can be treated on the level of the TGWD.

5.2 Damped Molecular Oscillator

Now, we investigate the anharmonic molecular oscillator with the potential given in Eq. (2.19), which is a physically more interesting system without a closed analytical solution for the system-bath case. First, similar to the harmonic oscillator case in the previous section, finite-bath results are compared with the dynamics for an infinite one. In a second subsection for an explicitly resonant bath, i.e. a bath consisting of only resonant and near-resonant modes, decoherence is compared with dissipation concerning the time scale of the particular process.

5.2.1 Comparison With an Infinite Bath

For the comparison of SCHD and SCBM results, the dimensionless potential parameters are chosen to be $D = 30$ and $\alpha = 0.08$, which gives a strong anharmonicity if the initial

Gaussian is centered at $s_i = 1$ with zero momentum and a width parameter $\gamma_s = 1$. Again, the mass is set to unity. For numerical reasons concerning the SCBM, an Ohmic spectral density with a quadratic algebraic cutoff is used

$$J_q(\omega) = \frac{\eta\omega}{(1 + \omega^2/\omega_c^2)^2}, \quad (5.15)$$

which is narrower than the one with a Drude-Lorentz cutoff. With the given parameters, the frequency of small oscillations around the minimum is $\omega_s = 0.62$. Thus the choice of the cutoff frequency $\omega_c = 5$ is sufficient to ensure resonant coupling. Since the resonant bath modes lead to the most effective dissipative coupling and the number of modes is to be kept small in the case of the SCHD, the Gaussian distribution of frequencies from Eq. (5.14) with $b = 0.65$ was chosen for the numerical calculations.

However, in the dissipative Morse oscillator we encounter a problem which is not present in the non-dissipative case. That is, the resonant harmonic bath modes are considerably influenced by the anharmonicity of the SOI. Hence, the SCHD may fail after a short time if *all* bath modes are treated on the level of the TGWD.

There are two possibilities to address this problem. One idea is based on the fact that the coupling coefficient c_i in the CL Hamiltonian and thus the effective coupling to every single bath mode decreases with increasing number of bath modes like $1/\sqrt{N_B}$. Hence, we could still treat the entire bath with TGWD if a high enough number of modes is taken such that every single mode is sufficiently weakly coupled, leaving its harmonicity nearly unperturbed on the observed time scale. With the SCHD scheme, 20 bath modes were found to be sufficient to attain a thermal equilibrium on the observed time scale. However, the limiting values differ significantly from those obtained with the SCBM and even more, an increase of the number of bath modes by a factor of five does not change the SCHD result considerably (not shown here). Therefore, this approach turns out to be impractical, since excessively many bath modes would be necessary, i.e. a decrease of the effective coupling by an order of magnitude would involve a hundredfold increase of the number of bath modes.

Another possibility to address the problem of the significant anharmonic influence on the resonant bath modes is to treat some of them on the more accurate level of the HK approximation in addition to the SOI. In practice, this means that the “most” resonant bath DOFs, i.e. the ones whose frequencies are closest to the anharmonic system’s frequency, are included into the multi-trajectory phase space integral. In Fig. 5.3, results obtained with SCBM and with SCHD (and 20 bath modes) are shown. The number of bath modes treated with the HK approximation, here called HK-modes, is varied and a convergence towards the SCBM result is clearly visible. For 3 HK-modes, the SCHD result for the position expectation value is very close to the SCBM result, while, obviously, the convergence of the variance for increasing number of HK-modes is slower. However, besides the circumstance that the second moment is much more sensitive to fluctuations in the HK phase space integral, it also reflects residual deviations from the correct reduced density much stronger. Still it is remarkable that treating only three out of twenty bath modes as HK-modes, i.e. the modes with frequencies $\omega_1 = 0.57$, $\omega_2 = 0.64$ and $\omega_3 = 0.71$, is sufficient to converge the graph towards the SCBM results. It should be noted that in the considered case the SCHD as well as the SCBM fail to maintain exact norm conservation for the anharmonic SOI with a deviation of 30-40% respectively 10-20 %. Thus the presented results are obtained via renormalization [119, 73, 120], i.e. by dividing the result by its norm.

In the case investigated above, the temperature and coupling strength are such, that

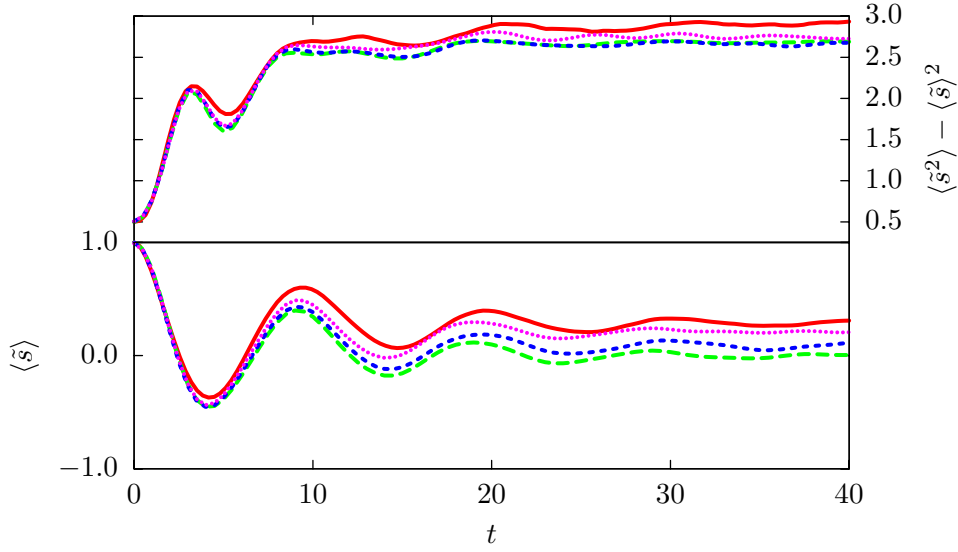


Figure 5.3: Variance and expectation value of position of the Morse oscillator for $\eta = 0.2$ and $\beta = 1.0$; solid line: SCBM result; long dashes: SCHD with 0 HK-modes; short dashes: SCHD with 1 HK-mode; dotted line: SCHD with 3 HK-modes; all SCHD results are for a total of 20 bath modes; For the SCHD results the number of necessary integration sampling points varies from 2×10^4 to 1×10^7 ; The number of trajectories taken to obtain the SCBM result is 1×10^7

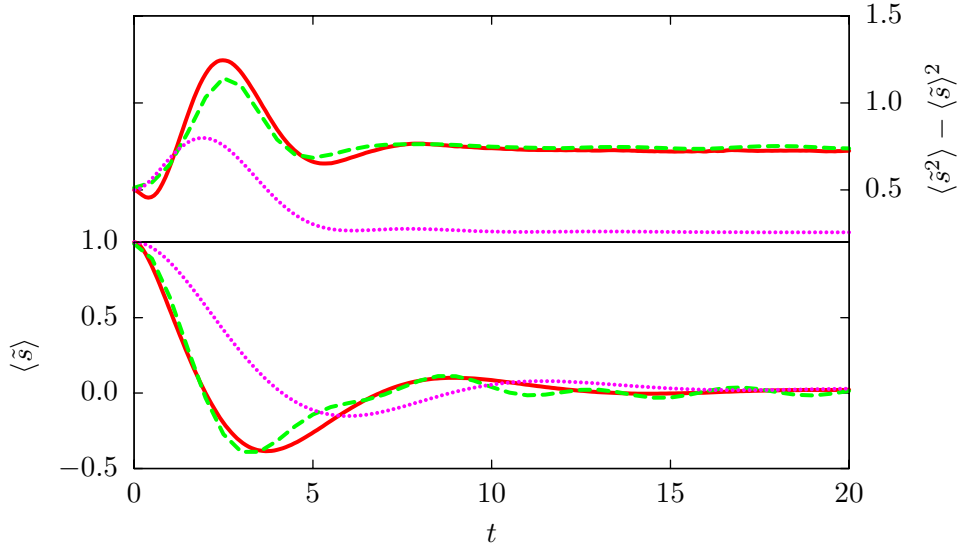


Figure 5.4: Variance and expectation value of position of the Morse oscillator for $\eta = 0.5$ and $\beta = 10.0$; solid line: SCBM result; dashed line: SCHD with 1 HK-mode and a total of 20 bath modes; dotted line: CL master equation result

also a Markovian approximation could be valid. That is either the quantum Brownian limit, valid for high temperatures and strictly Ohmic coupling, or the quantum optical limit, valid for weak coupling (more on this in [121]). In order to investigate a more demanding, typically non-Markovian quantum case, results for a lower temperature and stronger coupling are presented in Fig. 5.4. Here, for the SCHD one single HK-mode was already sufficient to obtain a good agreement with the SCBM result, which is probably due to the lower temperature of the bath leading to a narrower initial (thermal) state in position space of every single mode, which again is less affected by the anharmonicity of the SOI than a broader state. Thus the considered parameter regime is well covered by the explicit SCHD method. The small deviations between the two semiclassical results are due to the specific sampling of the bath frequencies and therefore due to the finiteness of the bath. For reasons of comparison, additionally the result gained with the high temperature Markovian CL master equation [8, 122] are displayed, showing a strong deviation from the two non-Markovian approaches, which are not restricted to high temperatures.

5.2.2 Dissipation vs Decoherence

So far, decoherence and dissipation have been explored separately depending on the cutoff frequency's magnitude compared to a typical system frequency. However, we want to compare the influence of each of these processes on the system dynamics in a finite bath, particularly in order to compare their different time scales. To this end, we choose the same parameters for the Morse oscillator and the same dissipative bath with frequencies distributed according to a Gaussian density as in the previous section. Also, the spectral density is of Ohmic form with a quadratic cutoff as described by Eq. (5.15).

For the estimation of the dissipation time scale, we consider the time evolution of the energy expectation value defined in Eq. (4.17) (for an elaborate calculation of the corresponding SCHD expression see Appendix D).

In Fig. 5.5, the energy expectation value is plotted for $\eta = 0.05$ as well as a bath with 20 modes and $\beta = 1000.0$ for a maximum time of about ten vibrational periods. The wave packet is started at $s_i = -3.0$. The inset of Fig. 5.5 shows the corresponding purity on a shorter time scale. For the estimation of the decoherence time we have to consider the circumstance that the decrease of the purity is weakened due to the relaxation of the system towards the ground state. Thus, fewer energy eigenstates become significantly occupied in time, yielding a mixed state with a decreasing basis. In other words, fewer eigenstates account for the mixed state in time. Thus, under the given conditions, the estimated decoherence time will represent a lower bound.

Also initially the energy expectation value increases slightly. The reason for this is the fact, that the interaction term in the CL Hamiltonian is not accounted for in the computation of the expectation value, although it also depends on the system DOF (more on this in Appendix D). However, for a sufficiently weak coupling, which is the case here, this contribution can be neglected.

Although the observed dynamics is non-Markovian, the mean course of both curves can be approximated by an exponential decay in each case. In doing so, we find a dissipation time of $\tau_{\text{diss}} = 20$ fs, which is higher by a factor of two than the decoherence time, i.e. $\tau_{\text{dec}} = 9$ fs. Even these results, obtained under the given conditions with a finite zero-temperature bath, still corroborate statements that decoherence always happens faster than dissipation [94, 123, 124, 76]

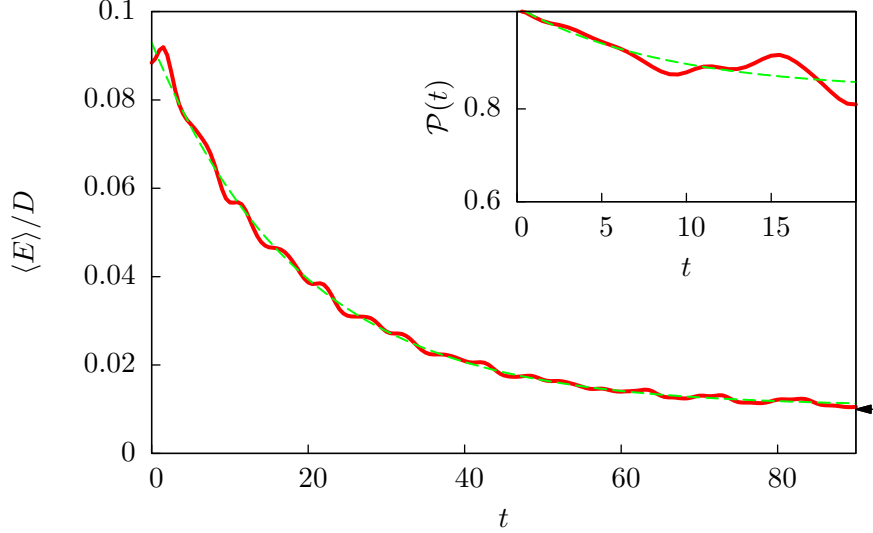


Figure 5.5: Time evolution of the energy expectation value for the initial Gaussian centered around $s_i = -3.0$, coupling strength $\eta = 0.05$ and $\beta = 1000.0$; Inset: Purity of the same system versus time; Dashed lines: exponential fits of the corresponding curves; The arrow marks the ground state energy of the Morse oscillator

5.2.3 Decoherence in a Resonant and Non-resonant Bath

Knowing that the bath temperature, coupling strength and the initial state strongly influence the coherence dynamics, in addition we want to know how far the choice of the bath modes affects the time-evolution of the purity. To this end we consider two different baths, a non-resonant and a resonant one. The non-resonant bath has a spectral density of Ohmic form with an exponential cutoff, which is given in Eq. (4.2), and with the cutoff frequency $\omega_c = 9.1 \times 10^{-5}$ a.u. The frequency distribution is the same as in Eq. (4.3) with a maximum frequency $\omega_{\max} = 5\omega_c$. With this choice, the effective coupling coefficient of the SOI DOF in the CL Hamiltonian in Eq. (2.6) becomes independent of the mode frequency and thus the same for every bath mode

$$\tilde{c} \equiv \frac{c_i}{\omega_i} = \sqrt{\frac{2}{a\pi}}. \quad (5.16)$$

Now we consider a resonant bath with the discrete spectral density

$$J(\omega) = \frac{\pi}{2} \sum_i \frac{c_i^2}{\omega_i} \delta(\omega - \omega_i) = \frac{\pi}{2} \sum_i \tilde{c} \omega_i \delta(\omega - \omega_i), \quad (5.17)$$

where the arbitrary choice $c_i = \tilde{c} \omega_i$ was made for the coupling coefficient. In doing so, we ensure that the effective coupling to every single bath mode is fixed and thus the equal for both the non-resonant and resonant case. This allows for the investigation of the influence of the choice of bath modes on the SOI dynamics. The bath frequencies of the resonant bath are chosen according to

$$\omega_i = \omega_1 + \frac{i}{N_B - 1} \Delta\omega, \quad (5.18)$$

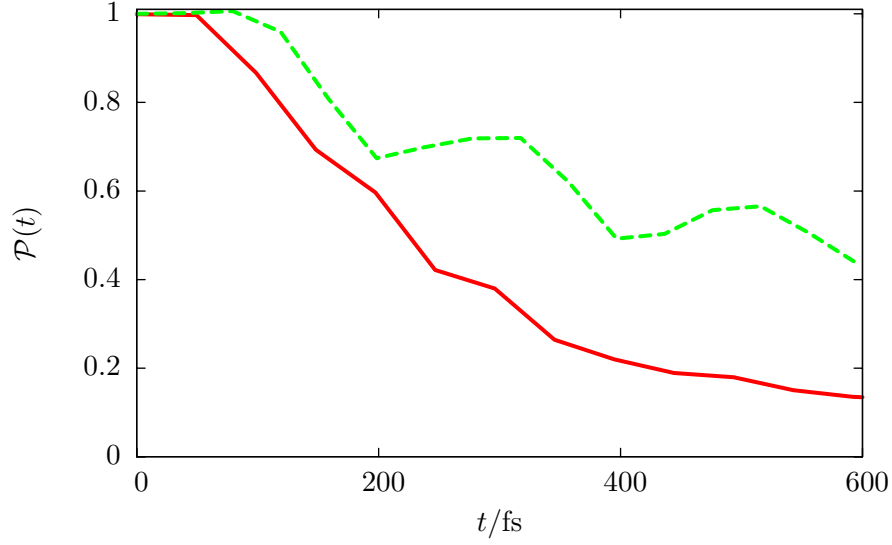


Figure 5.6: Purity for two different baths each with 20 bath modes, $\eta_{\text{eff}} = 0.25$ and zero temperature; solid line: resonant bath with frequencies chosen according to Eq. (5.18); dashed line: low frequency bath

with a lower bound $\omega_1 = 7.3 \times 10^{-4}$ a.u. and a range of $\Delta\omega = 4.6 \times 10^{-4}$ a.u. such that all bath frequencies are in the neighborhood of the resonance frequency. Both baths consist of 20 modes and have zero temperature. Again, the SOI is a Morse oscillator with parameters of the Iodine molecule given in Section 4.1, i.e. $D = 0.057$ a.u., $\alpha = 0.983$ a.u., $s_e = 5.04$ a.u. and the reduced mass of this system $M = 1.165 \times 10^5$ a.u..

In Fig. 5.6, the purities for the low-frequency and the resonant bath are plotted for a fixed coupling strength. Obviously, resonant coupling leads to an essentially stronger decoherence rate than the non-resonant one.

We note that, in the case of resonant coupling all bath modes are treated on the level of TGWD and thus the SCHD may become less accurate, as shown in Section 5.2.1. However, considering the zero temperature bath and the relatively short time scale of only three periods, the accuracy is sufficient for the investigation of the purity dynamics.

So far, only systems coupled to a harmonic bath were studied. In the next chapter, we turn to a molecular SOI, which is surrounded by a noble gas matrix with a specific structure forming the environment.

6 A realistic system - Iodine in a Krypton environment

The CL model is an appropriate model for the description of a thermal bath, whose specific form is generally unknown. Here, we go beyond the CL description of the bath in terms of harmonic oscillators and apply the SCHD to a system-bath problem, where we know the (microscopic) structure of the environment.

This particular study is motivated by a recent experiment investigating I_2 embedded in a van der Waals Krypton solid was investigated [125]. Within a pump-probe scenario, a so-called four-wave mixing experiment, the I_2 was laser-excited into a coherent vibrational cat-state superposition. As a result of the subsequent dissipative dynamics, coherent vibrations of the Krypton lattice were observed for many vibrational periods.

In the following, a simplified model for the Krypton cage will be presented in some detail. Subsequently we discuss the results obtained with the SCHD.

6.1 The Model

For the numerical treatment of the overall system, a simplification of the environment, i.e. the Krypton solid, is necessary. Thus, we reduce the Krypton matrix to the first micro-solvation shell, comprising 17 Kr atoms that are arranged as a double-icosahedron surrounding the I_2 molecule as shown in Fig. 6.1.

Within this treatment all atom-atom interactions are accounted for. Thus, the full potential is a sum over all pair potentials

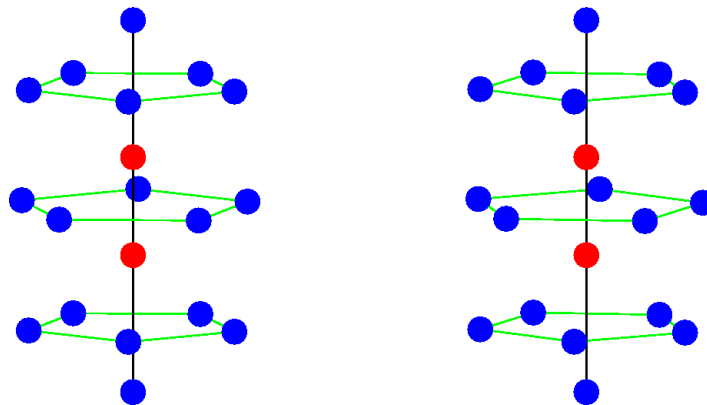


Figure 6.1: Stereoscopic image of I_2 in a Kr_{17} cage in equilibrium

Red: I atoms; Blue: Kr atoms

The I_2 has a common axis with two Kr atoms and the other 15 Kr atoms form three pentagons arranged around this axis

$$\mathcal{V} = \sum_{\substack{K,J=1 \\ K < J}}^{N_a} \mathcal{V}_{KJ}, \quad (6.1)$$

where $N_a = 19$ is the number of atoms and the capital letters are atom indices. Three kinds of pair potentials have to be considered, depending on the kind of atoms that interact. All potential parameters given below are taken from Ref. [126].

The rotation of the I_2 is not accounted for and thus the I-I interaction is described by the Morse potential in Eq. (2.19). We are only interested in the dynamics after the excitation of the I_2 and hence the Morse parameter for its electronic B-state are taken, i.e. $D_{\text{I-I}} = 0.021$ a.u., $\alpha_{\text{I-I}} = 0.98$ a.u. and $R_{\text{I-I,e}} = 5.7$ a.u., which now denotes the internuclear equilibrium distance of two I atoms, each with mass $m_{\text{I}} = 231323$ a.u.. Consequently, the period of the harmonic approximation is about 258 fs.

Regarding the I_2 -Kr interaction, we use a superposition of Σ and Π potentials of I_2

$$\mathcal{V}_{\text{I}_2\text{-Kr}} = \frac{1}{2} [\mathcal{V}_{\Sigma}(R_{\text{I}(1)\text{-Kr}}) + \mathcal{V}_{\Pi}(R_{\text{I}(1)\text{-Kr}})] + \frac{1}{2} [\mathcal{V}_{\Sigma}(R_{\text{I}(2)\text{-Kr}}) + \mathcal{V}_{\Pi}(R_{\text{I}(2)\text{-Kr}})] , \quad (6.2)$$

where the index $\text{I}(K)$ denotes the K th I atom. Both potentials can be modeled by the Morse potential, too. Here, the parameters $D_{\Sigma} = 0.001$ a.u., $\alpha_{\Sigma} = 0.79$ a.u. and $R_{\Sigma} = 7.05$ a.u. are used for the Σ part. Furthermore, the parameters for the Π part are $D_{\Pi} = 0.0006$ a.u., $\alpha_{\Pi} = 0.81$ a.u. and $R_{\Pi} = 8.1$ a.u.

Finally, the Kr-Kr interaction is of van der Waals type, which is approximated by the Lennard-Jones potential

$$\mathcal{V}_{\text{LJ}}(R_{KJ}) = 4\varepsilon \frac{\sigma^6}{R_{KJ}^6} \left(\frac{\sigma^6}{R_{KJ}^6} - 1 \right) + \varepsilon. \quad (6.3)$$

It looks very similar to the Morse potential shown in Fig. 2.4, except that usually the attractive force is weaker in the Lennard-Jones potential. The parameter ε is the asymptotic limit of the potential for $R_{KJ} \rightarrow \infty$ (similar to D in the Morse oscillator) and σ can be interpreted as the distance on the repulsive side of the potential, where $\mathcal{V}_{\text{LJ}}(\sigma) = \varepsilon$. The parameters are chosen as $\sigma = 6.8$ a.u. and $\varepsilon = 0.0009$ a.u. Furthermore, the mass of a Kr atom is $m_{\text{Kr}} = 152757$ a.u.

Since the overall system has 57 DOFs, we need to reduce the complexity of the problem. To this end, we introduce normal coordinates Q_j that are related to (mass-weighted) cartesian difference coordinates via a linear transformation

$$Q_j = \sum_k a_{kj} \tilde{q}_k \quad \tilde{q}_k = \sqrt{m_k} \Delta x_k, \quad (6.4)$$

with m_k the mass of the atom that is associated with the k th DOF. The coordinate Δx_k denotes the displacement from the equilibrium position of an atom in the $\text{I}_2\text{-Kr}_{17}$ cluster, while I_2 is in its electronic X-state (we note that, although the normal modes are determined with respect to the X-state, the dynamics studied later takes place on the B-surface). More precisely, the normal modes introduced here are actually “pseudo”-normal modes, since certain interactions between I and Kr atoms were neglected in the normal mode analysis [127]. This was done in order to obtain pure I_2 and Kr_2 stretching modes. More on normal

mode analysis in general and how to determine the transformation matrix with elements a_{kj} can be found in [59].

In this normal coordinate system, we can focus on the modes that are most strongly coupled to the I_2 , and thus reduce the effective size of the overall system. We found three normal modes of the Krypton shell that have a remarkably stronger coupling to the I_2 stretching mode than all other normal modes. These modes are the Kr_2 stretching mode and two “cage” modes, i.e. the sandclock and rugby ball mode. In Fig. 6.2 these Krypton normal modes as well as the I_2 mode are sketched and a normal mode index is assigned. For the numerical treatment of this system, these four normal modes will be considered.

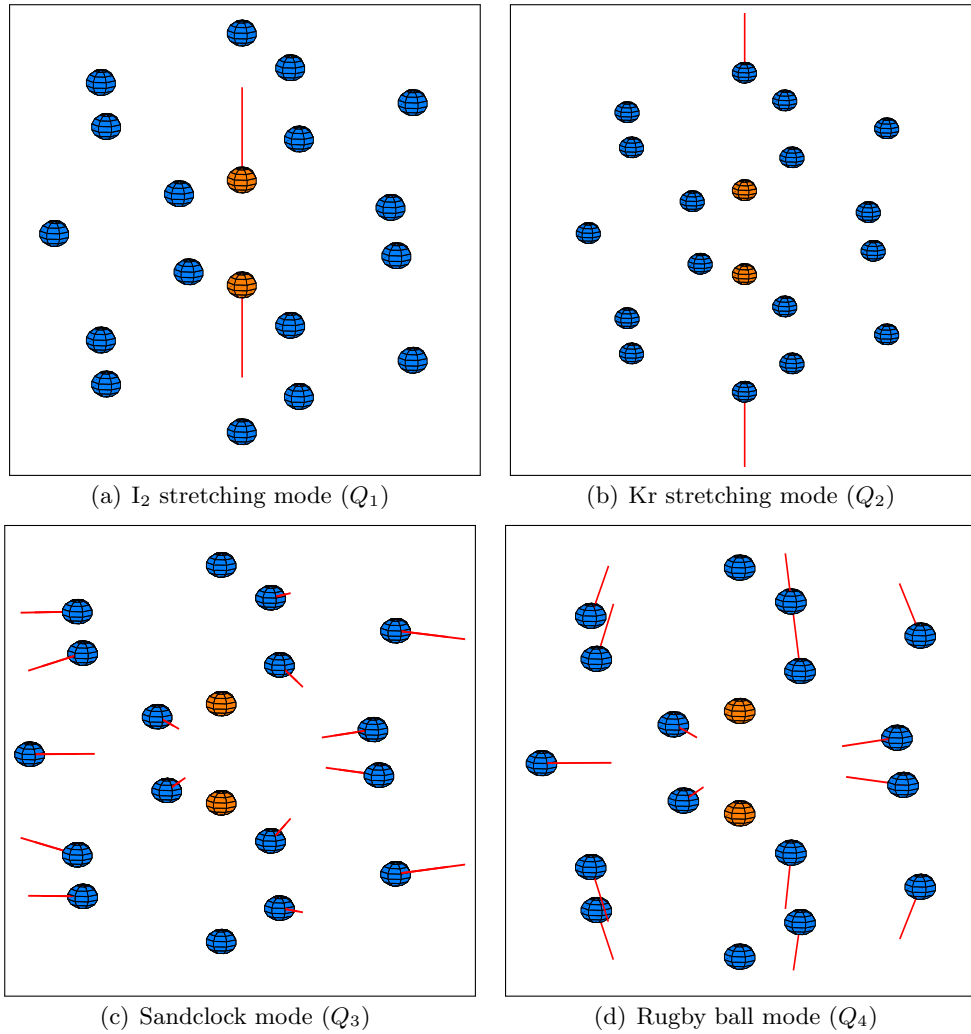


Figure 6.2: Normal modes of I_2 - Kr_{17} with the highest symmetry, where the modes shown in (b)-(d) have the strongest coupling to the I_2 mode in (a) (Figures were provided by M. Buchholz [127])

6.2 Vibrational Dynamics

With the presented model and the selected normal modes in place, we will now apply the SCHD to study the dynamics of this system. We note in passing, that we are interested in the dynamics of all considered DOFs. Thus, in contrast to the systems studied in the CL bath, there is no unique SOI here. In the experiment a double laser pulse prepares a coherent superposition, that is two distinct GWPs, on the B-surface of the I_2 , which is then taken as the “initial state” of the following dynamics in the I_2 DOF.

However, in this thesis, we choose an arbitrary initial cat-state as given in Eq. (4.6) since we are interested in the qualitative behavior of the system solely, without numerically determining the particular initial state. Hence, we place one GWP into the minimum of the B-state at $Q_{1,a} = 204.1$ a.u. and the other Gaussian on the repulsive side of the potential at $Q_{1,b} = 22.63$ a.u., each with zero initial momentum. Hence the latter GWP is centered around the 20th vibrational eigenstate. The width parameter of both Gaussians corresponds to the width of the ground state of the harmonic approximation or equivalently to the eigenfrequency of the I_2 stretching mode, i.e. $\gamma_1 = 22.25$ a.u.

In the other DOFs the respective GWP is initially located at the position that corresponds to the potential minimum, while the I_2 is in the X-state, i.e. $Q_i = 0$ ($i = 2...4$). Their width parameters correspond to the eigenfrequency of the particular normal mode, i.e. $\gamma_2 = 59.49$ a.u., $\gamma_3 = 61.54$ a.u. and $\gamma_4 = 69.83$ a.u., and they have zero initial momentum.

6.2.1 Three Normal Modes

In a first step, we compare three-dimensional SCHD results with full quantum ones. All reference quantum results have been obtained with the SPO and provided by M. Buchholz. First, the I_2 , Kr_2 and sandclock modes are considered, for which the purities are shown in Fig. 6.3 on a time scale in the order of 12 vibrational periods of the I_2 . Within the SCHD treatment, the I_2 mode is treated on the level of the HK approximation as well as the Kr_2 stretching mode, since its coupling to the I_2 mode is the strongest compared to all other normal modes. In contrast, we exploit the relatively weak coupling of the sandclock mode by treating this DOF on the level of TGWD. We find, that the agreement of the purities is very good, even for the sandclock mode, which is treated with a cruder approximation than the other modes. The largest deviation becomes manifest in the I_2 mode at larger times, where the SCHD result is below the full quantum one. However, up to this deviation, the quantum results are well reproduced by SCHD. We note, that for this system the deviation of the norm from unity is maximally 10% at larger times in the SCHD.

Now, the sandclock mode is replaced by the rugby ball mode. The corresponding purities are plotted in Fig. 6.4. Here the agreement of the SCHD with quantum results in all three modes is even better than in the previous case, except for times above $t = 2300$ fs, where the SCHD result for all modes is above the quantum one. Also, the norm deviates from unity by less than 15% at larger times. We note in passing, that for all SCHD results the necessary number of sampled trajectories is 10^5 , which is reasonable considering the eight-dimensional phase space integral and the length of the time scale.

The excellent agreement of the purities in the sandclock and rugby ball mode is surprising, the more so as both modes are treated on the level of an approximation in which the corresponding (reduced) density could be assumed to retain its Gaussian form. On the

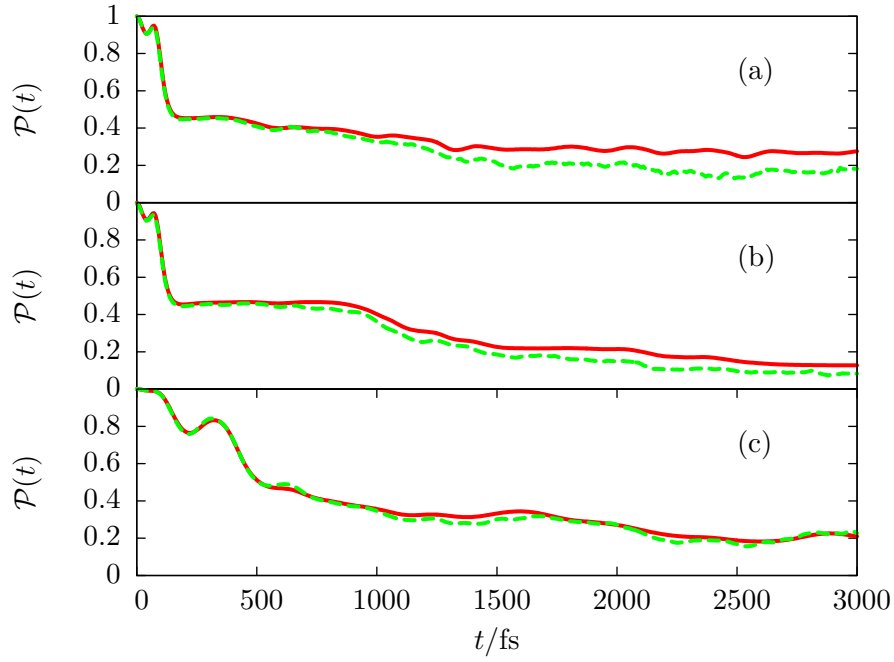


Figure 6.3: Time evolution of the purity of various normal modes for I_2Kr_{17} with I_2 , Kr_2 and sandclock mode; (a) I_2 stretching mode; (b) Kr_2 stretching mode; (c) Sandclock mode
solid lines: quantum results; dashed lines: SCHD results

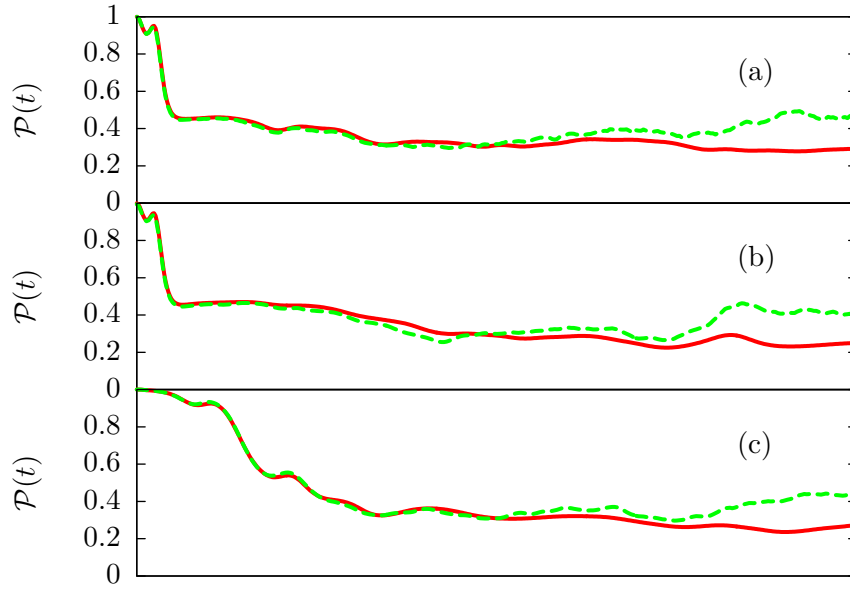


Figure 6.4: Time evolution of the purity of various normal modes for I_2Kr_{17} with I_2 , Kr_2 and rugby ball mode; (a) I_2 stretching mode; (b) Kr_2 stretching mode; (c) Rugby ball mode
solid lines: quantum results; dashed lines: SCHD results

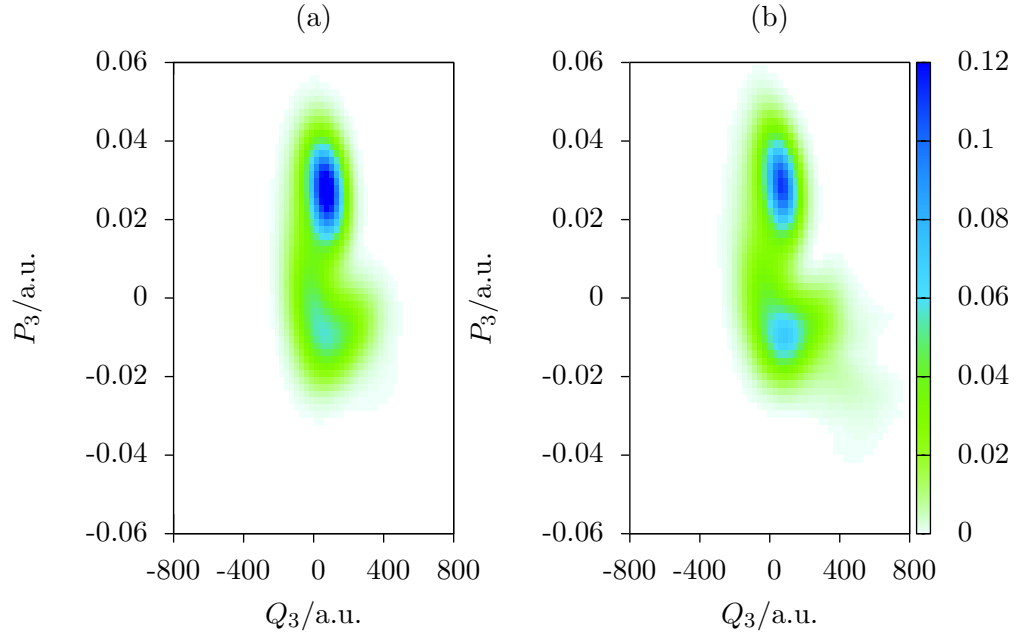


Figure 6.5: Snapshot of the sandclock mode Wigner function at 1320 fs considering three normal modes
 (a) full quantum result
 (b) SCHD result

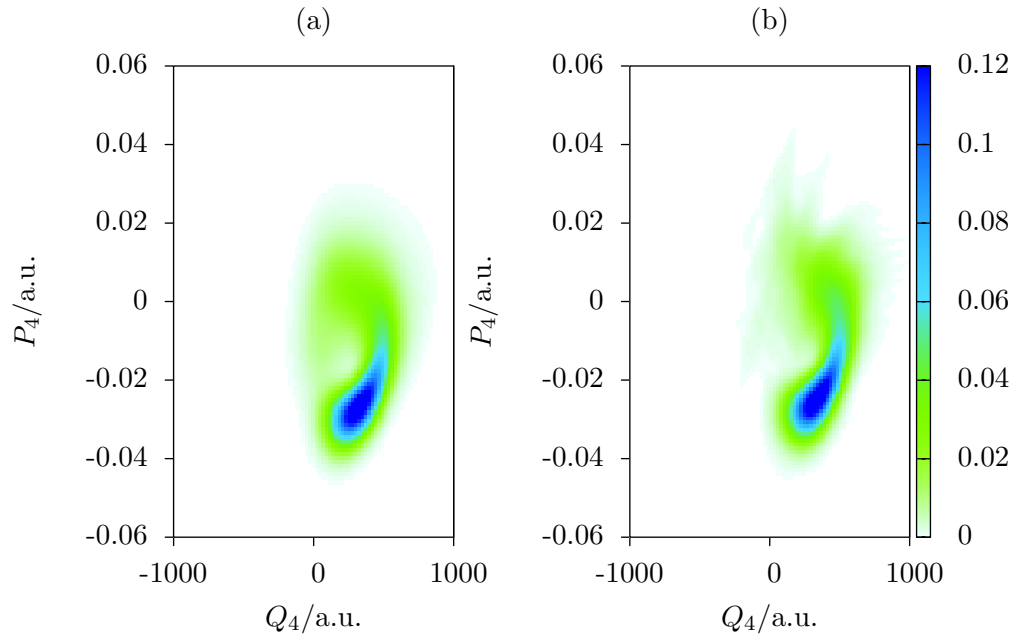


Figure 6.6: Snapshot of the rugby ball mode Wigner function at 1800 fs considering three normal modes
 (a) full quantum result
 (b) SCHD result

other hand, one might assume that in the full quantum treatment the initial Gaussian shape of the reduced density is distorted after a few periods due to the anharmonicity of the system. In order to shed light on this seemingly contradictory issue, we investigate the time evolution of the reduced density in the sandclock and rugby ball mode in more detail.

To this end, a snapshot of the SCHD Wigner function given in Appendix D is plotted in Fig. 6.5 for the sandclock mode at $t = 1320$ fs, which is after about five I_2 periods. Again, the SCHD result is compared with the full quantum one. The agreement of both results is obvious. Furthermore, we see that the initial superposition of two locally separated wave packets in the I_2 is reflected in the sandclock mode due to their mutual coupling. However, this superposition in the sandclock mode is incoherent, which is indicated by the lack of an interference pattern with negative parts between both “packets” in the Wigner function. The final aim of a larger project could be to find the conditions, for which a coherent superposition could be observed in the Krypton modes as was the case in the experiment. However, in this thesis we do not address this issue, since we want to investigate the properties of the SCHD and its capability of treating a system like the presented one. Returning to Fig. 6.5, one can see that both parts of the Wigner function are of slightly distorted Gaussian form, even in the SCHD. This circumstance suggests, that in the SCHD the TGWD DOFs generally do not keep their Gaussian shape. To see this more clearly, the Wigner function for the rugby ball mode is shown in Fig. 6.6 at time $t = 1800$ fs. The quantum result is very well reproduced by the SCHD and apparently its shape is different from the shape of a minimum uncertainty wave packet or a superposition of two of them.

How is it possible, that the reduced densities of the TGWD DOFs can deviate from a Gaussian shape in the SCHD and thus be so close to the accurate quantum results? To answer this question, we recall that the DOF on both levels of approximation, HK and TGWD, are coupled among each other via the classical dynamics. While the initial HK phase space points are sampled within the numerical integration, the initial phase space point of a TGWD DOF is fixed at the center of the corresponding initial GWP. However, due to the coupling to the HK DOFs, a trajectory associated with a TGWD DOF varies in the course of the HK phase space sampling. In other words, during the phase space integration, one obtains different trajectories in the TGWD DOFs, that emerge from a common initial phase space point. Therefore, strictly speaking, the integration over the HK DOFs comes along with an integration over a set of “thawed Gaussian”-trajectories in the SCHD, and thus the reduced density of a TGWD DOF is *not* restricted to a Gaussian shape. With this, we can conclude, that an approximation on the level of TGWD applied to a DOF, which is coupled to other HK DOFs, as in the SCHD, can still be accurate, even if weakly affected by anharmonic dynamics.

6.2.2 Four Normal Modes

So far, we have compared three-dimensional SCHD results with full quantum ones and found a good agreement. However, now we increase the number of DOFs by considering the most important normal modes, i.e. I_2 , Kr_2 , sandclock and rugby ball. This four-dimensional problem goes beyond the capability of a full quantum treatment with the SPO. In contrast, for the SCHD this is no restriction and thus it can be applied. Again, the phase space sampling within the framework of the integration is performed only for the I_2 and Kr_2 modes, while the rugby ball and sandclock modes are still treated on the level of TGWD. We note in passing, that also in the four-dimensional calculation 10^5 sampling

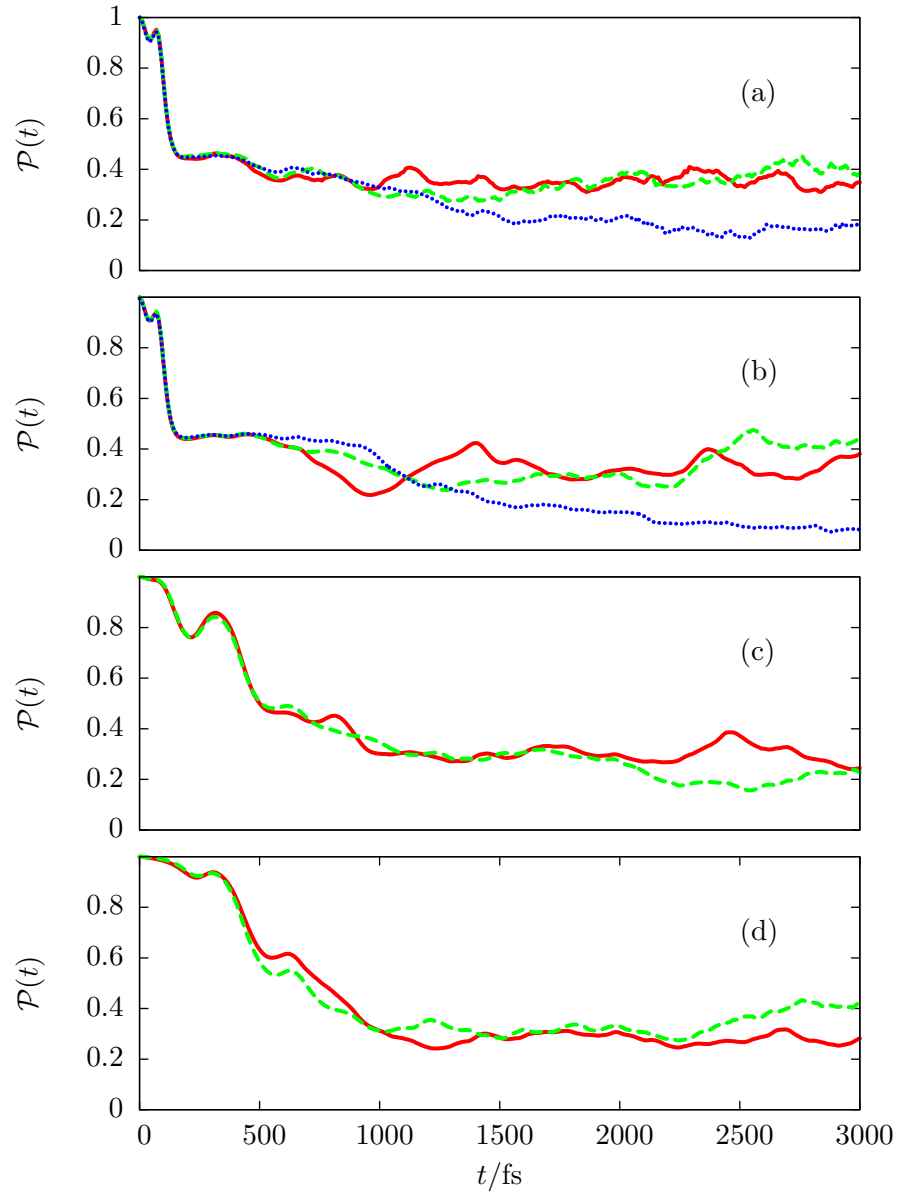


Figure 6.7: Time evolution of the SCHD purity of various normal modes

- (a) I_2 mode with: Kr_2 , sandclock and rugby ball mode (solid line); Kr_2 and rugby ball mode (dashed line); Kr_2 and sandclock mode (dotted line)
- (b) Kr_2 mode with: I_2 , sandclock and rugby ball mode (solid line); I_2 and rugby ball mode (dashed line); Kr_2 and sandclock mode (dotted line)
- (c) Sandclock mode with: I_2 , Kr_2 and rugby ball mode (solid line); I_2 and Kr_2 mode (dashed line)
- (d) Rugby ball mode with: I_2 , Kr_2 and sandclock mode (solid line); I_2 and Kr_2 mode (dashed line)

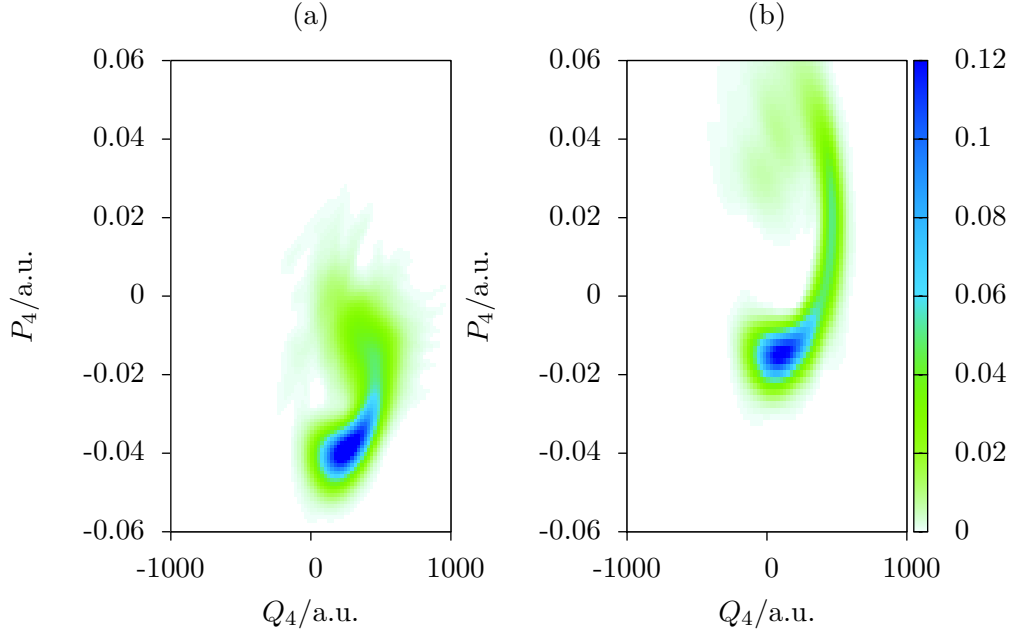


Figure 6.8: Snapshot of the rugby ball mode SCHD Wigner function at 1860 fs
 (a) with three normal modes
 (b) with four normal modes

points were used for the numerical Monte-Carlo integration.

In Fig. 6.7, the purities obtained with SCHD for each of the considered modes are plotted and compared for the three- and four-dimensional case. A comparison of the different purities for every normal mode reveals only small differences between results for the four- and three-dimensional case. Particularly the purities of the cage modes show only slight deviations between the results obtained for different numbers of DOFs. Hence, for the chosen initial state in the I_2 , we could assume that for a certain cage mode it is almost insignificant, whether or not the other cage mode is considered in the propagation.

However, the purity does not give all information about a state. It only reveals information about the “mixedness” of a state. Therefore, in order to see the influence of an additional normal mode on a subsystem, the Wigner functions of the rugby ball mode are shown in Fig. 6.8 for both the three- and four-dimensional case. The comparison of both snapshots, taken at the same time $t = 1800$ fs, shows clear differences, especially in the momentum width and also in the position of the maxima. Consequently, we conclude that indeed it is relevant for the dynamics of a cage mode, whether or not another cage mode is considered in the dynamics of the overall system.

In this chapter, we have shown, that the SCHD is also applicable to problems beyond the CL model. Furthermore, detailed investigations have revealed, that reduced densities for DOFs treated on the level of the TGWD within the SCHD do not necessarily keep their initial Gaussian shape, but rather approach the full quantum reference result, if weakly coupled to anharmonic HK DOFs.

As future work concerning the considered problem of $I_2\text{Kr}_{17}$, SCHD could be used for further investigations with varying initial conditions in the I_2 mode and addition of further normal modes, that are more weakly coupled to I_2 than the ones considered so far, so that

finally a coherent superposition in the Krypton cage could appear.

7 Summary and Outlook

In this thesis, open quantum systems in finite baths were studied. To this end, the so-called semiclassical hybrid method, which treats various DOFs of a multi-dimensional system on different levels of approximation, was extended to a density matrix description. The two approximations are the well-established HK method and the less accurate, but also computationally less costly TGWD.

To set the stage, in Chapter 2, the Caldeira-Leggett (CL) system-bath model used in this thesis was presented. Furthermore, a frequency blue shift appearing in bound open quantum systems was investigated for the harmonic and anharmonic Morse oscillator. As a result, we found that the blue shift becomes stronger with increasing coupling strength and if the cutoff frequency of the bath approaches the system's frequency. Then, in Chapter 3, the semiclassical hybrid method was extended in such a way, that it can be applied to thermal harmonic baths, in order to treat open quantum systems within the CL model. This method turns out to be very efficient in particular when treating systems in non-resonant baths, i.e. for baths whose frequencies are far away from a characteristic frequency of the SOI. In those systems, decoherence in the absence of dissipation could be studied thoroughly using the SCHD for the first time.

In Chapter 4 for the anharmonic Morse oscillator, effects of decoherence, namely the quenching of interference patterns and, ultimately, the quantum-to-classical transition, have been studied, as well as their dependence on various parameters like temperature and coupling strength. Furthermore, computing the purity with the SCHD as a quantitative measure of decoherence, additionally a strong dependence of decoherence on the initial state of the SOI as well as on the configuration of the bath was found, respectively confirmed.

Furthermore in Chapter 4, through the study of long time dynamics, the quantum revival phenomenon was investigated semiclassically. For this, again the anharmonic Morse oscillator was used as the model system. As a first step, the semiclassical mechanism of revivals in the case of a free system was studied with the HK SC-IVR. There, the quantum revival is a result of trajectories interfering constructively only in the phase space region the initial wave function is located at. Outside this region, the trajectory interference is destructive, thus giving no contribution to the revived wave function. In the next step, again baths of different sizes were coupled to this system. This way, depending on the bath size and particularly on the temperature, the revival is more or less partially suppressed. Now, the phase relations of the trajectories are blurred and thus their ability to interfere is reduced leading to a partial revival. For the largest regarded bath with the highest considered temperature, the revival is virtually fully suppressed resembling the classical result. Thus, using the SCHD, by variation of the bath temperature and size, the revival dynamics can be continuously tuned from a full revival to a full suppression of the revival.

The last study on decoherence in Chapter 4 was concerned with a fundamental scenario of quantum physics, the double slit experiment, was studied, where the CL system-bath model was extended by a form factor. Despite exhibiting chaotic dynamics, the semiclassical result of the uncoupled slit showed a good agreement with the quantum result. Having

proven to provide a result with a good accuracy in the bath-free case, the SCHD was then used in the coupled case for the investigation of the smoothing of the diffraction pattern as a manifestation of decoherence. This way, the dependence on the bath temperature, the coupling strength and the nonlinear DOF of the coupling, i.e. the coupling range, could be analyzed. For high enough temperatures this leads to a nearly classical diffraction pattern showing almost no interferences.

Moving on to resonant baths in Chapter 5, we have shown that SCHD can be used for the investigation of dissipative dynamics, too. To this end, the SCHD (which is obviously non-Markovian) was compared with an implicit non-Markovian method, i.e. the SCBM, where the influence of an infinite bath is mimicked by an average over a complex stochastic noise force. The purpose of this comparison was to find out, how the bath modes of the finite bath need to be chosen to capture the effect of the infinite bath.

The first test system was the dissipative harmonic oscillator, for which an analytic solution exists. Varying the distribution of frequencies for the SCHD finite bath, we find an excellent agreement with the analytic result for the distribution, that has the strongest emphasis on low-frequency modes. Moreover, the agreement of the analytic results with the SCHD was even better than with the SCBM.

As a more demanding model system, again the Morse oscillator coupled to a bath was chosen. Since the bath is a resonant one and thus the corresponding bath modes are significantly affected by the anharmonic system, this scenario is more challenging for the SCHD than the low-frequency bath configurations, particularly for higher temperatures. The approach towards this problem is to treat a small fraction of the bath on the level of the HK approximation, while the rest of the modes remain on the level of the TGWD. Using a frequency distribution, that gives an emphasis on resonant modes, we find that a bath consisting of only 20 modes is sufficient to reach a thermal equilibrium. Furthermore, a clear convergence towards the SCBM result is visible when increasing the number of modes treated on the level of the HK approximation in the SCHD. Also, a typically non-Markovian case, with stronger coupling and lower temperature than before, is fully reproduced by the SCHD, showing an excellent agreement with the SCBM, while the Markovian CL master equation fails to reproduce the transient behavior and the values of the equilibrated system. Finally the time scales of dissipation and decoherence were compared in the case of a finite zero temperature bath. We have confirmed the common statement, that the decoherence time is smaller than the time of dissipation. We have also shown, that a resonant bath strongly increases decoherence compared to a non-resonant one.

Finally, we went a step further and considered a system-bath problem beyond the CL model. We have studied an Iodine molecule in a coherent vibrational superposition surrounded by a Krypton environment, where all interactions are anharmonic. A final goal of this investigation is to find conditions, for which a coherent signature, i.e. a coherent superposition, can be observed in the Krypton environment for several vibrational periods as was the case in the corresponding experiment [125]. In this thesis, we set a starting point for this study by focussing on the properties of the SCHD in the framework of this system. We showed that the SCHD is an appropriate tool for the investigation of such systems. Furthermore, the investigation of DOFs treated on the level of TGWD has shown, that the respective reduced densities are not restricted to a Gaussian shape and instead show a high accuracy compared to quantum results.

Having treated both kinds of baths, the resonant and the non-resonant one, it can be stated in conclusion that the SCHD is capable of describing both of these cases, including

dissipation and pure decoherence, respectively. Especially for the non-resonant scenario, the SCHD is the method of choice, as it was shown to be a highly efficient method in that case. Furthermore, another computational advantage of the SCHD should be stressed, which all SC-IVRs that are based on coherent states have in common. The particular form of the propagator allows for the direct calculation of numerous expectation values and further measures, i.e. without a previous explicit knowledge of the reduced density.

Thus within the CL model, several other applications open up for the SCHD. In the field of atomic physics, it would be of interest to study atoms driven by laser fields and embedded in a thermal bath. Since decoherence is the more sensitive process than dissipation, it could manifest on time scales that are of interest here. Hence, quantum processes, that can be described semiclassically in this context, i.e. multiphoton processes like above threshold ionization and high harmonic generation [46], could be investigated in the presence of a non-resonant finite bath. With this, one could move away from the ideal description of an isolated quantum system closer to the more realistic experimental scenario.

Furthermore, the SCHD could be applied to a number of problems in molecular physics. Considering molecules in external laser fields, transitions between electronic surfaces under the influence of a thermal bath would be interesting to study [39, 40].

Applications also open up for the hybrid method regarding problems beyond the CL model. In the problem of I_2Kr_{17} , which was regarded in this thesis, the number of DOFs could be increased within the SCHD, so that one could get conditions that are closer to the experiment. Furthermore, similar problems of molecules in a noble gas environments (e.g. [128]) could be studied.

To improve the computational performance of the SCHD, it could be worthwhile to replace the HK part of the original method by a forward-backward treatment [50] (for the price of less accuracy).

Finally an advantage of more technical nature, the high parallelizability of the numerical integration, which all SC-IVRs have in common, can be exploited. To this end, a realization as a multi-GPU application via the computing architecture "Compute Unified Device Architecture" (CUDA) would allow for a faster computation than on a single CPU.

A Sampling the Bath Frequencies

Several densities, according to which the frequencies of the finite bath are chosen, are used in this thesis. In this appendix the specific sampling of the frequencies for different frequency distributions is given. Generally, the frequency of a particular distribution is chosen by solving the equation

$$\int_0^{\omega_j} d\omega \rho_f = j \quad j \in \mathbb{N} \quad (\text{A.1})$$

for the j th bath mode.

A.1 Exponential Density

The first density of frequencies, which is of exponential form, was used in the low-frequency bath cases in Chapter 4. Similarly to the Lorentzian density case, it is related to a spectral density of Ohmic form with an exponential cutoff

$$\rho_f^{(e)}(\omega) = a_e \frac{J_e(\omega)}{\omega} = a_e \eta e^{-\omega/\omega_c} . \quad (\text{A.2})$$

It is normalized via the factor

$$a_e = \frac{N_B}{\eta \omega_c} \left(1 - e^{-\omega_{\max}/\omega_c}\right)^{-1} , \quad (\text{A.3})$$

while the frequencies

$$\omega_j = -\omega_c \ln \left[1 - \frac{j}{a_e \eta \omega_c}\right] = -\omega_c \ln \left[1 - \frac{j}{N_B} \left(1 - e^{-\omega_{\max}/\omega_c}\right)\right] \quad (\text{A.4})$$

are logarithmically distributed.

A.2 “Inverse Square Root” Distribution

Another density of frequencies which was used in Section 5.1 depends on the inverse square root of the frequency

$$\rho_f^{(\text{sq})}(\omega) = a_{\text{sq}} \omega^{-1/2} . \quad (\text{A.5})$$

Using the normalization condition

$$\int_0^{\omega_{\max}} d\omega \rho_f^{(\text{sq})} = N_B \quad j \in \mathbb{N} \quad (\text{A.6})$$

yields the normalization coefficient

$$a_{\text{sq}} = \frac{N_{\text{B}}}{2\sqrt{\omega_{\text{max}}}}. \quad (\text{A.7})$$

Then using Eq. (A.1) the j th frequency can be sampled straightforwardly giving

$$\omega_j^{(\text{sq})} = \frac{j^2}{N_{\text{B}}^2} \omega_{\text{max}}, \quad (\text{A.8})$$

which depends quadratically on the mode index.

A.3 Lorentzian Density

As a third frequency distribution we used in Section 5.1 one of Lorentzian form, such that it is adapted to the corresponding spectral density with a Drude-Lorentz cutoff

$$\rho_{\text{f}}^{(\text{L})}(\omega) = a_{\text{L}} \frac{J_{\text{D}}(\omega)}{\omega} = a_{\text{L}} \frac{\eta}{1 + \omega^2/\omega_{\text{c}}^2} \quad (\text{A.9})$$

Here, the normalization factor becomes

$$\begin{aligned} N_{\text{B}} &= a_{\text{L}} \omega_{\text{c}} \eta \int_0^{\frac{\omega_{\text{max}}}{\omega_{\text{c}}}} d\tilde{\omega} \frac{1}{1 + \tilde{\omega}^2} \\ \rightarrow a_{\text{L}} &= \frac{N_{\text{B}}}{\arctan\left(\frac{\omega_{\text{max}}}{\omega_{\text{c}}}\right) \omega_{\text{c}} \eta} \end{aligned} \quad (\text{A.10})$$

and accordingly the frequency of every bath mode is

$$\omega_j^{(\text{L})} = \omega_{\text{c}} \tan \left[\frac{\arctan\left(\frac{\omega_{\text{max}}}{\omega_{\text{c}}}\right)}{N_{\text{B}}} j \right], \quad (\text{A.11})$$

which goes with the tangent of the mode index.

A.4 Gaussian Density of Frequencies

Finally, the last frequency distribution that we have used in Section 5.1 and 5.2 is of Gaussian form giving an emphasis on a region around some central frequency, which is chosen to be the frequency of the SOI

$$\rho_{\text{f}}^{(\text{G})}(\omega) = a_{\text{G}} e^{-b(\omega - \omega_{\text{s}})^2}, \quad (\text{A.12})$$

so that resonant and near-resonant bath modes are sampled. Again applying the normalization condition (A.6)

$$\begin{aligned}
N_B &= a_G \int_0^{\omega_{\max}} d\omega \, e^{-b(\omega - \omega_s)^2} \\
&= \frac{a_G}{\sqrt{b}} \int_{-\sqrt{b}\omega_s}^{\sqrt{b}(\omega_{\max} - \omega_s)} d\tilde{\omega} \, e^{-\tilde{\omega}^2}
\end{aligned} \tag{A.13}$$

yields

$$a_G = \frac{2N_B\sqrt{b}}{\sqrt{\pi}} \left\{ \operatorname{erf}(\sqrt{b}\omega_s) - \operatorname{erf}\left[\sqrt{b}(\omega_s - \omega_{\max})\right] \right\}^{-1}, \tag{A.14}$$

with the error function erf [66]. Analogously, the frequencies are sampled

$$\begin{aligned}
j &= \frac{a_G\sqrt{\pi}}{2\sqrt{b}} \left\{ \operatorname{erf}(\sqrt{b}\omega_s) - \operatorname{erf}\left[\sqrt{b}(\omega_s - \omega_j^{(G)})\right] \right\}^{-1} \\
\rightarrow \omega_j^{(G)} &= \omega_s - \frac{1}{\sqrt{b}} \operatorname{erf}^{-1} \left[\operatorname{erf}(\sqrt{b}\omega_s) - \frac{2\sqrt{b}}{a_G\sqrt{\pi}} j \right],
\end{aligned} \tag{A.15}$$

so that they are distributed according to the given density of frequencies.

B Symplectic Integration

The underlying dynamics of semiclassical methods is classical. Consequently, Hamilton's equations

$$\begin{aligned}\dot{\mathbf{q}} &= \frac{\partial \mathcal{H}}{\partial \mathbf{p}} \\ \dot{\mathbf{p}} &= -\frac{\partial \mathcal{H}}{\partial \mathbf{q}}\end{aligned}\tag{B.1}$$

need to be solved. Numerically, this can be carried out using a symplectic integrator [129]. It ensures the preservation of the volume of a propagated region in phase space, which is also known as Liouville's theorem. The trajectories are then propagated via

$$\begin{aligned}\mathbf{p}^{(j)} &= \mathbf{p}^{(j-1)} - b_j \Delta t \frac{\partial \mathcal{H}}{\partial \mathbf{q}} \Big|_{\mathbf{q}^{(j-1)}} \quad (j = 1..m) \\ \mathbf{q}^{(j)} &= \mathbf{q}^{(j-1)} + a_j \Delta t \frac{\partial \mathcal{H}}{\partial \mathbf{p}} \Big|_{\mathbf{p}^{(j)}} \quad (j = 1..m),\end{aligned}\tag{B.2}$$

for one time step with step size Δt . The specific order and scheme of symplectic integration is characterized by the coefficients a_j and b_j , which also set the number of intermediate steps per full time step. Here, the second order leapfrog (or position Verlet) scheme is used, where $a_{1/2} = 0.5$, $b_1 = 0$ and $b_2 = 1$.

In contrast to classical mechanics, additionally elements of the monodromy matrix are included in the semiclassical theory. To obtain their equations of motion, it should first be recalled, that the monodromy matrix determines the time evolution of small deviations $\delta \mathbf{p}_t = \tilde{\mathbf{p}}_t - \mathbf{p}_t$ and $\delta \mathbf{q}_t = \tilde{\mathbf{q}}_t - \mathbf{q}_t$ and thus reads

$$\begin{pmatrix} \delta \mathbf{p}_t \\ \delta \mathbf{q}_t \end{pmatrix} = \mathbf{M} \begin{pmatrix} \delta \mathbf{p}_i \\ \delta \mathbf{q}_i \end{pmatrix},\tag{B.3}$$

with the initial deviations $\delta \mathbf{p}_i$ and $\delta \mathbf{q}_i$. On the other hand, the time derivatives of the deviations can be Taylor expanded up to first order, so that

$$\begin{pmatrix} \delta \dot{\mathbf{p}}_t \\ \delta \dot{\mathbf{q}}_t \end{pmatrix} = \begin{pmatrix} \mathbf{0} & -\frac{\partial^2 \mathcal{H}}{\partial \mathbf{q} \partial \mathbf{q}^T} \\ \frac{\partial^2 \mathcal{H}}{\partial \mathbf{p} \partial \mathbf{p}^T} & \mathbf{0} \end{pmatrix} \begin{pmatrix} \delta \mathbf{p}_t \\ \delta \mathbf{q}_t \end{pmatrix} \Rightarrow \dot{\mathbf{M}} = \begin{pmatrix} \mathbf{0} & -\frac{\partial^2 \mathcal{H}}{\partial \mathbf{q} \partial \mathbf{q}^T} \\ \frac{\partial^2 \mathcal{H}}{\partial \mathbf{p} \partial \mathbf{p}^T} & \mathbf{0} \end{pmatrix} \mathbf{M}\tag{B.4}$$

The monodromy matrix is symplectic as well, since

$$\mathbf{M}^T \mathbf{J} \mathbf{M} = \mathbf{J} \quad \mathbf{J} = \begin{pmatrix} \mathbf{0} & \mathbf{1} \\ -\mathbf{1} & \mathbf{0} \end{pmatrix}\tag{B.5}$$

and therefore the symplectic integration scheme

$$\begin{aligned}
 \mathbf{m}_{11}^{(j)} &= \mathbf{m}_{11}^{(j-1)} - b_j \Delta t \frac{\partial^2 \mathcal{H}}{\partial \mathbf{q} \partial \mathbf{q}^T} \bigg|_{\mathbf{q}^{(j-1)}} \mathbf{m}_{21}^{(j-1)} \\
 \mathbf{m}_{12}^{(j)} &= \mathbf{m}_{12}^{(j-1)} - b_j \Delta t \frac{\partial^2 \mathcal{H}}{\partial \mathbf{q} \partial \mathbf{q}^T} \bigg|_{\mathbf{q}^{(j-1)}} \mathbf{m}_{22}^{(j-1)} \\
 \mathbf{m}_{21}^{(j)} &= \mathbf{m}_{21}^{(j-1)} + a_j \Delta t \frac{\partial^2 \mathcal{H}}{\partial \mathbf{p} \partial \mathbf{p}^T} \bigg|_{\mathbf{p}^{(j)}} \mathbf{m}_{11}^{(j-1)} \\
 \mathbf{m}_{22}^{(j)} &= \mathbf{m}_{22}^{(j-1)} + a_j \Delta t \frac{\partial^2 \mathcal{H}}{\partial \mathbf{p} \partial \mathbf{p}^T} \bigg|_{\mathbf{p}^{(j)}} \mathbf{m}_{12}^{(j-1)}
 \end{aligned} \tag{B.6}$$

can be applied.

B.1 Derivatives for the Caldeira-Leggett Model

For the CL model, the gradients of the Hamiltonian needed in Eqs. (B.2) read (assuming a SOI with one DOF and unit masses for the bath DOFs as usual)

$$\begin{aligned}
 \frac{\partial \mathcal{H}}{\partial \mathbf{q}} &= \begin{pmatrix} \frac{\partial \mathcal{V}}{\partial q_S} + \sum_{i=1}^{N_B} \frac{c_i}{\omega_i} \left(\omega_i q_i + \frac{c_i}{\omega_i} q_S \right) \\ \omega_1 \left(\omega_1 q_1 + \frac{c_1}{\omega_1} q_S \right) \\ \vdots \\ \omega_{N_B} \left(\omega_{N_B} q_{N_B} + \frac{c_{N_B}}{\omega_{N_B}} q_S \right) \end{pmatrix} \\
 \frac{\partial \mathcal{H}}{\partial \mathbf{p}} &= \begin{pmatrix} p_S/M \\ \mathbf{p}_B \end{pmatrix}.
 \end{aligned} \tag{B.7}$$

Furthermore the second derivatives of the Hamiltonian with respect to position (the Hessian), needed in Eqs. (B.6), read

$$\frac{\partial^2 \mathcal{H}}{\partial \mathbf{q} \partial \mathbf{q}^T} = \begin{pmatrix} \frac{\partial^2 \mathcal{V}}{\partial q_S^2} + \sum_{i=1}^{N_B} \left(\frac{c_i}{\omega_i} \right)^2 & c_1 & \cdots & c_{N_B} \\ c_1 & \omega_1^2 & & \mathbf{0} \\ \vdots & & \ddots & \\ c_{N_B} & \mathbf{0} & & \omega_{N_B}^2 \end{pmatrix}, \tag{B.8}$$

with $\mathbf{0}$ denoting the nondiagonal vanishing elements of the bath submatrix of the second derivative. The second derivatives with respect to the momentum are trivially just the inverses of the masses.

B.2 Derivatives for the I₂Kr₁₇ Problem

In the treatment of Iodine in a Krypton shell, we introduce normal coordinates, which are linked to mass-weighted cartesian displacement coordinates via a linear transformation

$$Q_j = \sum_{k=1}^N a_{kj} \tilde{q}_k \iff \tilde{q}_k = \sum_{j=1}^N a_{kj} Q_j. \quad (\text{B.9})$$

Here, l_{kj} are the elements of the transformation matrix and $\tilde{q}_k = \sqrt{m_k} \Delta x_k$, where Δx_k is the deviation from the equilibrium position of a particular DOF with mass m_k in the N -dimensional $I_2\text{Kr}_{17}$ system.

We propagate in normal coordinates and hence, the first derivatives with respect to them give

$$\begin{aligned} \frac{\partial \mathcal{H}}{\partial P_j} &= \frac{\partial \mathcal{T}}{\partial P_j} = P_j \\ \frac{\partial \mathcal{H}}{\partial Q_j} &= \frac{\partial \mathcal{V}}{\partial Q_j} = \sum_{k=1}^N \frac{\partial \mathcal{V}}{\partial \tilde{q}_k} \frac{\partial \tilde{q}_k}{\partial Q_j} = \sum_{k=1}^N a_{kj} \frac{\partial \mathcal{V}}{\partial \tilde{q}_k}. \end{aligned} \quad (\text{B.10})$$

The second derivatives of the Hamiltonian with respect to the normal coordinates and their conjugate momenta read

$$\begin{aligned} \frac{\partial^2 \mathcal{T}}{\partial P_j \partial P_i} &= \delta_{ji} \\ \frac{\partial^2 \mathcal{V}}{\partial Q_j \partial Q_i} &= \frac{\partial}{\partial Q_j} \left(\sum_{k=1}^N \frac{\partial \mathcal{V}}{\partial \tilde{q}_k} a_{ki} \right) = \sum_{k,l=1}^N a_{lj} a_{ki} \frac{\partial^2 \mathcal{V}}{\partial \tilde{q}_k \partial \tilde{q}_l}. \end{aligned} \quad (\text{B.11})$$

However, the overall potential is a sum of analytically given potentials, that are functions of distances between the atoms, which again can be written as functions of the displacement coordinates

$$\begin{aligned} R_{KJ} &= \left\{ \left[\left(x_{K,1}^0 + \frac{\tilde{q}_{K,1}}{\sqrt{m_K}} \right) - \left(x_{J,1}^0 + \frac{\tilde{q}_{J,1}}{\sqrt{m_J}} \right) \right]^2 + \left[\left(x_{K,2}^0 + \frac{\tilde{q}_{K,2}}{\sqrt{m_K}} \right) - \left(x_{J,2}^0 + \frac{\tilde{q}_{J,2}}{\sqrt{m_J}} \right) \right]^2 \right. \\ &\quad \left. + \left[\left(x_{K,3}^0 + \frac{\tilde{q}_{K,3}}{\sqrt{m_K}} \right) - \left(x_{J,3}^0 + \frac{\tilde{q}_{J,3}}{\sqrt{m_J}} \right) \right]^2 \right\}^{1/2}, \end{aligned} \quad (\text{B.12})$$

where the index now consists of two parts, of which the first part (capital letter) labels the atom and the second part the internal DOF of an atom. Furthermore, $x_{K,\nu}^0$ ($\nu = 1, 2, 3$) is the equilibrium position coordinate. Hence the first derivative of the potential with respect to the displacement coordinates yields

$$\frac{\partial \mathcal{V}}{\partial \tilde{q}_{K,\nu}} = \sum_{I \neq K}^{N_a} \frac{\partial \mathcal{V}}{\partial R_{KI}} \frac{\partial R_{KI}}{\partial \tilde{q}_{K,\nu}} \quad (\nu = 1, 2, 3), \quad (\text{B.13})$$

with the number of atoms $N_a = N/3$ and the displacement coordinate derivatives of the distance

$$\frac{\partial R_{KJ}}{\partial \tilde{q}_{K,\nu}} = \frac{\left(x_{K,\nu}^0 + \frac{\tilde{q}_{K,\nu}}{\sqrt{m_K}}\right) - \left(x_{J,\nu}^0 + \frac{\tilde{q}_{J,\nu}}{\sqrt{m_J}}\right)}{R_{KJ}\sqrt{m_J}} = \frac{\partial R_{JK}}{\partial \tilde{q}_{K,\nu}}. \quad (\text{B.14})$$

For the second derivatives we obtain two equations, depending on the atom index of both displacement coordinates

$$J \neq K : \quad \frac{\partial^2 \mathcal{V}}{\partial \tilde{q}_{J,\mu} \partial \tilde{q}_{K,\nu}} = \frac{\partial^2 \mathcal{V}}{\partial R_{KJ}^2} \frac{\partial R_{KJ}}{\partial \tilde{q}_{K,\nu}} \frac{\partial R_{KJ}}{\partial \tilde{q}_{J,\mu}} + \frac{\partial \mathcal{V}}{\partial R_{KJ}} \frac{\partial^2 R_{KJ}}{\partial \tilde{q}_{J,\mu} \partial \tilde{q}_{K,\nu}} \quad (\text{B.15})$$

$$J = K, \mu \neq \nu : \quad \frac{\partial^2 \mathcal{V}}{\partial \tilde{q}_{K,\mu} \partial \tilde{q}_{K,\nu}} = \sum_{I \neq K} \left(\frac{\partial \mathcal{V}}{\partial R_{KI}} \frac{\partial^2 R_{KI}}{\partial \tilde{q}_{K,\nu} \partial \tilde{q}_{K,\mu}} + \frac{\partial^2 \mathcal{V}}{\partial R_{KI}^2} \frac{\partial R_{KI}}{\partial \tilde{q}_{K,\mu}} \frac{\partial R_{KI}}{\partial \tilde{q}_{K,\nu}} \right), \quad (\text{B.16})$$

which consist of the second derivatives of the distances giving two equation

$$\begin{aligned} \frac{\partial^2 R_{KJ}}{\partial \tilde{q}_{K,\nu} \partial \tilde{q}_{J,\mu}} &= - \frac{\left(x_{K,\nu}^0 + \frac{\tilde{q}_{K,\nu}}{\sqrt{m_K}}\right) - \left(x_{J,\nu}^0 + \frac{\tilde{q}_{J,\nu}}{\sqrt{m_J}}\right)}{R_{KJ}^2 \sqrt{m_K}} \frac{\partial R_{KJ}}{\partial \tilde{q}_{J,\mu}} - \frac{\delta_{\nu\mu}}{R_{KJ} \sqrt{m_K} \sqrt{m_J}} \\ &= - \frac{\left[\left(x_{K,\nu}^0 + \frac{\tilde{q}_{K,\nu}}{\sqrt{m_K}}\right) - \left(x_{J,\nu}^0 + \frac{\tilde{q}_{J,\nu}}{\sqrt{m_J}}\right)\right] \left[\left(x_{K,\mu}^0 + \frac{\tilde{q}_{K,\mu}}{\sqrt{m_K}}\right) - \left(x_{J,\mu}^0 + \frac{\tilde{q}_{J,\mu}}{\sqrt{m_J}}\right)\right]}{R_{KJ}^3 \sqrt{m_K} \sqrt{m_J}} \\ &\quad - \frac{\delta_{\nu\mu}}{R_{KJ} \sqrt{m_K} \sqrt{m_J}} \end{aligned} \quad (\text{B.17})$$

$$\begin{aligned} \frac{\partial^2 R_{KJ}}{\partial \tilde{q}_{K,\nu} \partial \tilde{q}_{K,\mu}} &= - \frac{\left(x_{K,\nu}^0 + \frac{\tilde{q}_{K,\nu}}{\sqrt{m_K}}\right) - \left(x_{J,\nu}^0 + \frac{\tilde{q}_{J,\nu}}{\sqrt{m_J}}\right)}{R_{KJ}^2 \sqrt{m_K}} \frac{\partial R_{KJ}}{\partial \tilde{q}_{K,\mu}} + \frac{\delta_{\nu\mu}}{R_{KJ} m_K} \\ &= - \frac{\left[\left(x_{K,\nu}^0 + \frac{\tilde{q}_{K,\nu}}{\sqrt{m_K}}\right) - \left(x_{J,\nu}^0 + \frac{\tilde{q}_{J,\nu}}{\sqrt{m_J}}\right)\right] \left[\left(x_{K,\mu}^0 + \frac{\tilde{q}_{K,\mu}}{\sqrt{m_K}}\right) - \left(x_{J,\mu}^0 + \frac{\tilde{q}_{J,\mu}}{\sqrt{m_J}}\right)\right]}{R_{KJ}^3 m_K} \\ &\quad + \frac{\delta_{\nu\mu}}{R_{KJ} m_K}, \end{aligned} \quad (\text{B.18})$$

depending on the atom indices of the derivation variables.

C From Herman-Kluk to Thawed Gaussian Wave Packet Dynamics

In order to show, that the approximation made for some DOFs in the HK wave function leading to the SCHD indeed shifts the accuracy of the respective DOFs to the level of the TGWD, the original TGWD wave function is derived in detail from the HK approximation in this appendix [55].

We start with the N -dimensional HK wave function

$$\Psi_\alpha(\mathbf{x}, t) = \int \frac{d^N q d^N p}{(2\pi\hbar)^N} \langle \mathbf{x} | g_\gamma(\mathbf{q}_t, \mathbf{p}_t) \rangle \sqrt{\det[\mathbf{h}(\mathbf{q}, \mathbf{p}, t)]} e^{iS/\hbar} \langle g_\gamma(\mathbf{q}, \mathbf{p}) | \Psi_\alpha(0) \rangle, \quad (\text{C.1})$$

which initially is a GWP centered around $(\mathbf{q}_\alpha, \mathbf{p}_\alpha)$. Now, for *all* of the N DOFs the action is expanded up to second order around the center of the initial Gaussian

$$\begin{aligned} S(\mathbf{q}, \mathbf{p}, t) \approx S(\mathbf{q}_\alpha, \mathbf{p}_\alpha, t) &+ \mathbf{p}_{\alpha,t}^T \mathbf{m}_{21} \delta \mathbf{p} + (\mathbf{p}_{\alpha,t}^T \mathbf{m}_{22} - \mathbf{p}_\alpha^T) \delta \mathbf{q} + \frac{1}{2} \delta \mathbf{p}^T \mathbf{m}_{11}^T \mathbf{m}_{21} \delta \mathbf{p} \\ &+ \frac{1}{2} \delta \mathbf{q}^T \mathbf{m}_{12}^T \mathbf{m}_{22} \delta \mathbf{q} + \frac{1}{2} \delta \mathbf{p}^T \mathbf{m}_{21}^T \mathbf{m}_{12} \delta \mathbf{q}, \end{aligned} \quad (\text{C.2})$$

with the deviations of the integration phase space variables from the initial wave packet center $\delta \mathbf{q} = \mathbf{q} - \mathbf{q}_\alpha$ and $\delta \mathbf{p} = \mathbf{p} - \mathbf{p}_\alpha$. In addition, the final momentum and position is first order expanded similar to Eqs. (3.23) and (3.24), but now again for *all* DOFs

$$\mathbf{p}_t \approx \mathbf{p}_{\alpha,t} + \mathbf{m}_{11} \delta \mathbf{p} + \mathbf{m}_{12} \delta \mathbf{q} \quad (\text{C.3})$$

$$\mathbf{q}_t \approx \mathbf{q}_{\alpha,t} + \mathbf{m}_{21} \delta \mathbf{p} + \mathbf{m}_{22} \delta \mathbf{q}. \quad (\text{C.4})$$

With the resulting Gaussian form of the integrand, the phase space integral in Eq. (C.1) can be calculated analytically by making use of the multidimensional Gaussian integral formula given in Eq. (2.36) and thus the resulting wave function reads

$$\Psi_\alpha(\mathbf{x}, t) = \frac{1}{(2\hbar)^N} \sqrt{\frac{\det[\mathbf{h}(\mathbf{q}, \mathbf{p}, t)]}{\det \bar{\mathbf{A}}}} \left(\frac{\det \gamma}{\pi^N} \right)^{1/4} \exp \left\{ \frac{1}{4} \bar{\mathbf{b}}^T \bar{\mathbf{A}}^{-1} \bar{\mathbf{b}} + c \right\}, \quad (\text{C.5})$$

with the N -dimensional vector

$$\bar{\mathbf{b}}^T = (\mathbf{x} - \mathbf{q}_{\alpha,t})^T (\mathbf{u}^T, \mathbf{v}^T), \quad (\text{C.6})$$

the symmetric $2N \times 2N$ matrix

$$\bar{\mathbf{A}} = \begin{pmatrix} \mathbf{a}_{11} & \mathbf{a}_{12} \\ \mathbf{a}_{12}^T & \mathbf{a}_{22} \end{pmatrix} = \begin{pmatrix} \frac{\gamma^{-1}}{4\hbar^2} + \frac{\mathbf{u}\mathbf{m}_{21}}{2} & \frac{i}{4\hbar} + \frac{\mathbf{m}_{21}^T \mathbf{v}^T}{2} \\ \frac{i}{4\hbar} + \frac{\mathbf{v}\mathbf{m}_{21}}{2} & \frac{\gamma}{4} + \frac{\mathbf{v}\mathbf{m}_{22}}{2} \end{pmatrix} \quad (\text{C.7})$$

and the scalar

$$c = -\frac{1}{2}(\mathbf{x} - \mathbf{q}_{\alpha,t})^T \boldsymbol{\gamma} (\mathbf{x} - \mathbf{q}_{\alpha,t}) + \frac{i}{\hbar} \mathbf{p}_{\alpha,t}^T \cdot (\mathbf{x} - \mathbf{q}_{\alpha,t}) + \frac{i}{\hbar} S(\mathbf{q}, \mathbf{p}, t). \quad (\text{C.8})$$

It also contains the abbreviations

$$\mathbf{u} \equiv \mathbf{m}_{21}^T \boldsymbol{\gamma} + \frac{i}{\hbar} \mathbf{m}_{11}^T \quad \mathbf{v} \equiv \mathbf{m}_{22}^T \boldsymbol{\gamma} + \frac{i}{\hbar} \mathbf{m}_{12}^T. \quad (\text{C.9})$$

In order to see, that Eq. (C.5) is indeed the TGWD wave function, it needs to be transformed. First, the vector-matrix-vector product in the exponent is evaluated. For this, the inverse of a symmetric block matrix is needed, which is given by

$$\begin{pmatrix} \mathbf{a}_{11} & \mathbf{a}_{12} \\ \mathbf{a}_{12}^T & \mathbf{a}_{22} \end{pmatrix}^{-1} = \begin{pmatrix} \mathbf{d}^{-1} & -\mathbf{d}^{-1} \mathbf{a}_{12} \mathbf{a}_{22}^{-1} \\ -\mathbf{e}^{-1} \mathbf{a}_{12}^T \mathbf{a}_{11}^{-1} & \mathbf{e}^{-1} \end{pmatrix}, \quad (\text{C.10})$$

with the abbreviations $\mathbf{d} = \mathbf{a}_{11} - \mathbf{a}_{12} \mathbf{a}_{22}^{-1} \mathbf{a}_{12}^T$ and $\mathbf{e} = \mathbf{a}_{22} - \mathbf{a}_{12}^T \mathbf{a}_{11}^{-1} \mathbf{a}_{12}$. Then the expression in the exponent of Eq. (C.5) becomes

$$\begin{aligned} & (\mathbf{u}^T, \mathbf{v}^T) \mathbf{A}^{-1} \begin{pmatrix} \mathbf{u} \\ \mathbf{v} \end{pmatrix} \\ &= \mathbf{u}^T \mathbf{d}^{-1} \mathbf{u} + \mathbf{v}^T \mathbf{e}^{-1} \mathbf{v} - \mathbf{u}^T \mathbf{d}^{-1} \mathbf{a}_{12} \mathbf{a}_{22}^{-1} \mathbf{v} - \mathbf{v}^T \mathbf{e}^{-1} \mathbf{a}_{12}^T \mathbf{a}_{11}^{-1} \mathbf{u} \\ &= \mathbf{u}^T (\mathbf{a}_{22} \mathbf{d})^{-1} \mathbf{a}_{22} \mathbf{u} + \mathbf{v}^T (\mathbf{a}_{11} \mathbf{e})^{-1} \mathbf{a}_{11} \mathbf{v} - \mathbf{u}^T (\mathbf{a}_{22} \mathbf{d})^{-1} \mathbf{a}_{22} \mathbf{a}_{12} \mathbf{a}_{22}^{-1} \mathbf{v} \\ & \quad - \mathbf{v}^T (\mathbf{a}_{11} \mathbf{e})^{-1} \mathbf{a}_{11} \mathbf{a}_{12}^T \mathbf{a}_{11}^{-1} \mathbf{u} \\ & \stackrel{(\text{C.14})}{=} \mathbf{u}^T \boldsymbol{\gamma} \left(\frac{1}{8\hbar^2} \mathbf{m}_{22} + \frac{i}{8\hbar} \mathbf{m}_{21} \boldsymbol{\gamma} \right)^{-1} (\mathbf{v} - i\hbar \mathbf{a}_{22} \mathbf{u} \mathbf{m}_{22} \mathbf{a}_{22}^{-1} \boldsymbol{\gamma} \mathbf{m}_{22}^{-1})^{-1} (\mathbf{a}_{22} \mathbf{u} - \mathbf{a}_{22} \mathbf{a}_{12} \mathbf{a}_{22}^{-1} \mathbf{v}) \\ & \quad + \mathbf{v}^T \left(\frac{1}{8\hbar^2} \mathbf{m}_{22} + \frac{i}{8\hbar} \mathbf{m}_{21} \boldsymbol{\gamma} \right)^{-1} (-i\hbar \mathbf{u} + \mathbf{a}_{11} \mathbf{v} \mathbf{m}_{21} \mathbf{a}_{11}^{-1} \boldsymbol{\gamma}^{-1} \mathbf{m}_{21}^{-1})^{-1} \\ & \quad \times (\mathbf{a}_{11} \mathbf{v} - \mathbf{a}_{11} \mathbf{a}_{12}^T \mathbf{a}_{11}^{-1} \mathbf{u}) \quad (\text{C.11}) \end{aligned}$$

$$\begin{aligned} & \stackrel{(\text{C.16})}{=} \mathbf{u}^T \boldsymbol{\gamma} \left(\frac{1}{8\hbar^2} \mathbf{m}_{22} + \frac{i}{8\hbar} \mathbf{m}_{21} \boldsymbol{\gamma} \right)^{-1} \left(\frac{\mathbf{v}^{-1} \boldsymbol{\gamma} \mathbf{u}}{4} + \frac{\mathbf{m}_{22} \mathbf{u}}{2} + \frac{i}{4\hbar} - \frac{\mathbf{m}_{22} \mathbf{u}}{2} \right) (1 - i\hbar \mathbf{v}^{-1} \boldsymbol{\gamma} \mathbf{u})^{-1} \\ & \quad + \mathbf{v}^T \left(\frac{1}{8\hbar^2} \mathbf{m}_{22} + \frac{i}{8\hbar} \mathbf{m}_{21} \boldsymbol{\gamma} \right)^{-1} \left(\frac{1}{4\hbar^2} + \frac{\mathbf{m}_{21} \boldsymbol{\gamma} \mathbf{u}}{2} - \frac{i\mathbf{v}^{-1} \boldsymbol{\gamma} \mathbf{u}}{4\hbar} - \frac{\mathbf{m}_{21} \boldsymbol{\gamma} \mathbf{u}}{2} \right) \\ & \quad \times (1 - i\hbar \mathbf{v}^{-1} \boldsymbol{\gamma} \mathbf{u})^{-1} \quad (\text{C.12}) \end{aligned}$$

$$\begin{aligned} &= i\hbar \mathbf{u}^T \boldsymbol{\gamma} \left(\frac{1}{2} \mathbf{m}_{22} + \frac{i\hbar}{2} \mathbf{m}_{21} \boldsymbol{\gamma} \right)^{-1} + \mathbf{v}^T \left(\frac{1}{2} \mathbf{m}_{22} + \frac{i\hbar}{2} \mathbf{m}_{21} \boldsymbol{\gamma} \right)^{-1} \\ &= 2 (i\hbar \mathbf{u}^T \boldsymbol{\gamma} + \mathbf{v}^T) (\mathbf{m}_{22} + i\hbar \mathbf{m}_{21} \boldsymbol{\gamma})^{-1}, \quad (\text{C.13}) \end{aligned}$$

where in Eq. (C.11) the two relations

$$\begin{aligned}
\mathbf{a}_{11}\mathbf{e} &= \mathbf{a}_{11}\mathbf{a}_{22} - \mathbf{a}_{11}\mathbf{a}_{12}^T\mathbf{a}_{11}^{-1}\mathbf{a}_{12} \\
&= \left(\frac{\gamma^{-1}}{4\hbar^2} + \frac{\mathbf{u}\mathbf{m}_{21}}{2}\right)\left(\frac{\gamma}{4} + \frac{\mathbf{v}\mathbf{m}_{22}}{2}\right) - \mathbf{a}_{11}\left(\frac{\imath}{4\hbar} + \frac{\mathbf{v}\mathbf{m}_{21}}{2}\right)\mathbf{a}_{11}^{-1}\left(-\frac{\imath}{4\hbar} + \frac{\mathbf{u}\mathbf{m}_{22}}{2}\right) \\
&= \frac{\gamma^{-1}}{8\hbar^2}\mathbf{v}\mathbf{m}_{22} + \frac{1}{8}\mathbf{u}\mathbf{m}_{21}\gamma + \frac{1}{4}\mathbf{u}\mathbf{m}_{21}\mathbf{v}\mathbf{m}_{22} - \frac{\imath}{4\hbar}\frac{\mathbf{u}\mathbf{m}_{22}}{2} + \frac{\imath}{8\hbar}\mathbf{a}_{11}\mathbf{v}\mathbf{m}_{21}\mathbf{a}_{11}^{-1} \\
&\quad - \frac{1}{4}\mathbf{a}_{11}\mathbf{v}\mathbf{m}_{21}\mathbf{a}_{11}^{-1}\mathbf{u}\mathbf{m}_{22} \\
&= \frac{1}{8}\mathbf{u}\left(\mathbf{m}_{21}\gamma - \frac{\imath}{\hbar}\mathbf{m}_{22}\right) + \frac{\gamma^{-1}}{8\hbar^2}\mathbf{v}\mathbf{m}_{22} + \frac{1}{2}\left(\mathbf{a}_{11} - \frac{\gamma^{-1}}{4\hbar^2}\right)\mathbf{v}\mathbf{m}_{22} + \frac{\imath}{8\hbar}\mathbf{a}_{11}\mathbf{v}\mathbf{m}_{21}\mathbf{a}_{11}^{-1} \\
&\quad - \frac{1}{4}\mathbf{a}_{11}\mathbf{v}\mathbf{m}_{21}\mathbf{a}_{11}^{-1}\mathbf{u}\mathbf{m}_{21}\mathbf{m}_{21}^{-1}\mathbf{m}_{22} \\
&= -\imath\hbar\mathbf{u}\left(\frac{\imath}{8\hbar}\mathbf{m}_{21}\gamma + \frac{1}{8\hbar^2}\mathbf{m}_{22}\right) + \frac{1}{2}\mathbf{a}_{11}\mathbf{v}\mathbf{m}_{22} + \frac{\imath}{8\hbar}\mathbf{a}_{11}\mathbf{v}\mathbf{m}_{21}\mathbf{a}_{11}^{-1} \\
&\quad - \frac{1}{2}\mathbf{a}_{11}\mathbf{v}\mathbf{m}_{21}\mathbf{a}_{11}^{-1}\left(\mathbf{a}_{11} - \frac{\gamma^{-1}}{4\hbar^2}\right)\mathbf{m}_{21}^{-1}\mathbf{m}_{22} \\
&= -\imath\hbar\mathbf{u}\left(\frac{\imath}{8\hbar}\mathbf{m}_{21}\gamma + \frac{1}{8\hbar^2}\mathbf{m}_{22}\right) + \frac{\imath}{8\hbar}\mathbf{a}_{11}\mathbf{v}\mathbf{m}_{21}\mathbf{a}_{11}^{-1}\gamma^{-1}\mathbf{m}_{21}^{-1}\mathbf{m}_{21}\gamma \\
&\quad + \frac{1}{8\hbar^2}\mathbf{a}_{11}\mathbf{v}\mathbf{m}_{21}\mathbf{a}_{11}^{-1}\gamma^{-1}\mathbf{m}_{21}^{-1}\mathbf{m}_{22} \\
&= (-\imath\hbar\mathbf{u} + \mathbf{a}_{11}\mathbf{v}\mathbf{m}_{21}\mathbf{a}_{11}^{-1}\gamma^{-1}\mathbf{m}_{21}^{-1})\left(\frac{\imath}{8\hbar}\mathbf{m}_{21}\gamma + \frac{1}{8\hbar^2}\mathbf{m}_{22}\right) \tag{C.14}
\end{aligned}$$

and

$$\begin{aligned}
\mathbf{a}_{22}\mathbf{d} &= \mathbf{a}_{22}(\mathbf{a}_{11} - \mathbf{a}_{12}\mathbf{a}_{22}^{-1}\mathbf{a}_{12}^T) = \mathbf{a}_{22}\mathbf{a}_{11} - \mathbf{a}_{22}\mathbf{a}_{12}\mathbf{a}_{22}^{-1}\mathbf{a}_{12}^T \\
&= \left(\frac{\gamma}{4} + \frac{\mathbf{v}\mathbf{m}_{22}}{2}\right)\left(\frac{\gamma^{-1}}{4\hbar^2} + \frac{\mathbf{u}\mathbf{m}_{21}}{2}\right) - \mathbf{a}_{22}\left(-\frac{\imath}{4\hbar} + \frac{\mathbf{u}\mathbf{m}_{22}}{2}\right)\mathbf{a}_{22}^{-1}\left(\frac{\imath}{4\hbar} + \frac{\mathbf{v}\mathbf{m}_{21}}{2}\right) \\
&= \frac{\gamma}{8}\mathbf{u}\mathbf{m}_{21} + \frac{1}{8\hbar^2}\mathbf{v}\mathbf{m}_{22}\gamma^{-1} + \frac{1}{4}\mathbf{v}\mathbf{m}_{22}\mathbf{u}\mathbf{m}_{21} + \frac{\imath}{8\hbar}\mathbf{v}\mathbf{m}_{21} - \frac{\imath}{8\hbar}\mathbf{a}_{22}\mathbf{u}\mathbf{m}_{22}\mathbf{a}_{22}^{-1} \\
&\quad - \frac{1}{4}\mathbf{a}_{22}\mathbf{u}\mathbf{m}_{22}\mathbf{a}_{22}^{-1}\mathbf{v}\mathbf{m}_{21} \\
&= \mathbf{v}\left(\frac{1}{8\hbar^2}\mathbf{m}_{22}\gamma^{-1} + \frac{\imath}{8\hbar}\mathbf{m}_{21}\right) + \frac{\gamma}{8}\mathbf{u}\mathbf{m}_{21} + \frac{1}{2}\left(\mathbf{a}_{22} - \frac{\gamma}{4}\right)\mathbf{u}\mathbf{m}_{21} - \frac{\imath}{8\hbar}\mathbf{a}_{22}\mathbf{u}\mathbf{m}_{22}\mathbf{a}_{22}^{-1} \\
&\quad - \frac{1}{4}\mathbf{a}_{22}\mathbf{u}\mathbf{m}_{22}\mathbf{a}_{22}^{-1}\mathbf{v}\mathbf{m}_{22}\mathbf{m}_{22}^{-1}\mathbf{m}_{21} \\
&= \mathbf{v}\left(\frac{1}{8\hbar^2}\mathbf{m}_{22}\gamma^{-1} + \frac{\imath}{8\hbar}\mathbf{m}_{21}\right) + \frac{1}{2}\mathbf{a}_{22}\mathbf{u}\mathbf{m}_{21} - \frac{\imath}{8\hbar}\mathbf{a}_{22}\mathbf{u}\mathbf{m}_{22}\mathbf{a}_{22}^{-1} \\
&\quad - \frac{1}{2}\mathbf{a}_{22}\mathbf{u}\mathbf{m}_{22}\mathbf{a}_{22}^{-1}\left(\mathbf{a}_{22} - \frac{\gamma}{4}\right)\mathbf{m}_{22}^{-1}\mathbf{m}_{21} \\
&= \mathbf{v}\left(\frac{1}{8\hbar^2}\mathbf{m}_{22}\gamma^{-1} + \frac{\imath}{8\hbar}\mathbf{m}_{21}\right) - \frac{\imath}{8\hbar}\mathbf{a}_{22}\mathbf{u}\mathbf{m}_{22}\mathbf{a}_{22}^{-1}\gamma\mathbf{m}_{22}^{-1}\mathbf{m}_{22}\gamma^{-1} \\
&\quad + \frac{1}{8}\mathbf{a}_{22}\mathbf{u}\mathbf{m}_{22}\mathbf{a}_{22}^{-1}\gamma\mathbf{m}_{22}^{-1}\mathbf{m}_{21}
\end{aligned}$$

$$= (\mathbf{v} - i\hbar \mathbf{a}_{22} \mathbf{u} \mathbf{m}_{22} \mathbf{a}_{22}^{-1} \gamma \mathbf{m}_{22}^{-1}) \left(\frac{i}{8\hbar} \mathbf{m}_{21} + \frac{1}{8\hbar^2} \mathbf{m}_{22} \gamma^{-1} \right) \quad (\text{C.15})$$

are applied. Furthermore in Eq. (C.12) we make use of the relations

$$\begin{aligned} & (-i\hbar \mathbf{u} + \mathbf{a}_{11} \mathbf{v} \mathbf{m}_{21} \mathbf{a}_{11}^{-1} \gamma^{-1} \mathbf{m}_{21}^{-1})^{-1} \mathbf{a}_{11} \mathbf{v} \\ &= \mathbf{m}_{21} (-i\hbar \mathbf{v}^{-1} \mathbf{a}_{11}^{-1} \mathbf{u} \mathbf{m}_{21} + \mathbf{m}_{21} \mathbf{a}_{11}^{-1} \gamma^{-1})^{-1} \\ &= \mathbf{m}_{21} \left(-2i\hbar \mathbf{v}^{-1} \mathbf{a}_{11}^{-1} \left(\mathbf{a}_{11} - \frac{\gamma^{-1}}{4\hbar^2} \right) + \mathbf{m}_{21} \mathbf{a}_{11}^{-1} \gamma^{-1} \right)^{-1} \\ &= \mathbf{m}_{21} \left(-2i\hbar \mathbf{v}^{-1} + \frac{i}{2\hbar} \mathbf{v}^{-1} \mathbf{a}_{11}^{-1} \gamma^{-1} + \mathbf{m}_{21} \mathbf{a}_{11}^{-1} \gamma^{-1} \right)^{-1} \\ &= \mathbf{m}_{21} \gamma \mathbf{a}_{11} \left(-2i\hbar \gamma \left(\frac{\gamma^{-1}}{4\hbar^2} + \frac{\mathbf{u} \mathbf{m}_{21}}{2} \right) + \frac{i}{2\hbar} + \mathbf{v} \mathbf{m}_{21} \right)^{-1} \mathbf{v} \\ &= \mathbf{m}_{21} \gamma \mathbf{a}_{11} \mathbf{m}_{21}^{-1} (1 - i\hbar \mathbf{v}^{-1} \gamma \mathbf{u})^{-1} \\ &= \mathbf{m}_{21} \gamma \left(\frac{\gamma^{-1}}{4\hbar^2} + \frac{\mathbf{u} \mathbf{m}_{21}}{2} \right) \mathbf{m}_{21}^{-1} (1 - i\hbar \mathbf{v}^{-1} \gamma \mathbf{u})^{-1} \\ &= \left(\frac{1}{4\hbar^2} + \frac{\mathbf{m}_{21} \gamma \mathbf{u}}{2} \right) (1 - i\hbar \mathbf{v}^{-1} \gamma \mathbf{u})^{-1} \end{aligned} \quad (\text{C.16})$$

$$\begin{aligned} & (-i\hbar \mathbf{u} + \mathbf{a}_{11} \mathbf{v} \mathbf{m}_{21} \mathbf{a}_{11}^{-1} \gamma^{-1} \mathbf{m}_{21}^{-1})^{-1} \mathbf{a}_{11} \mathbf{a}_{12}^T \mathbf{a}_{11}^{-1} \mathbf{u} \\ &= \mathbf{m}_{21} (-i\hbar \mathbf{a}_{11}^{-1} \mathbf{u} \mathbf{m}_{21} + \mathbf{v} \mathbf{m}_{21} \mathbf{a}_{11}^{-1} \gamma^{-1})^{-1} \mathbf{a}_{12}^T \mathbf{a}_{11}^{-1} \mathbf{u} \\ &= \mathbf{m}_{21} \left(-2i\hbar \mathbf{a}_{11}^{-1} \left(\mathbf{a}_{11} - \frac{\gamma^{-1}}{4\hbar^2} \right) + 2 \left(\mathbf{a}_{12}^T - \frac{i}{4\hbar} \right) \mathbf{a}_{11}^{-1} \gamma^{-1} \right)^{-1} \mathbf{a}_{12}^T \mathbf{a}_{11}^{-1} \mathbf{u} \\ &= \mathbf{m}_{21} \left(-2i\hbar + \frac{i}{2\hbar} \mathbf{a}_{11}^{-1} \gamma^{-1} + 2 \mathbf{a}_{12}^T \mathbf{a}_{11}^{-1} \gamma^{-1} - \frac{i}{2\hbar} \mathbf{a}_{11}^{-1} \gamma^{-1} \right)^{-1} \mathbf{a}_{12}^T \mathbf{a}_{11}^{-1} \mathbf{u} \\ &= \mathbf{m}_{21} \left(-2i\hbar \mathbf{a}_{11} (\mathbf{a}_{12}^T)^{-1} + 2\gamma^{-1} \right)^{-1} \mathbf{u} \\ &= \frac{1}{2} \mathbf{m}_{21} \mathbf{a}_{12}^T (-i\hbar \mathbf{a}_{11} + \gamma^{-1} \mathbf{a}_{12}^T)^{-1} \mathbf{u} \\ &= \frac{1}{2} \mathbf{m}_{21} \mathbf{a}_{12}^T \left(-i\hbar \left(\frac{\gamma^{-1}}{4\hbar^2} + \frac{\mathbf{u} \mathbf{m}_{21}}{2} \right) + \gamma^{-1} \left(\frac{i}{4\hbar} + \frac{\mathbf{v} \mathbf{m}_{21}}{2} \right) \right)^{-1} \mathbf{u} \\ &= \mathbf{m}_{21} \mathbf{a}_{12}^T (-i\hbar \mathbf{u} \mathbf{m}_{21} + \gamma^{-1} \mathbf{v} \mathbf{m}_{21})^{-1} \mathbf{u} \\ &= \mathbf{m}_{21} \mathbf{a}_{12}^T \mathbf{m}_{21}^{-1} (\mathbf{u}^{-1} \gamma^{-1} \mathbf{v} - i\hbar)^{-1} \\ &= \mathbf{m}_{21} \mathbf{a}_{12}^T \mathbf{m}_{21}^{-1} \mathbf{v}^{-1} \gamma \mathbf{u} (1 - i\hbar \mathbf{v}^{-1} \gamma \mathbf{u})^{-1} \\ &= \mathbf{m}_{21} \left(\frac{i}{4\hbar} + \frac{\mathbf{v} \mathbf{m}_{21}}{2} \right) (\mathbf{v} \mathbf{m}_{21})^{-1} \gamma \mathbf{u} (1 - i\hbar \mathbf{v}^{-1} \gamma \mathbf{u})^{-1} \\ &= \left(\frac{i \mathbf{v}^{-1} \gamma \mathbf{u}}{4\hbar} + \frac{\mathbf{m}_{21} \gamma \mathbf{u}}{2} \right) (1 - i\hbar \mathbf{v}^{-1} \gamma \mathbf{u})^{-1} \end{aligned} \quad (\text{C.17})$$

$$\begin{aligned}
& (\mathbf{v} - i\hbar \mathbf{a}_{22} \mathbf{u} \mathbf{m}_{22} \mathbf{a}_{22}^{-1} \gamma \mathbf{m}_{22}^{-1})^{-1} \mathbf{a}_{22} \mathbf{u} \\
&= \mathbf{m}_{22} (\mathbf{u}^{-1} \mathbf{a}_{22}^{-1} \mathbf{v} \mathbf{m}_{22} - i\hbar \mathbf{m}_{22} \mathbf{a}_{22}^{-1} \gamma)^{-1} \\
&= \mathbf{m}_{22} \left(2\mathbf{u}^{-1} \mathbf{a}_{22}^{-1} \left(\mathbf{a}_{22} - \frac{\gamma}{4} \right) - i\hbar \mathbf{m}_{22} \mathbf{a}_{22}^{-1} \gamma \right)^{-1} \\
&= \mathbf{m}_{22} \left(2\mathbf{u}^{-1} - \frac{1}{2} \mathbf{u}^{-1} \mathbf{a}_{22}^{-1} \gamma - i\hbar \mathbf{m}_{22} \mathbf{a}_{22}^{-1} \gamma \right)^{-1} \\
&= \mathbf{m}_{22} \gamma^{-1} \mathbf{a}_{22} \left(2\mathbf{u}^{-1} \gamma^{-1} \mathbf{a}_{22} - \frac{1}{2} \mathbf{u}^{-1} - i\hbar \mathbf{m}_{22} \right)^{-1} \\
&= \mathbf{m}_{22} \gamma^{-1} \mathbf{a}_{22} (\gamma^{-1} \mathbf{v} \mathbf{m}_{22} - i\hbar \mathbf{u} \mathbf{m}_{22})^{-1} \mathbf{u} \\
&= \mathbf{m}_{22} \gamma^{-1} \mathbf{a}_{22} \mathbf{m}_{22}^{-1} (\mathbf{u}^{-1} \gamma^{-1} \mathbf{v} - i\hbar)^{-1} \\
&= \mathbf{m}_{22} \gamma^{-1} \mathbf{a}_{22} \mathbf{m}_{22}^{-1} \mathbf{v}^{-1} \gamma \mathbf{u} (1 - i\hbar \mathbf{v}^{-1} \gamma \mathbf{u})^{-1} \\
&= \mathbf{m}_{22} \gamma^{-1} \left(\frac{\gamma}{4} + \frac{\mathbf{v} \mathbf{m}_{22}}{2} \right) (\mathbf{v} \mathbf{m}_{22})^{-1} \gamma \mathbf{u} (1 - i\hbar \mathbf{v}^{-1} \gamma \mathbf{u})^{-1} \\
&= \left(\frac{\mathbf{v}^{-1} \gamma \mathbf{u}}{4} + \frac{\mathbf{m}_{22} \mathbf{u}}{2} \right) (1 - i\hbar \mathbf{v}^{-1} \gamma \mathbf{u})^{-1}
\end{aligned} \tag{C.18}$$

$$\begin{aligned}
& (\mathbf{v} - i\hbar \mathbf{a}_{22} \mathbf{u} \mathbf{m}_{22} \mathbf{a}_{22}^{-1} \gamma \mathbf{m}_{22}^{-1})^{-1} \mathbf{a}_{22} \mathbf{a}_{12} \mathbf{a}_{22}^{-1} \mathbf{v} \\
&= \mathbf{m}_{22} (\mathbf{a}_{22}^{-1} \mathbf{v} \mathbf{m}_{22} - i\hbar \mathbf{u} \mathbf{m}_{22} \mathbf{a}_{22}^{-1} \gamma)^{-1} \mathbf{a}_{12} \mathbf{a}_{22}^{-1} \mathbf{v} \\
&= \mathbf{m}_{22} \left(2\mathbf{a}_{22}^{-1} \left(\mathbf{a}_{22} - \frac{\gamma}{4} \right) - i\hbar \left(\mathbf{m}_{21}^T \mathbf{v}^T + \frac{i}{\hbar} \right) \mathbf{a}_{22}^{-1} \gamma \right)^{-1} \mathbf{a}_{12} \mathbf{a}_{22}^{-1} \mathbf{v} \\
&= \mathbf{m}_{22} \left(2 - \frac{1}{2} \mathbf{a}_{22}^{-1} \gamma - i\hbar \left(2\mathbf{a}_{12} + \frac{i}{2\hbar} \right) \mathbf{a}_{22}^{-1} \gamma \right)^{-1} \mathbf{a}_{12} \mathbf{a}_{22}^{-1} \mathbf{v} \\
&= \mathbf{m}_{22} \left(2 - \frac{1}{2} \mathbf{a}_{22}^{-1} \gamma - 2i\hbar \mathbf{a}_{12} \mathbf{a}_{22}^{-1} \gamma + \frac{1}{2} \mathbf{a}_{22}^{-1} \gamma \right)^{-1} \mathbf{a}_{12} \mathbf{a}_{22}^{-1} \mathbf{v} \\
&= \mathbf{m}_{22} (2\mathbf{a}_{22} \mathbf{a}_{12}^{-1} - 2i\hbar \gamma)^{-1} \mathbf{v} \\
&= \frac{1}{2} \mathbf{m}_{22} \mathbf{a}_{12} (\mathbf{a}_{22} - i\hbar \gamma \mathbf{a}_{12})^{-1} \mathbf{v} \\
&= \frac{1}{2} \mathbf{m}_{22} \mathbf{a}_{12} \left(\frac{\gamma}{4} + \frac{\mathbf{v} \mathbf{m}_{22}}{2} - i\hbar \gamma \left(\frac{i}{4\hbar} + \frac{\mathbf{m}_{21}^T \mathbf{v}^T}{2} \right) \right)^{-1} \mathbf{v} \\
&= \frac{1}{2} \mathbf{m}_{22} \mathbf{a}_{12} \left(\frac{\gamma}{2} + \frac{\mathbf{v} \mathbf{m}_{22}}{2} - i\hbar \gamma \frac{\mathbf{u} \mathbf{m}_{22} - \frac{i}{\hbar}}{2} \right)^{-1} \mathbf{v} \\
&= \mathbf{m}_{22} \left(\frac{i}{4\hbar} + \frac{\mathbf{u} \mathbf{m}_{22}}{2} - \frac{i}{2\hbar} \right) \mathbf{m}_{22}^{-1} (1 - i\hbar \mathbf{v}^{-1} \gamma \mathbf{u})^{-1} \\
&= \left(-\frac{i}{4\hbar} + \frac{\mathbf{m}_{22} \mathbf{u}}{2} \right) (1 - i\hbar \mathbf{v}^{-1} \gamma \mathbf{u})^{-1}.
\end{aligned} \tag{C.19}$$

In Eq. (C.19), the equation

$$\mathbf{m}_{21}^T \mathbf{v}^T = \mathbf{u} \mathbf{m}_{22} - \frac{i}{\hbar} \mathbf{1} \tag{C.20}$$

was used, which can be obtained using Eqs. (C.9) together with the symplecticity property

$$\mathbf{m}_{22}^T \mathbf{m}_{11} - \mathbf{m}_{12}^T \mathbf{m}_{21} = \mathbf{1}, \quad (\text{C.21})$$

which again is equivalent with Eq. (B.5). Eventually, the determinant of the matrix $\bar{\mathbf{A}}$ needs to be evaluated. In doing so, we resort to the determinant formula for block matrices

$$\det \begin{pmatrix} \mathbf{a}_{11} & \mathbf{a}_{12} \\ \mathbf{a}_{12}^T & \mathbf{a}_{22} \end{pmatrix} = \det \mathbf{a}_{11} \det (\mathbf{a}_{22} - \mathbf{a}_{12}^T \mathbf{a}_{11}^{-1} \mathbf{a}_{12}). \quad (\text{C.22})$$

Noting that $\mathbf{a}_{11} (\mathbf{a}_{22} - \mathbf{a}_{12}^T \mathbf{a}_{11}^{-1} \mathbf{a}_{12}) = \mathbf{a}_{11} \mathbf{e}$, which was rearranged in Eq. (C.14), the determinant of $\bar{\mathbf{A}}$ reads

$$\begin{aligned} \det \bar{\mathbf{A}} &= \det (\mathbf{a}_{11} \mathbf{e}) \\ &= \det (-i\hbar \mathbf{u} + \mathbf{a}_{11} \mathbf{v} \mathbf{m}_{21} \mathbf{a}_{11}^{-1} \gamma^{-1} \mathbf{m}_{21}^{-1}) \det \left(\frac{i}{8\hbar} \mathbf{m}_{21} \gamma + \frac{1}{8\hbar^2} \mathbf{m}_{22} \right). \end{aligned} \quad (\text{C.23})$$

The first determinant in this equation can be further simplified

$$\begin{aligned} &\det [-i\hbar \mathbf{u} + \mathbf{a}_{11} \mathbf{v} \mathbf{m}_{21} \mathbf{a}_{11}^{-1} \gamma^{-1} \mathbf{m}_{21}^{-1}] \\ &= \det [-i\hbar \mathbf{u} \mathbf{m}_{21} \gamma + \mathbf{a}_{11} \mathbf{m}_{21}^T \mathbf{v}^T \mathbf{a}_{11}^{-1}] \det [(\mathbf{m}_{21} \gamma)^{-1}] \\ &= \det \left[-2i\hbar \left(\mathbf{a}_{11} - \frac{\gamma^{-1}}{4\hbar^2} \right) \gamma + \mathbf{a}_{11} \mathbf{m}_{21}^T \mathbf{v}^T \mathbf{a}_{11}^{-1} \right] \det [(\mathbf{m}_{21} \gamma)^{-1}] \\ &= \det \left[-2i\hbar \mathbf{a}_{11} \gamma + \frac{i}{2\hbar} + \mathbf{a}_{11} \mathbf{m}_{21}^T \mathbf{v}^T \mathbf{a}_{11}^{-1} \right] \det [(\mathbf{m}_{21} \gamma)^{-1}] \\ &= \det (\mathbf{a}_{11}) \det \left[-2i\hbar \gamma + \frac{i}{2\hbar} \mathbf{a}_{11}^{-1} + \mathbf{m}_{21}^T \mathbf{v}^T \mathbf{a}_{11}^{-1} \right] \det [(\mathbf{m}_{21} \gamma)^{-1}] \\ &= \det \left[-2i\hbar \gamma \mathbf{a}_{11} + \frac{i}{2\hbar} + \mathbf{m}_{21}^T \mathbf{v}^T \right] \det [(\mathbf{m}_{21} \gamma)^{-1}] \\ &= \det [-i\hbar \gamma \mathbf{u} \mathbf{m}_{21} + \mathbf{v} \mathbf{m}_{21}] \det (\gamma^{-1}) \det (\mathbf{m}_{21}^{-1}) \\ &= \det [-i\hbar \mathbf{u} + \gamma^{-1} \mathbf{v}] \\ &= \det \left[-i\hbar \gamma \mathbf{m}_{21} + \mathbf{m}_{11} + \gamma \mathbf{m}_{22} \gamma^{-1} + \frac{i}{\hbar} \mathbf{m}_{12} \gamma^{-1} \right] \\ &= 2^N \det \mathbf{h}. \end{aligned} \quad (\text{C.24})$$

Employing Eqs. (C.23), (C.24) and (C.13), Eq. (C.5) finally becomes

$$\begin{aligned}
\Psi_\alpha(\mathbf{x}, t) &= \frac{1}{(2\hbar)^N} \sqrt{\frac{\det[\mathbf{h}(\mathbf{q}, \mathbf{p}, t)]}{\det \bar{\mathbf{A}}}} \left(\frac{\det \gamma}{\pi^N} \right)^{1/4} \exp \left\{ \frac{1}{4} \bar{\mathbf{b}}^T \bar{\mathbf{A}}^{-1} \bar{\mathbf{b}} + c \right\} \\
&= \frac{1}{(2\hbar)^N} \left(\frac{\det \gamma}{\pi^N} \right)^{1/4} [(2\hbar)^{2N} \det (\imath \hbar \mathbf{m}_{21} \gamma + \mathbf{m}_{22})]^{-1/2} \\
&\quad \times \exp \left\{ 2(\mathbf{x} - \mathbf{q}_{\alpha, t})^T (\imath \hbar \mathbf{u}^T \gamma + \mathbf{v}^T) (\mathbf{m}_{22} + \imath \hbar \mathbf{m}_{21} \gamma)^{-1} (\mathbf{x} - \mathbf{q}_{\alpha, t}) \right. \\
&\quad \left. - \frac{1}{2} (\mathbf{x} - \mathbf{q}_{\alpha, t})^T \gamma (\mathbf{x} - \mathbf{q}_{\alpha, t}) + \frac{\imath}{\hbar} \mathbf{p}_{\alpha, t}^T \cdot (\mathbf{x} - \mathbf{q}_{\alpha, t}) + \frac{\imath}{\hbar} S(\mathbf{q}, \mathbf{p}, t) \right\} \\
&= \left(\frac{\det \gamma}{\pi^N} \right)^{1/4} [\det (\imath \hbar \mathbf{m}_{21} \gamma + \mathbf{m}_{22})]^{-1/2} \\
&\quad \times \exp \left\{ -\frac{1}{2} (\mathbf{x} - \mathbf{q}_{\alpha, t})^T \left(\mathbf{m}_{11} \gamma + \frac{1}{\imath \hbar} \mathbf{m}_{12} \right) (\mathbf{m}_{22} + \imath \hbar \mathbf{m}_{21} \gamma)^{-1} (\mathbf{x} - \mathbf{q}_{\alpha, t}) \right. \\
&\quad \left. + \frac{\imath}{\hbar} \mathbf{p}_{\alpha, t}^T \cdot (\mathbf{x} - \mathbf{q}_{\alpha, t}) + \frac{\imath}{\hbar} S(\mathbf{q}, \mathbf{p}, t) \right\}, \tag{C.25}
\end{aligned}$$

which is the original expression of TGWD given by Heller [56]. Again, it should be stressed, that the obtained wave function depends on a single classical trajectory only.

D Expectation Values, Survival Probability and the Wigner Function in SCHD

An advantage of the SCHD is the Gaussian form of the integrand in the reduced density expression of Eq. (3.35) allowing for a partial analytical calculation of a number of quantities based on the density, like expectation values, so that in all cases finally only the phase space integral occurring in the SCHD needs to be performed numerically. Hence, in this appendix SCHD expressions for expectations values required in this thesis as well as the Wigner function and the survival probability are derived for SOIs with one DOF as used in this thesis. In addition, an expression for the survival probability within the LSC-IVR will be given, which provides the classical results. In all cases, the initial state is a Gaussian centered around (q_α, p_α) .

D.1 The Wigner Function

We consider a one-dimensional SOI. Then in density matrix formalism the Wigner function is defined as

$$W(s, \tilde{p}_s) = \frac{1}{\pi\hbar} \int d\zeta \langle s - \zeta | \hat{\rho} | s + \zeta \rangle e^{2i\tilde{p}_s\zeta/\hbar}. \quad (\text{D.1})$$

For reasons of clarity, the momentum of the Wigner representation \tilde{p}_s is introduced to distinguish it from the system momentum p_s , which is part of the phase space integration variables in the SCHD. Inserting the SCHD expression of the reduced density from Eq. (3.35), the ζ -dependent terms in the exponent of Eq. (D.1) then give

$$\begin{aligned} e &= (s - \zeta - q_{\alpha,s,t})^2 \Lambda_{11} + 2(s - \zeta - q_{\alpha,s,t})(s + \zeta - q_{\alpha,s,t}) \Lambda_{12} + (s + \zeta - q_{\alpha,s,t})^2 \Lambda_{22} \\ &\quad + \sigma_1(s - \zeta - q_{\alpha,s,t}) + \sigma_2(s + \zeta - q_{\alpha,s,t}) + \frac{2i}{\hbar} \tilde{p}_s \zeta \\ &= \left[\zeta^2 - 2\zeta(s - q_{\alpha,s,t}) + (s - q_{\alpha,s,t})^2 \right] \Lambda_{11} - 2[\zeta - (s - q_{\alpha,s,t})][\zeta + s - q_{\alpha,s,t}] \Lambda_{12} + \frac{2i}{\hbar} \tilde{p}_s \zeta \\ &\quad + \left[\zeta^2 + 2\zeta(s - q_{\alpha,s,t}) + (s - q_{\alpha,s,t})^2 \right] \Lambda_{22} - [\zeta - (s - q_{\alpha,s,t})] \sigma_1 + [\zeta + s - q_{\alpha,s,t}] \sigma_2 \\ &= -(-\Lambda_{11} + 2\Lambda_{12} - \Lambda_{22}) \zeta^2 + \left[-2(s - q_{\alpha,s,t}) \Lambda_{11} + 2(q_{\alpha,s,t} - q_\alpha) \Lambda_{12} \right. \\ &\quad \left. + 2(s - q_{\alpha,s,t}) \Lambda_{22} - \sigma_1 + \sigma_2 + \frac{2i}{\hbar} \tilde{p}_s \right] \zeta + (s - q_{\alpha,s,t})^2 \Lambda_{11} + (s - q'_{\alpha,s,t})^2 \Lambda_{22} \\ &\quad + 2(s - q_{\alpha,s,t})(s - q'_{\alpha,s,t}) \Lambda_{12} + (s - q_{\alpha,s,t}) \sigma_1 + (s - q'_{\alpha,s,t}) \sigma_2. \end{aligned} \quad (\text{D.2})$$

This is now an exponent of quadratic form in ζ , for which the integral in Eq. (D.1) can be calculated analytically by applying the Gaussian integration formula given in Eq. (2.36). The Wigner function then becomes

$$\begin{aligned}
 W(s, \tilde{p}_s) &= \int \frac{d^{N_{\text{hk}}} p_{\text{hk}} d^{N_{\text{hk}}} q_{\text{hk}} d^{N_{\text{hk}}} p'_{\text{hk}} d^{N_{\text{hk}}} q'_{\text{hk}}}{(2\hbar)^{2N} \pi^{2N_{\text{hk}}} \pi \hbar} \left(\prod_{i=1}^{N_B} (1 - e^{-\beta \omega_i \hbar}) \right) \sqrt{\frac{\det(\gamma) R(R')^*}{\det(\mathbf{A}) \det(\mathbf{H})}} \\
 &\quad \times \sqrt{\frac{1}{(-\Lambda_{11} + 2\Lambda_{12} - \Lambda_{22})}} \exp \left\{ \tilde{e} + h + \frac{i}{\hbar} (S - S') \right\} \\
 &\quad \times \langle g_{\gamma_S}(q_S, p_S) | \Psi_\alpha \rangle \langle \Psi_\alpha | g_{\gamma_S}(q'_S, p'_S) \rangle K_{\text{hb}}, \tag{D.3}
 \end{aligned}$$

where the expression

$$\begin{aligned}
 \tilde{e} &= \frac{1}{2\Lambda_{12} - \Lambda_{11} - \Lambda_{22}} \left[-(\tilde{s} - q_\alpha) \Lambda_{11} + (\tilde{s} - q'_\alpha) \Lambda_{22} + (q'_\alpha - q_\alpha) \Lambda_{12} - \frac{\sigma_1}{2} + \frac{\sigma_2}{2} + \frac{i}{\hbar} \tilde{p}_s \right]^2 \\
 &\quad + (s - q_{\alpha, s, t})^2 \Lambda_{11} + (s - q'_{\alpha, s, t})^2 \Lambda_{22} + 2(s - q_{\alpha, s, t})(s - q'_{\alpha, s, t}) \Lambda_{12} \\
 &\quad + (s - q_{\alpha, s, t}) \sigma_1 + (s - q'_{\alpha, s, t}) \sigma_2 \tag{D.4}
 \end{aligned}$$

results from the integration over ζ . This term can be reorganized into a clearer form yielding an expression that is quadratic in s and \tilde{p}_s

$$\begin{aligned}
 \tilde{e} &= \begin{pmatrix} s - q_{\alpha, s, t} \\ s - q'_{\alpha, s, t} \end{pmatrix}^T \mathbf{\Upsilon} \begin{pmatrix} s - q_{\alpha, s, t} \\ s - q'_{\alpha, s, t} \end{pmatrix} + \mathbf{\chi}^T \begin{pmatrix} s - q_{\alpha, s, t} \\ s - q'_{\alpha, s, t} \end{pmatrix} \\
 &\quad - \frac{1}{\hbar^2 (-\Lambda_{11} + 2\Lambda_{12} - \Lambda_{22})} \tilde{p}_s^2 + \frac{2i [(q'_{\alpha, s, t} - q_{\alpha, s, t}) \Lambda_{12} - \frac{\sigma_1}{2} + \frac{\sigma_2}{2}]}{\hbar (-\Lambda_{11} + 2\Lambda_{12} - \Lambda_{22})} \tilde{p}_s \\
 &\quad + \frac{[(q'_{\alpha, s, t} - q_{\alpha, s, t}) \Lambda_{12} - \frac{\sigma_1}{2} + \frac{\sigma_2}{2}]^2}{-\Lambda_{11} + 2\Lambda_{12} - \Lambda_{22}}, \tag{D.5}
 \end{aligned}$$

with the matrix

$$\mathbf{\Upsilon} = \begin{pmatrix} \frac{\Lambda_{11}^2}{2\Lambda_{12} - \Lambda_{11} - \Lambda_{22}} + \Lambda_{11} & \frac{\Lambda_{11}\Lambda_{22}}{2\Lambda_{12} - \Lambda_{11} - \Lambda_{22}} - \Lambda_{12} \\ \frac{\Lambda_{11}\Lambda_{22}}{2\Lambda_{12} - \Lambda_{11} - \Lambda_{22}} - \Lambda_{12} & \frac{\Lambda_{22}^2}{2\Lambda_{12} - \Lambda_{11} - \Lambda_{22}} + \Lambda_{22} \end{pmatrix} \tag{D.6}$$

and the vector

$$\mathbf{\chi} = \begin{pmatrix} -\frac{\frac{2i}{\hbar} \tilde{p}_s \Lambda_{11} + 2 [(q'_{\alpha, s, t} - q_{\alpha, s, t}) \Lambda_{12} - \frac{\sigma_1}{2} + \frac{\sigma_2}{2}] \Lambda_{11}}{-\Lambda_{11} + 2\Lambda_{12} - \Lambda_{22}} + \sigma_1 \\ \frac{\frac{2i}{\hbar} \tilde{p}_s \Lambda_{22} + 2 [(q'_{\alpha, s, t} - q_{\alpha, s, t}) \Lambda_{12} - \frac{\sigma_1}{2} + \frac{\sigma_2}{2}] \Lambda_{22}}{-\Lambda_{11} + 2\Lambda_{12} - \Lambda_{22}} + \sigma_2 \end{pmatrix}. \tag{D.7}$$

Thus as in the semiclassical hybrid reduced density, only the numerical calculation of the phase space integral is left in order to obtain the SCHD Wigner function.

D.2 Some Expectation Values

In the following SCHD expressions for the norm and some expectation values are derived, in which the energy expectation value for the Morse oscillator will be given.

D.2.1 Energy Expectation Value for the Morse Oscillator

The energy expectation value in reduced density formalism is given by

$$\langle E \rangle = \text{tr}(\mathcal{H}_s \hat{\rho}_s) = \int ds \langle s | \mathcal{T} \hat{\rho}_s | s \rangle + \int ds \langle s | \mathcal{V} \hat{\rho}_s | s \rangle. \quad (\text{D.8})$$

First the kinetic contribution is evaluated using the SCHD reduced density expression again. For reasons of clarity and comprehensibility, the s - and s' -dependent parts are considered solely, and thus the kinetic expectation value reads

$$\begin{aligned} & \int ds \langle s | \mathcal{T} \hat{\rho}_s | s \rangle \\ &= -\frac{\hbar^2}{2m} \int ds ds' \delta(s' - s) \frac{\partial^2}{\partial s^2} \langle s' | \hat{\rho}_s | s \rangle \\ &\sim -\frac{\hbar^2}{2m} \int ds ds' \delta(s' - s) \exp \left\{ \Lambda_{22} (s' - q'_{\alpha,s,t})^2 + \sigma_2 (s' - q'_{\alpha,s,t}) \right\} \\ &\quad \times \frac{\partial^2}{\partial s^2} \exp \left\{ \Lambda_{11} (s - q_{\alpha,s,t})^2 + 2\Lambda_{12} (s - q_{\alpha,s,t}) (s' - q'_{\alpha,s,t}) + \sigma_1 (s - q_{\alpha,s,t}) \right\} \\ &= -\frac{\hbar^2}{2m} \int ds ds' \delta(s' - s) \left\{ 2\Lambda_{11} + [2\Lambda_{11} (s - q_{\alpha,s,t}) + 2\Lambda_{12} (s' - q'_{\alpha,s,t}) + \sigma_1]^2 \right\} \\ &\quad \times \exp \left\{ \Lambda_{22} (s' - q'_{\alpha,s,t})^2 + \sigma_2 (s' - q'_{\alpha,s,t}) \right. \\ &\quad \left. + \Lambda_{11} (s - q_{\alpha,s,t})^2 + 2\Lambda_{12} (s - q_{\alpha,s,t}) (s' - q'_{\alpha,s,t}) + \sigma_1 (s - q_{\alpha,s,t}) \right\} \\ &= -\frac{\hbar^2}{2m} \int ds \left\{ 2\Lambda_{11} + \underbrace{[2(\Lambda_{11} + \Lambda_{12})s + (\sigma_1 - 2\Lambda_{11}q_{\alpha,s,t} - 2\Lambda_{12}q'_{\alpha,s,t})]}_{\equiv \kappa_1} \right\}^2 \\ &\quad \times \exp \left\{ -\underbrace{(-\Lambda_{11} - \Lambda_{22} - 2\Lambda_{12})s^2}_{\equiv \Omega_1} \right. \\ &\quad \left. + \underbrace{[-2\Lambda_{11}q_{\alpha,s,t} - 2\Lambda_{22}q'_{\alpha,s,t} - 2\Lambda_{12}(q_{\alpha,s,t} + q'_{\alpha,s,t}) + \sigma_1 + \sigma_2]s}_{\equiv \Omega_2} \right. \\ &\quad \left. + \underbrace{\Lambda_{11}q_{\alpha,s,t}^2 + 2\Lambda_{12}q_{\alpha,s,t}q'_{\alpha,s,t} + \Lambda_{22}q_{\alpha,s,t}'^2 - \sigma_1q_{\alpha,s,t} - \sigma_2q'_{\alpha,s,t}}_{\equiv \Omega_3} \right\} \\ &= -\frac{\hbar^2}{2m} \int ds \left\{ \kappa_1^2 s^2 + 2\kappa_1\kappa_2 s + 2\Lambda_{11} + \kappa_2^2 \right\} \exp \left\{ -\Omega_1 \left(s - \frac{\Omega_2}{2\Omega_1} \right)^2 + \frac{\Omega_2^2}{4\Omega_1} + \Omega_3 \right\}. \end{aligned} \quad (\text{D.9})$$

The obtained integral can be solved by making use of the Gaussian integration formula in Eq. (2.36) as well as the following two formulas

$$\int_{-\infty}^{\infty} dx x e^{-a(x-b)^2} = b \sqrt{\frac{\pi}{a}} \quad \text{Re}(a) > 0 \quad (\text{D.10})$$

$$\int_{-\infty}^{\infty} dx x^2 e^{-a(x-b)^2} = \frac{1 + 2ab^2}{2a} \sqrt{\frac{\pi}{a}} \quad \text{Re}(a) > 0, \quad (\text{D.11})$$

which basically can be derived by partial integration and applying the Gaussian integration formula again. Hence, the kinetic part of the energy expectation value becomes

$$\begin{aligned} & \int ds \langle s | \mathcal{T} \hat{\rho}_S | s \rangle \\ &= -\frac{\hbar^2}{2m} \int \frac{d^{N_{\text{hk}}} p_{\text{hk}} d^{N_{\text{hk}}} q_{\text{hk}} d^{N_{\text{hk}}} p'_{\text{hk}} d^{N_{\text{hk}}} q'_{\text{hk}}}{(2\hbar)^{2N} \pi^{2N_{\text{hk}}}} \left[\prod_{i=1}^{N_{\text{B}}} (1 - e^{-\beta \omega_i \hbar}) \right] \sqrt{\frac{\det(\gamma) R(R')^*}{\det(\mathbf{A}) \det(\mathbf{H})}} \\ & \quad \times \sqrt{\frac{1}{\Omega_1}} \left[\frac{\kappa_1^2}{2\Omega_1} + \left(\frac{\kappa_1^2 \Omega_2^2}{4\Omega_1^2} + \frac{\kappa_1 \kappa_2 \Omega_2}{\Omega_1} + 2\Lambda_{11} + \kappa_2^2 \right) \right] \exp \left\{ \frac{\Omega_2^2}{4\Omega_1} + \Omega_3 \right\} \\ & \quad \times \exp \left\{ h + \frac{i}{\hbar} (S - S') \right\} \langle g_{\gamma_S}(q_S, p_S) | \Psi_\alpha \rangle \langle \Psi_\alpha | g_{\gamma_S}(q'_S, p'_S) \rangle K_{\text{hb}}. \quad (\text{D.12}) \end{aligned}$$

Turning to the potential expectation value, one has to be careful, since within the CL model the identification of the SOI potential contribution is not as straightforward as the one of the SOI kinetic contribution. In principle, for the potential part every term has to be considered, that depends on the system's position s , i.e. the Morse potential, the counter and the coupling term in the CL Hamiltonian given in Eq. (2.5). The main problem is the coupling term, since the SOI DOFs cannot be separated from the bath DOFs and thus this term always depends on *all* DOFs. Thus, it gives a contribution to the energy of the overall system, though it cannot be fully assigned to any of the subsystems, neither the SOI nor the bath. Nevertheless, for small coupling strengths this issue can be ignored, since the coupling term is assumed to be much smaller than the actual SOI potential, i.e. the Morse potential, and thus can be neglected. Therefore, the potential expectation value can be written as the expectation value of an effective potential $\mathcal{V} \rightarrow \mathcal{V}_{\text{eff}}$, which is composed of the system's Morse potential and the quadratic counter term

$$\int ds \langle s | \mathcal{V}_{\text{eff}} \hat{\rho}_S | s \rangle = \int ds D (1 - e^{-\alpha s})^2 \rho_S(s) + \sum_{i=1}^{N_{\text{B}}} \frac{c_i^2}{2\omega_i^2 m_i} \int ds s^2 \rho_S(s). \quad (\text{D.13})$$

Focusing on the s -dependent parts of the SCHD expression and considering the relation

$$\begin{aligned} \begin{pmatrix} s - q_{\alpha, s, t} \\ s - q'_{\alpha, s, t} \end{pmatrix}^T \mathbf{\Lambda} \begin{pmatrix} s - q_{\alpha, s, t} \\ s - q'_{\alpha, s, t} \end{pmatrix} + \boldsymbol{\sigma} \begin{pmatrix} s - q_{\alpha, s, t} \\ s - q'_{\alpha, s, t} \end{pmatrix} &= -\Omega_1 s^2 + \Omega_2 s + \Omega_3 \\ &= -\Omega_1 \left(s - \frac{\Omega_2}{2\Omega_1} \right)^2 + \frac{\Omega_2^2}{4\Omega_1} + \Omega_3, \quad (\text{D.14}) \end{aligned}$$

with the abbreviations introduced in Eq. (D.9), the Morse part then reads

$$\begin{aligned}
 & \int ds D (1 - e^{-\alpha s})^2 \rho_s(s) \\
 & \sim D \int ds (1 - 2e^{-\alpha s} + e^{-2\alpha s}) \exp\{-\Omega_1 s^2 + \Omega_2 s + \Omega_3\} \\
 & = D \int ds e^{-\Omega_1 s^2 + \Omega_3} [\exp\{\Omega_2 s\} - 2 \exp\{(\Omega_2 - \alpha) s\} + \exp\{(\Omega_2 - 2\alpha) s\}] \\
 & = D \sqrt{\frac{\pi}{\Omega_1}} \left[\exp\left\{\frac{\Omega_2^2}{4\Omega_1}\right\} - 2 \exp\left\{\frac{(\Omega_2 - \alpha)^2}{4\Omega_1}\right\} + \exp\left\{\frac{(\Omega_2 - 2\alpha)^2}{4\Omega_1}\right\} \right] e^{\Omega_3}. \quad (D.15)
 \end{aligned}$$

The counter term can be calculated by applying Eq. (D.14) and making use of Eq. (D.11)

$$\begin{aligned}
 & \underbrace{\sum_{i=1}^{N_B} \frac{c_i^2}{2\omega_i^2 m_i}}_{\equiv F = \text{const.}} \int ds s^2 \rho_s(s) = F \int ds s^2 \exp\left\{-\Omega_1 \left(s - \frac{\Omega_2}{2\Omega_1}\right)^2\right\} \\
 & = F \sqrt{\frac{\pi}{\Omega_1}} \left(\frac{1}{2\Omega_1} + \frac{\Omega_2^2}{4\Omega_1^2} \right), \quad (D.16)
 \end{aligned}$$

where again only the s -dependent terms are considered. Summing up everything, the potential expectation value finally yields

$$\begin{aligned}
 & \int ds \langle s | \mathcal{V}_{\text{eff}} \hat{\rho}_S | s \rangle \\
 & = \int \frac{d^{N_{\text{hk}}} p_{\text{hk}} d^{N_{\text{hk}}} q_{\text{hk}} d^{N_{\text{hk}}} p'_{\text{hk}} d^{N_{\text{hk}}} q'_{\text{hk}}}{(2\hbar)^{2N} \pi^{2N_{\text{hk}}}} \left[\prod_{i=1}^{N_B} (1 - e^{-\beta \omega_i \hbar}) \right] \sqrt{\frac{\det(\boldsymbol{\gamma}) R(R')^*}{\det(\mathbf{A}) \det(\mathbf{H})}} \sqrt{\frac{1}{\Omega_1}} \\
 & \quad \times \left[D \exp\left\{\frac{\Omega_2^2}{4\Omega_1}\right\} - 2D \exp\left\{\frac{(\Omega_2 - \alpha)^2}{4\Omega_1}\right\} \right. \\
 & \quad \left. + D \exp\left\{\frac{(\Omega_2 - 2\alpha)^2}{4\Omega_1}\right\} + F \left(\frac{1}{2\Omega_1} + \frac{\Omega_2^2}{4\Omega_1^2} \right) \exp\left\{\frac{\Omega_2^2}{4\Omega_1}\right\} \right] \\
 & \quad \times \exp\left\{\Omega_3 + h + \frac{i}{\hbar}(S - S')\right\} \langle g_{\gamma_S}(q_S, p_S) | \Psi_\alpha \rangle \langle \Psi_\alpha | g_{\gamma_S}(q'_S, p'_S) \rangle K_{\text{hb}} \quad (D.17)
 \end{aligned}$$

in case, the SOI is a Morse oscillator.

D.2.2 Norm, Position Expectation Value and Second Moment of Position

Having derived the energy expectation value, the calculation of the position expectation value, its second moment and the norm, i.e. $\text{tr}(\hat{\rho}_S)$, is straightforward, since the same integration formulas can be applied as before. Again, considering only the s -dependent parts included in the SCHD expression of the norm and the regarded expectation values we obtain

$$\begin{aligned}
 G_{\text{tr}(\hat{\rho}_S)} &= \int ds \exp \left\{ -\Omega_1 \left(s - \frac{\Omega_2}{2\Omega_1} \right)^2 + \frac{\Omega_2^2}{4\Omega_1} + \Omega_3 \right\} \\
 &= \sqrt{\frac{\pi}{\Omega_1}} \exp \left\{ +\frac{\Omega_2^2}{4\Omega_1} + \Omega_3 \right\}
 \end{aligned} \tag{D.18}$$

$$\begin{aligned}
 G_{\langle s \rangle} &= \int ds s \exp \left\{ -\Omega_1 \left(s - \frac{\Omega_2}{2\Omega_1} \right)^2 + \frac{\Omega_2^2}{4\Omega_1} + \Omega_3 \right\} \\
 &= \sqrt{\frac{\pi}{\Omega_1}} \frac{\Omega_2}{2\Omega_1} \exp \left\{ +\frac{\Omega_2^2}{4\Omega_1} + \Omega_3 \right\}
 \end{aligned} \tag{D.19}$$

$$\begin{aligned}
 G_{\langle s^2 \rangle} &= \int ds s^2 \exp \left\{ -\Omega_1 \left(s - \frac{\Omega_2}{2\Omega_1} \right)^2 + \frac{\Omega_2^2}{4\Omega_1} + \Omega_3 \right\} \\
 &= \sqrt{\frac{\pi}{\Omega_1}} \left(\frac{1}{2\Omega_1} + \frac{\Omega_2^2}{4\Omega_1^2} \right) \exp \left\{ +\frac{\Omega_2^2}{4\Omega_1} + \Omega_3 \right\},
 \end{aligned} \tag{D.20}$$

where the Eqs. (2.36), (D.10) and (D.11) are used and Eq. (D.14) is considered. The respective expectation value then becomes

$$\begin{aligned}
 i &= \int \frac{d^{N_{\text{hk}}} p_{\text{hk}} d^{N_{\text{hk}}} q_{\text{hk}} d^{N_{\text{hk}}} p'_{\text{hk}} d^{N_{\text{hk}}} q'_{\text{hk}}}{(2\hbar)^{2N} \pi^{2N_{\text{hk}}} \sqrt{\pi}} \left[\prod_{i=1}^{N_{\text{B}}} (1 - e^{-\beta \omega_i \hbar}) \right] \sqrt{\frac{\det(\boldsymbol{\gamma}) R(R')^*}{\det(\mathbf{A}) \det(\mathbf{H})}} G_i \\
 &\quad \times \exp \left\{ h + \frac{i}{\hbar} (S - S') \right\} \langle g_{\gamma_S}(q_S, p_S) | \Psi_\alpha \rangle \langle \Psi_\alpha | g_{\gamma_S}(q'_S, p'_S) \rangle K_{\text{hb}}, \tag{D.21}
 \end{aligned}$$

where i stands for $\text{tr}(\hat{\rho}_S)$, $\langle s \rangle$ and $\langle s^2 \rangle$.

D.3 Survival Probability...

D.3.1 ... within SCHD

In density formalism, the survival probability equals the trace over the time-evolved (reduced) density operator with the initial density operator

$$C(t) = \text{tr}[\hat{\rho}_i \hat{\rho}(t)], \tag{D.22}$$

which is nothing else but the expectation value of the initial state. For the derivation of the SCHD expression of the survival probability, as before, only the terms involved in the integration necessary to perform the trace, i.e. the s - and s' -dependent terms, will be regarded giving

$$\begin{aligned}
J &= \int ds ds' \Psi_\alpha^*(s) \rho_s(s, s'; t) \Psi_\alpha(s') \\
&= \sqrt{\frac{\gamma_s}{\pi}} \int ds ds' \exp \left\{ -\frac{\gamma_s}{2} [(s - q_\alpha)^2 + (s' - q_\alpha)^2] + \Lambda_{11}(s - q_{\alpha, s, t})^2 + \Lambda_{22}(s' - q'_{\alpha, s, t})^2 \right. \\
&\quad \left. + 2\Lambda_{12}(s - q_{\alpha, s, t})(s' - q'_{\alpha, s, t}) + \sigma_1(s - q_{\alpha, s, t}) + \sigma_2(s' - q'_{\alpha, s, t}) \right\} \\
&= \sqrt{\frac{\gamma_s}{\pi}} \int ds ds' \exp \left\{ -\begin{pmatrix} s \\ s' \end{pmatrix}^T \mathbf{\Gamma} \begin{pmatrix} s \\ s' \end{pmatrix} + \boldsymbol{\xi}^T \begin{pmatrix} s \\ s' \end{pmatrix} \right. \\
&\quad \left. - \gamma_s q_\alpha^2 + \begin{pmatrix} q_{\alpha, s, t} \\ q'_{\alpha, s, t} \end{pmatrix}^T \mathbf{\Lambda} \begin{pmatrix} q_{\alpha, s, t} \\ q'_{\alpha, s, t} \end{pmatrix} + \boldsymbol{\sigma}^T \begin{pmatrix} q_{\alpha, s, t} \\ q'_{\alpha, s, t} \end{pmatrix} \right\} \\
&= \sqrt{\frac{\gamma_s \pi}{\det \mathbf{\Gamma}}} \exp \left\{ \frac{1}{4} \boldsymbol{\xi}^T \mathbf{\Gamma}^{-1} \boldsymbol{\xi} - \gamma_s q_\alpha^2 + \begin{pmatrix} q_{\alpha, s, t} \\ q'_{\alpha, s, t} \end{pmatrix}^T \mathbf{\Lambda} \begin{pmatrix} q_{\alpha, s, t} \\ q'_{\alpha, s, t} \end{pmatrix} + \boldsymbol{\sigma}^T \begin{pmatrix} q_{\alpha, s, t} \\ q'_{\alpha, s, t} \end{pmatrix} \right\}. \quad (D.23)
\end{aligned}$$

Here, the determinant and inverse of the introduced 2×2 matrix $\mathbf{\Gamma}$ is

$$\det(\mathbf{\Gamma}) = \left(\frac{\gamma_s}{2} - \Lambda_{11} \right) \left(\frac{\gamma_s}{2} - \Lambda_{22} \right) - \Lambda_{12}^2 \quad (D.24)$$

$$\mathbf{\Gamma}^{-1} = \frac{1}{\det(\mathbf{\Gamma})} \begin{pmatrix} \frac{\gamma_s}{2} - \Lambda_{22} & \Lambda_{12} \\ \Lambda_{12} & \frac{\gamma_s}{2} - \Lambda_{11} \end{pmatrix} \quad (D.25)$$

and furthermore the new vector reads

$$\boldsymbol{\xi} = \begin{pmatrix} \gamma_s q_\alpha - 2\Lambda_{11} q_{\alpha, s, t} - 2\Lambda_{12} q'_{\alpha, s, t} + \sigma_1 \\ \gamma_s q_\alpha - 2\Lambda_{22} q'_{\alpha, s, t} - 2\Lambda_{12} q_{\alpha, s, t} + \sigma_2 \end{pmatrix}. \quad (D.26)$$

Thus in summary, we obtain the SCHD survival probability

$$\begin{aligned}
C(t) &= \int \frac{d^{N_{\text{hk}}} p_{\text{hk}} d^{N_{\text{hk}}} q_{\text{hk}} d^{N_{\text{hk}}} p'_{\text{hk}} d^{N_{\text{hk}}} q'_{\text{hk}}}{(2\hbar)^{2N} \pi^{2N_{\text{hk}}} \sqrt{\pi}} \left[\prod_{i=1}^{N_B} (1 - e^{-\beta \omega_i \hbar}) \right] \sqrt{\frac{\det(\boldsymbol{\gamma}) R(R')^*}{\det(\mathbf{A}) \det(\mathbf{H})}} J \\
&\quad \times \exp \left\{ h + \frac{i}{\hbar} (S - S') \right\} \langle g_{\gamma_s}(q_s, p_s) | \Psi_\alpha \rangle \langle \Psi_\alpha | g_{\gamma_s}(q'_s, p'_s) \rangle K_{\text{hb}}, \quad (D.27)
\end{aligned}$$

so that it can be computed without the explicit calculation of the reduced density matrix, too.

D.3.2 ... within the LSC-IVR

As the final part of this chapter, the LSC-IVR expression for the survival probability is to be sketched as well. To this end, the LSC-IVR time-correlation function from Eq. (3.12) is the starting point

$$\tilde{C}_{AB}(t) = \iint \frac{d^N q d^N p}{(2\pi\hbar)^N} A^w(\mathbf{p}, \mathbf{q}) B^w(\mathbf{p}_t, \mathbf{q}_t). \quad (D.28)$$

The operator \hat{A} is the same as in the derivation of the LSC-IVR reduced density, since the initial state has not changed. However, now the operator \hat{B} is chosen to be the initial state density operator, i.e. $|\Psi_\alpha\rangle\langle\Psi_\alpha|$, with $p_\alpha = 0$. The corresponding Wigner function

$$\begin{aligned}
 B^w &= \int d^N \zeta \, e^{-i\mathbf{p}_t \cdot \boldsymbol{\zeta} / \hbar} \langle \mathbf{q}_t + \frac{\boldsymbol{\zeta}}{2} | \hat{B} | \mathbf{q}_t - \frac{\boldsymbol{\zeta}}{2} \rangle = \int d^N \zeta \, e^{-i\mathbf{p}_t \cdot \boldsymbol{\zeta} / \hbar} \langle \mathbf{q}_t + \frac{\boldsymbol{\zeta}}{2} | \Psi_\alpha \rangle \langle \Psi_\alpha | \mathbf{q}_t - \frac{\boldsymbol{\zeta}}{2} \rangle \\
 &= \int d\zeta_s \, e^{-ip_{s,t}\zeta_s/\hbar} \langle q_{s,t} + \frac{\zeta_s}{2} | \Psi_\alpha \rangle \langle \Psi_\alpha | q_{s,t} - \frac{\zeta_s}{2} \rangle \prod_{i=1}^{N_B} \int d\zeta_i \, e^{-ip_{i,t}\zeta_i/\hbar} \underbrace{\langle q_{i,t} + \frac{\zeta_i}{2} | q_{i,t} - \frac{\zeta_i}{2} \rangle}_{=\delta(\zeta_i)} \\
 &= \sqrt{\frac{\gamma_s}{\pi}} \int d\zeta_s \, \exp \left\{ -\frac{\gamma_s}{2} \left(q_{s,t} + \frac{\zeta_s}{2} - q_\alpha \right)^2 - \frac{\gamma_s}{2} \left(q_{s,t} - \frac{\zeta_s}{2} - q_\alpha \right)^2 - \frac{i}{\hbar} p_{s,t} \zeta_s \right\} \\
 &= \sqrt{\frac{\gamma_s}{\pi}} \int d\zeta_s \, \exp \left\{ -\gamma_s (q_{s,t} - q_\alpha)^2 - \frac{\gamma_s}{4} \zeta_s^2 - \frac{i}{\hbar} p_{s,t} \zeta_s \right\} \\
 &= 2 \exp \left\{ -\gamma_s (q_{s,t} - q_\alpha)^2 - \frac{1}{\hbar^2 \gamma_s} p_{s,t}^2 \right\} \tag{D.29}
 \end{aligned}$$

is of Gaussian form in both the final position and momentum centered around the mean position and momentum of the initial GWP.

Bibliography

- [1] D. P. DiVincenzo
“The Physical Implementation of Quantum Computation”
Fortschritte der Physik **21**, 771 (2000)
- [2] M. A. Nielsen and I. L. Chuang
Quantum Computation and Quantum Information
Cambridge University Press (2000)
- [3] P. Hänggi, P. Talkner and M. Borkovec
“Reaction-rate theory: fifty years after Kramers”
Rev. Mod. Phys. **62**, 251 (1990)
- [4] H.-P. Breuer and F. Petruccione
The Theory of Open Quantum Systems
Oxford University Press, Oxford (2002)
- [5] P. Hänggi and G.-L. Ingold
“Fundamental Aspects of Quantum Brownian Motion”
Chaos **15**, 026105 (2005)
- [6] U. Weiss
Quantum Dissipative Systems
World Scientific, Singapore third edition (2008)
- [7] R. P. Feynman and F. L. Vernon
“The theory of a general quantum system interacting with a linear dissipative system”
Annals of Physics **24**, 118–173 (1963)
- [8] A. O. Caldeira and A. J. Leggett
“Path integral approach to quantum Brownian motion”
Physica A **121**, 587 (1983)
- [9] M. Winterstetter and W. Domcke
“Path-integral approach to resonant electron-molecule scattering”
Phys. Rev. A **47**, 2838 (1993)
- [10] F. Grossmann
“A semiclassical approach to dissipation in quantum mechanics”
J. Chem. Phys. **103**, 3696 (1995)
- [11] N. Makri
“Quantum Dissipative Dynamics”
J. Phys. Chem. **102**, 4414 (1998)

- [12] J. T. Stockburger and H. Grabert
“Exact c -Number Representation of Non-Markovian Quantum Dissipation”
Phys. Rev. Lett. **88**, 170407 (2002)
- [13] B. Hu, P. Paz and Y. Zhang
“Quantum Brownian motion in a general environment: Exact master equation with nonlocal dissipation and colored noise”
Phys. Rev. D **45**, 2843 (1992)
- [14] P. Saalfrank
“Stochastic wave packet vs. direct density matrix solution of Liouville-von Neumann equations for photodesorption problems”
Chem. Phys. **211**, 265 (1996)
- [15] W. Strunz, L. Diosi and N. Gisin
“Open system dynamics with non-Markovian quantum trajectories”
Phys. Rev. Lett. **82**, 1801 (1999)
- [16] D. Kohen and D. J. Tannor
“Phase Space Approach to Dissipative Molecular Dynamics”
Adv. Chem. Phys. **111**, 219 (2000)
- [17] E. Pollak
“Transition-state theory for tunneling in dissipative media”
Phys. Rev. A **33**, 4244 (1986)
- [18] W. Hontscha and P. Hänggi
“Phenomenological shortcut to dissipative dynamics”
Phys. Rev. A **36**, 2359 (1987)
- [19] E. Pollak
“Continuum limit semiclassical initial value representation for dissipative systems”
J. Chem. Phys. **127**, 074505 (2007)
- [20] J. M. Moix and E. Pollak
“Semiclassical initial value series representation in the continuum limit: Application to vibrational relaxation”
J. Chem. Phys. **129**, 064515 (2008)
- [21] W. Hontscha, P. Hänggi and E. Pollak
“Numerical study of tunneling in a dissipative system”
Phys. Rev. B **41**, 2210 (1990)
- [22] J. Cao, L. W. Ungar and G. A. Voth
“A novel method for simulating quantum dissipative systems”
J. Chem. Phys. **104**, 4189 (1996)
- [23] H. Wang, X. Song, D. Chandler and W. Miller
“Semiclassical study of electronically nonadiabatic dynamics in the condensed-phase: Spin-boson problem with Debye spectral density”
J. Chem. Phys. **110**, 4828 (1999)

-
- [24] R. Martinazzo, M. Nest, P. Saalfrank and G. F. Tondardini
“A local coherent-state approximation to system-bath quantum dynamics”
J. Chem. Phys. **125**, 194102 (2006)
- [25] H. Wang and M. Thoss
“From coherent motion to localization: dynamics of the spin-boson model at zero temperature”
New J. Phys. **10**, 115005 (2008)
- [26] I. Burghardt, M. Nest and G. A. Worth
“Multiconfigurational system-bath dynamics using Gaussian wave packets: Energy relaxation and decoherence induced by a finite-dimensional bath”
J. Chem. Phys. **119**, 5364 (2003)
- [27] Y. Elran and P. Brumer
“Decoherence in an anharmonic oscillator coupled to a thermal environment: A semi-classical forward-backward approach”
J. Chem. Phys. **121**, 2673 (2004)
- [28] E. Pollak, J. Shao and D. H. Zhang
“Effects of initial correlations on the dynamics of dissipative systems”
Phys. Rev. E **77**, 021107 (2008)
- [29] A. O. Caldeira and A. J. Leggett
“Influence of dissipation on quantum tunneling in macroscopic systems”
Phys. Rev. Lett. **46**, 211 (1981)
- [30] J. A. Fleck, J. R. Morris and M. D. Feit
“Time-dependent propagation of high energy laser beams through the atmosphere”
App. Phys. A **10**, Issue 2, 129 (1976)
- [31] H.-D. Meyer, U. Manthe and L. S. Cederbaum
“The multi-configurational time-dependent Hartree approach”
Chem. Phys. Lett. **165**, 73 (1990)
- [32] J. H. Van Vleck
“The correspondence principle in the statistical interpretation of quantum mechanics”
Proc. Natl. Acad. Sci. **14**, 178 (1928)
- [33] M. C. Gutzwiller
Chaos in Classical and Quantum Mechanics
Springer (1990)
- [34] W. H. Miller
“Classical S Matrix: Numerical Application to Inelastic Collision”
J. Chem. Phys. **53**, 3578 (1970)
- [35] E. J. Heller
“Time-dependent approach to semiclassical dynamics”
J. Chem. Phys. **62**, 1544 (1975)

- [36] E. J. Heller
“Frozen Gaussians: A very simple semiclassical approximation”
J. Chem. Phys. **75**, 2923 (1981)
- [37] K. G. Kay
“Integral expressions for the semiclassical time-dependent propagator”
J. Chem. Phys. **100**, 4377 (1994)
- [38] M. F. Herman and E. Kluk
“A semiclassical justification for the use of non-spreading wavepackets in dynamics calculations”
Chem. Phys. **91**, 27 (1984)
- [39] X. Sun and W. H. Miller
“Semiclassical initial value representation for electronically nonadiabatic molecular dynamics”
J. Chem. Phys. **106**, 6343 (1997)
- [40] F. Grossmann
“Semiclassical wave packet propagation on potential surfaces coupled by ultrashort laser pulses”
Phys. Rev. A **60**, 1791 (1999)
- [41] D. A. McCormack
“An evaluation of the semiclassical Herman-Kluk (HK) propagator for molecule-surface reaction scattering”
J. Chem. Phys. **112**, 992 (2000)
- [42] M. Thoss, W. H. Miller and G. Stock
“Semiclassical description of nonadiabatic quantum dynamics: Application to the $S_1 - S_2$ conical intersection in pyrazine”
J. Chem. Phys. **112**, 10282 (2000)
- [43] K. Giese and O. Kühn
“Semiclassical tunneling splittings from short time dynamics: Herman-Kluk-propagation and harmonic inversion”
J. Chem. Phys. **120**, 4107 (2004)
- [44] C. Harabati and K. G. Kay
“Semiclassical initial value calculations of the collinear helium atom”
J. Chem. Phys. **127**, 084104 (2009)
- [45] M. Ceotto, S. Atahan, G. F. Tantardini and A. Aspuru-Guzik
“Multiple coherent states for first-principles semiclassical initial value representation molecular dynamics”
J. Chem. Phys. **130**, 234113 (2009)
- [46] G. van de Sand and J.-M. Rost
“Irregular Orbits Generate Higher Harmonics”
Phys. Rev. Lett. **83**, 524 (1999)

-
- [47] G. van de Sand and J.-M. Rost
“Semiclassical description of multiphoton processes”
Phys. Rev. A **62**, 053403 (2000)
- [48] M. Spanner
“Strong Field Tunnel Ionization by Real-Valued Classical Trajectories”
Phys. Rev. Lett. **90**, 233005 (2003)
- [49] S. Yoshida, F. Grossmann, E. Persson and J. Burgdörfer
“Semiclassical analysis of quantum localization of the periodically kicked Rydberg atom”
Phys. Rev. A **69**, 043410 (2004)
- [50] X. Sun and W. H. Miller
“Forward-backward initial value representation for semiclassical time correlation functions”
J. Chem. Phys. **110**, 6635 (1999)
- [51] H. Wang, M. Thoss, K. L. Sørge, R. Gelabert, X. Giménez and W. H. Miller
“Semiclassical description of quantum coherence effects and their quenching: A forward-backward initial value representation study”
J. Chem. Phys. **114**, 2562 (2001)
- [52] R. Gelabert, X. Giménez, M. Thoss, H. Wang and W. H. Miller
“Semiclassical description of diffraction and its quenching by the forward-backward version of the initial value representation”
J. Chem. Phys. **114**, 2572 (2001)
- [53] M. Thoss, H. Wang and W. H. Miller
“Generalized forward-backward initial value representation for the calculation of correlation functions in complex systems”
J. Chem. Phys. **114**, 9220 (2001)
- [54] M. Thoss and H. Wang
“Semiclassical Description of Molecular Dynamics Based on Initial-Value Representation Methods”
Annu. Rev. Phys. Chem. **55**, 299 (2004)
- [55] F. Grossmann
“A semiclassical hybrid approach to many particle quantum dynamics”
J. Chem. Phys. **125**, 014111 (2006)
- [56] E. J. Heller
“Wavepacket dynamics and quantum chaos”
In M. J. Giannoni, A. Voros and J. Zinn-Justin, editors, “Chaos et Physique Quantique/Chaos and Quantum Physics, Proc. Les Houches Summer School, Session LII (1989)”, North-Holland, Amsterdam (1991)
- [57] W. Koch, F. Grossmann, J. T. Stockburger and J. Ankerhold
“Non-Markovian semiclassical dynamics”
Phys. Rev. Lett. **100**, 230402 (2008)

- [58] A. J. Leggett, S. Chakravarty, A. T. dorsey, M. P. Fisher, A. Garg and W. Zwerger
“Dynamics of the dissipative two-state system”
Rev. Mod. Phys. **59**, 1 (1987)
- [59] E. B. Wilson, J. C. Decius and P. Cross
Molecular Vibrations
McGraw-Hill, New York (1955)
- [60] W. H. Press, B. P. Flannery, S. A. Teukolsky and W. T. Vetterling
Numerical Recipes: The Art of Scientific Computing
Cambridge University Press (2007)
- [61] P. M. Morse
“Diatomic molecules according to the wave mechanics. II. Vibrational levels”
Phys. Rev. **34**, 57 (1929)
- [62] W. H. Miller
“The Semiclassical Initial Value Representation: A Potentially Practical Way of Adding Quantum Effects to Classical Molecular Dynamics Simulations”
J. Phys. Chem. A **105**, 2942 (2001)
- [63] H.-U. Finzel, H. Frank, H. Hoinkes, M. Luschka, H. Nahr, H. Wilsch and U. Wonka
“Atom-surface scattering with velocity-selected H and D atomic beams from LiF and NaF (001)”
Surf. Sci. **49**, 577 (1975)
- [64] M. Persson, J. Strömquist, L. Bengtsson, B. Jackson, D. Shalashilin and B. Hammer
“A first-principles potential energy surface for Eley-Rideal reaction dynamics of H atoms on Cu(111)”
J. Chem. Phys. **110**, 2240 (1999)
- [65] J. A. C. Gallas
“Some matrix elements for Morse oscillators”
Phys. Rev. A **21**, 1829 (1980)
- [66] I. N. Bronstein, K. A. Semendjajew, G. Musiol and H. Mühlig
Taschenbuch der Mathematik
Verlag Harri Deutsch, Frankfurt am Main (2008)
- [67] D. ter Haar
“The Vibrational Levels of an Anharmonic Oscillator”
Phys. Rev. **70**, 222 (1946)
- [68] M. E. Goggin and P. W. Milonni
“Driven Morse oscillator: Classical chaos, quantum theory, and photodissociation”
Phys. Rev. A **37**, 796 (1988)
- [69] V. Averbukh and N. Moiseyev
“Classical versus quantum harmonic-generation spectrum of a driven anharmonic oscillator in the high-frequency regime”
Phys. Rev. A **57**, 1345 (1998)

-
- [70] K. Toukan and A. Rahman
“Molecular-dynamics study of atomic motions in water”
Phys. Rev. B **31**, 2643 (1985)
- [71] F. Pichierri, J. Botina and N. Rahman
“Intramolecular dynamics from a statistical analysis of vibrational levels: Application of two coupled Morse oscillator models to the HCN molecule”
Phys. Rev. A **53**, 2624 (1995)
- [72] M. Peyrard and A. R. Bishop
“Statistical Mechanics of a Nonlinear Model for DNA Denaturation”
Phys. Rev. Lett. **62**, 2755 (1989)
- [73] C. Harabati, J. M. Rost and F. Grossmann
“Long-time and unitary properties of semiclassical initial value representations”
The Journal of Chemical Physics **120**, 26 (2004)
- [74] J. S. Bader, B. J. Berne, E. Pollak and P. Hänggi
“The energy relaxation of a nonlinear oscillator coupled to a linear bath”
J. Chem. Phys. **104**, 1111 (1996)
- [75] B. R. Holstein
“The harmonic oscillator propagator”
Am. J. Phys. **66**, 583 (1998)
- [76] M. Schlosshauer
Decoherence and Quantum-To-Classical Transition
Springer, Berlin (2007)
- [77] J. v. Neumann
Mathematische Grundlagen der Quantenmechanik (Mathematical Foundations of Quantum Mechanics)
Springer, Berlin (1955)
- [78] N. A. Peters, T.-C. Wei and P. G. Kwiat
“Mixed-state sensitivity of several quantum information benchmarks”
Phys. Rev. A **70**, 052309 (2004)
- [79] G. Barinova, N. Markovic and G. Nyman
“Split operator method in hyperspherical coordinates: Application to CH_2I_2 and $OCIO$ ”
J. Chem. Phys. **111**, 6705 (1999)
- [80] M. H. Beck, A. Jäckle, G. A. Worth and H.-D. Meyer
“The multiconfiguration time-dependent Hartree method: A highly efficient algorithm for propagating wavepackets”
Phys. Rep. **324**, 1 (2000)
- [81] J. Zanghellini, M. Kitzler, T. Brabec and A. Scrinzi
“Testing the multi-configuration time-dependent Hartree–Fock method”
J. Phys. B **37**, 763 (2004)

- [82] E. Runge and E. K. U. Gross
“Density-Functional Theory for Time-Dependent Systems”
Phys. Rev. Lett. **52**, 997 (1984)
- [83] F. Grossmann
“Semiclassical Real-Time Tunneling by Multiple Spawning of Classical Trajectories”
Phys. Rev. Lett. **85**, 903 (2000)
- [84] S. C. Creagh and N. D. Whelan
“Complex Periodic Orbits and Tunneling in Chaotic Potentials”
Phys. Rev. Lett. **77**, 4975 (1996)
- [85] S. Levit and U. Smilansky
“A new approach to Gaussian path integrals and the evaluation of the semiclassical propagator”
Annals of Physics **103**, 198 (1977)
- [86] M. F. Herman
“Time reversal and unitarity in the frozen Gaussian approximation for semiclassical scattering”
J. Chem. Phys. **85**, 2069 (1986)
- [87] K. Kay
“Semiclassical Initial Value Treatment of Atoms and Molecules”
Annu. Rev. Phys. Chem. **56**, 25 (2005)
- [88] F. Grossmann
“A hierarchy of semiclassical approximations based on Gaussian wavepackets”
Comments At. Mol Phys. **34**, 141 (1999)
- [89] E. Kluk, M. F. Herman and H. L. Davis
“Comparison of the propagation of semiclassical frozen Gaussian wave functions with quantum propagation for a highly excited anharmonic oscillator”
J. Chem. Phys. **84**, 326 (1986)
- [90] H. Wang, X. Sun and W. H. Miller
“Semiclassical approximations for the calculation of thermal rate constants for chemical reactions in complex molecular systems”
J. Chem. Phys. **108**, 9726 (1998)
- [91] X. Sun, H. Wang and W. H. Miller
“Semiclassical theory of electronically nonadiabatic dynamics: Results of a linearized approximation to the initial value representation”
J. Chem. Phys. **109**, 7064 (1998)
- [92] H. Lo, S. Popescu and T. Spiller
Introduction to Quantum Computation and Information
World Scientific (1998)
- [93] C. Macchiavello, G. M. Palma and A. Zeilinger
Quantum Computation and Quantum Information Theory
World Scientific (2000)

-
- [94] W. Zurek
“Decoherence and the Transition from Quantum to Classical - *Revisited*”
Los Alamos Science **27**, 2 (2002)
- [95] M. S. Bartlett
“Negative probability”
Proc. Cambridge Philos. Soc. **41**, 71 (1945)
- [96] N. Spagnolo, C. Vitelli, T. D. Angelis, F. Sciarrino and F. D. Martini
“Wigner-function theory and decoherence of the quantum-injected optical parametric amplifier”
Phys. Rev. A **80**, 032318 (2009)
- [97] J. Parker and C. R. Stroud
“Coherence and Decay of Rydberg Wave Packets”
Phys. Rev. Lett. **56**, 716 (1986)
- [98] J. A. Yeazell, M. Mallalieu and C. R. Stroud
“Observation of the Collapse and Revival of a Rydberg Electronic Wave Packet”
Phys. Rev. Lett. **64**, 2007 (1990)
- [99] O. Knospe and R. Schmidt
“Revivals of wave packets: General theory and application to Rydberg clusters”
Phys. Rev. A **54**, 1154 (1996)
- [100] G. Raithel, W. D. Phillips and S. L. Rolston
“Collapse and Revivals of Wave Packets in Optical Lattices”
Phys. Rev. Lett. **81**, 3615 (1998)
- [101] S. Tomsovic and J. H. Lefebvre
“Can Wave Packet Revivals Pccur in Chaotic Quantum Systems?”
Phys. Rev. Lett. **79**, 3629 (1997)
- [102] M. J. J. Vrakking, D. M. Villeneuve and A. Stolow
“Observation of fractional revivals of a molecular wave packet”
Phys. Rev. A **54**, R37 (1996)
- [103] M. Gühr, H. Ibrahim and N. Schwentner
“Controlling vibrational wave packet revivals in condensed phase: Dispersion and coherence for Br₂ in solid Ar”
Phys. Chem. Chem. Phys. **6**, 5353 (2004)
- [104] M. Spanner, E. A. Shapiro and M. Ivanov
“Coherent Control of Rotational Wave-Packet Dynamics via Fractional Revivals”
Phys. Rev. Lett. **92**, 093001–1 (2004)
- [105] B. Grüner, M. Schlesinger, P. Heister, W. T. Strunz, F. Stienkemeier and M. Mudrich
“Vibrational relaxation and decoherence of Rb₂ attached to helium nanodroplets”
arXiv:1011.0924v1 (2010)

- [106] R. W. Robinett
 “Quantum wave packet revivals”
Phys. Rep. **392**, 1 (2004)
- [107] E. J. Heller and S. Tomsovic
 “Postmodern Quantum Mechanics”
Phys. Today **46**, 38 (1993)
- [108] Z. Wang and E. J. Heller
 “Semiclassical investigation of the revival phenomena in a one-dimensional system”
J. Phys. A **42**, 285304 (2009)
- [109] O. Carnal and J. Mlynek
 “Young’s Double-Slit Experiment with Atoms: A Simple Atom Interferometer”
Phys. Rev. Lett. **66**, 2689 (1991)
- [110] U. Sinha, C. Couteau, T. Jennewein, R. Laflamme and G. Weihs
 “Ruling Out Multi-Order Interference in Quantum Mechanics”
Science **329**, 418 (2010)
- [111] G. Casati and T. Prosen
 “Quantum chaos and the double-slit experiment”
Phys. Rev. A **72**, 032111 (2005)
- [112] C.-M. Goletz, F. Grossmann and S. Tomsovic
 “Investigating quantum transport with an initial value representation of the semi-classical propagator”
Phys. Rev. E **80**, 031101 (2009)
- [113] K. G. Kay
 “Semiclassical propagation for multidimensional systems by an initial value method”
J. Chem. Phys. **101**, 2250 (1994)
- [114] M. Spanner, V. S. Batista and P. Brumer
 “Is the Filinov integral conditioning technique useful in semiclassical initial value representation methods?”
J. Chem. Phys. **122**, 084111 (2005)
- [115] G. Käb
 “Mean field Ehrenfest quantum/classical simulation of vibrational energy relaxation in a simple liquid”
Phys. Rev. E **66**, 046117 (2002)
- [116] W. Koch, F. Grossmann, J. T. Stockburger and J. Ankerhold
 “Semiclassical non-Markovian Brownian motion in anharmonic potentials”
Chem. Phys. **370**, 34 (2010)
- [117] R. Karrlein and H. Grabert
 “Exact time evolution and master equations for the damped harmonic oscillator”
Phys. Rev. E **55**, 153 (1996)

-
- [118] H. Grabert, P. Schramm and G.-L. Ingold
“Quantum brownian motion: The functional integral approach”
Phys. Rep. **168**, 115 (1988)
- [119] M. Thoss and G. Stock
“Mapping approach to the semiclassical description of nonadiabatic quantum dynamics”
Phys. Rev. A **59**, 64 (1999)
- [120] S. Zhang and E. Pollak
“A prefactor free semiclassical initial value series representation of the propagator”
The Journal of Chemical Physics **121**(8), 3384–3392 (2004)
- [121] H.-P. Breuer and F. Petruccione
The Theory of Open Quantum Systems
Oxford University Press, Oxford (2002)
- [122] F. Grossmann and W. Koch
“A finite-difference implementation of the Caldeira-Leggett master equation”
J. Chem. Phys. **130**, 034105 (2009)
- [123] W. Zurek
“Decoherence and the Transition from Quantum to Classical”
Phys. Today **44**, 10 (1991)
- [124] D. J. Tannor
Introduction to Quantum Mechanics: A Time-Dependent Perspective
University Science Books, Sausalito (2007)
- [125] D. Segale, M. Karavatis, E. Fredj and V. A. Apkarian
“Quantum coherent dissipation: A glimpse of the ‘cat’”
J. Chem. Phys. **122**, 111104 (2005)
- [126] M. Ovchinnikov and V. A. Apkarian
“Condensed phase spectroscopy from mixed-order semiclassical molecular dynamics: Absorption, emission, and resonant Raman spectra of I₂ isolated in solid Kr”
J. Chem. Phys. **105**, 10312 (1996)
- [127] M. Buchholz
Diploma Thesis
TU Dresden (2011)
- [128] G. Tao and W. H. Miller
“Semiclassical description of vibrational quantum coherence in a three dimensional I₂Ar_n ($n \leq 6$) cluster: A forward-backward initial value representation implementation”
J. Chem. Phys. **130**, 184108 (2009)
- [129] F. Grossmann
Theoretical Femtosecond Physics
Springer, Berlin (2008)

List of Publications

1. I. Gilary, Y. Sajeev, M. F. Ciappina, A. Croy, C.-M. Goletz, S. Klaiman, M. Sindelka, M. Winter, W. Wustmann and N. Moiseyev
“Suppression of Photoionization by a Static Field”
Phys. Rev. Lett. **101**, 163002 (2008)
2. C.-M. Goletz and F. Grossmann
“Decoherence and dissipation in a molecular system coupled to an environment: An application of semiclassical hybrid dynamics”
J. Chem. Phys. **130**, 244107 (2009)
3. C.-M. Goletz, F. Grossmann and S. Tomsovic “Investigating quantum transport with an initial value representation of the semiclassical propagator”
Phys. Rev. E **80**, 031101 (2009)
4. C.-M. Goletz, W. Koch and F. Grossmann “Semiclassical dynamics of open quantum systems: Comparing the finite with the infinite perspective”
Chem. Phys. **375**, 227 (2010)

Danksagung

Auch wenn auf der Titelseite der Dissertation nur mein Name steht, gibt es viele Menschen, die ihren Anteil daran haben haben, ohne womöglich sogar davon zu wissen. Es ist mir ein Bedürfnis, diesen Menschen meinen Dank auszudrücken.

Zunächst möchte ich Frank Großmann für seine fachliche, intensive Betreuung danken, die mir ein tieferes Verständnis der Physik ermöglichte, mich anfangs auch mal vor dem Betreten falscher Pfade bewahrte und meine Entwicklung als Physiker förderte. Aber nicht nur die fachliche Betreuung sondern auch das menschliche Miteinander habe ich als sehr angenehm empfunden, was mitunter auch zu interessanten Gesprächen über den Tellerrand der Physik hinaus führte.

Prof. Rüdiger Schmidt möchte ich danken, daß er sich als mein Doktorvater zur Verfügung gestellt und mir somit die Möglichkeit gegeben hat, in seiner Arbeitsgruppe die Dissertation anzufertigen. Die sozialen Veranstaltungen, wie beispielsweise Wanderungen, die ihm wichtig waren und auf seine Initiative hin zustande kamen, waren für mich eine Bereicherung.

Desweiteren möchte ich der gesamten Gruppe in ihren wechselnden Besetzungen, die ich in den Jahren erlebt habe, für interessante und oft fruchtbare Gespräche, aber auch gemeinsame Aktivitäten außerhalb des Institusgebäudes, danken. Ich darf behaupten, dass ich mich in der Gruppe sehr wohl gefühlt habe. An dieser Stelle möchte ich meinem Zimmerkollegen Werner zusätzlich für seine Hilfe, die insbesondere meine Linux- und Programmierkenntnisse erweitert hat, danken.

Ich hatte das Glück, zweimal jeweils einen Monat an einem ausländischen Forschungsinstitut gastieren zu dürfen. In diesem Zusammenhang möchte ich sowohl Steve Tomsovic als auch David Tannor für die sehr angenehme Gastfreundschaft danken.

Es ist nicht selbstverständlich Leute zu finden, die sich die Arbeit machen, ein Manuskript, das anfangs mit mehr oder weniger Fehlern gespickt ist, gegenzulesen. All jenen, die diese Arbeit auf sich genommen haben, möchte ich an dieser Stelle ebenfalls danken.

Für gewöhnlich werden die eigenen Eltern und Familie gegen Ende der Danksagung erwähnt, so auch hier. Der Grund ist aber nicht der, dass sie in meiner Dankesliste eine niedrigere Priorität haben als alle, die vorher kamen. Ganz im Gegenteil, ich habe meinen Eltern aber auch meinen Geschwistern sehr viel zu verdanken. Sie waren rat- und orientierunggebende Begleiter in meinem Leben, ohne mich jedoch irgendwohin zu drängen, und haben stets meine Begeisterung für die Naturwissenschaften, insbesondere natürlich für die Physik, unterstützt.

Nicht zuletzt gilt mein Dank Charlotte für ihre Geduld, ihr Mutmachen, ihr offenes Ohr und dafür dass sie mir den Rücken gestärkt hat.

Es mag eine Floskel sein, aber nirgendwo trifft die Aussage, dass diese Arbeit ohne all die hier erwähnten und unerwähnten Menschen nicht so gelungen wäre, mehr zu als hier.

Erklärung

Hiermit versichere ich, dass die vorliegende Arbeit ohne unzulässige Hilfe Dritter und ohne Benutzung anderer als der angegebenen Hilfsmittel angefertigt habe; die aus fremden Quellen direkt oder indirekt übernommenen Gedanken sind als solche kenntlich gemacht. Die Arbeit wurde bisher weder im In- noch im Ausland in gleicher oder ähnlicher Form einer anderen Prüfungsbehörde vorgelegt.

Die Dissertation wurde an der Technischen Universität Dresden unter Betreuung von Herrn Prof. Dr. Rüdiger Schmidt angefertigt.

Ich erkenne die Promotionsordnung der Fakultät Mathematik und Naturwissenschaften an der Technischen Universität Dresden vom 20.03.2000 mit allen Änderungssatzungen bis zum 17.07.2008 an.

Dresden, den 10. Februar 2011

Christoph-Marian Goletz